CONTROL METHODS FOR COMPENSATION AND INHIBITION OF MUSCLE FATIGUE IN NEUROPROSTHETIC DEVICES

by

Nicholas A. Kirsch

BS in Mechanical Engineering, University of Pittsburgh, 2009

MS in Mechanical Engineering, University of Pittsburgh, 2012

Submitted to the Graduate Faculty of

the Swanson School of Engineering in partial fulfillment

of the requirements for the degree of

PhD in Mechanical Engineering

University of Pittsburgh

2016

UNIVERSITY OF PITTSBURGH

SWANSON SCHOOL OF ENGINEERING

This dissertation was presented

by

Nicholas A. Kirsch

It was defended on

March 21, 2016

and approved by

Nitin Sharma, PhD, Assistant Professor

William Clark, PhD, Professor

Daniel Cole, PhD, Associate Professor

Zhi-Hong Mao, PhD, Associate Professor

Mark Redfern, PhD, Professor

Jeffrey Vipperman, PhD, Professor

Dissertation Director: Nitin Sharma, PhD, Assistant Professor

CONTROL METHODS FOR COMPENSATION AND INHIBITION OF MUSCLE FATIGUE IN NEUROPROSTHETIC DEVICES

Nicholas A. Kirsch, PhD

University of Pittsburgh, 2016

For individuals that suffer from paraplegia activities of daily life are greatly inhibited. With over 5,000 new cases of paraplegia each year in the United States alone there is a clear need to develop technologies to restore lower extremity function to these individuals. One method that has shown promise for restoring functional movement to paralyzed limbs is the use of functional electrical stimulation (FES), which is the application of electrical stimulation to produce a muscle contraction and create a functional movement. This technique has been shown to be able to restore numerous motor functions in persons with disability; however, the application of the electrical stimulation can cause rapid muscle fatigue, limiting the duration that these devices may be used. As an alternative some research has developed fully actuated orthoses to restore motor function via electric motors. These devices have been shown to be capable of achieving greater walking durations than FES systems; however, these systems can be significantly larger and heavier. To develop smaller and more efficient systems some research has explored hybrid neuroprostheses that use both FES and electric motors. However, these hybrid systems present new research challenges.

In this dissertation novel control methods to compensate/inhibit muscle fatigue in neuro-prosthetic and hybrid neuroprosthetic devices are developed. Some of these methods seek to compensate for the effects of fatigue by using fatigue dynamics in the control development or by minimizing the amount of stimulation used to produce a desired movement. Other control methods presented here seek to inhibit the effects of muscle fatigue by adding an electric motor as additional actuation. These control methods use either switching or cooperative

control of FES and an electric motor to achieve longer durations of use than systems that strictly use FES. Finally, the necessity for the continued study of hybrid gait restoration systems is facilitated through simulations of walking with a hybrid neuroprosthesis. The results of these simulations demonstrate the potential for hybrid neuroprosthesis gait restoration devices to be more efficient and achieve greater walking durations than systems that use strictly FES or strictly electric motors.

TABLE OF CONTENTS

LIST OF TABLES

LIST OF FIGURES

x

1.0 INTRODUCTION

Each year in the United States approximately 12,500 people suffer a spinal cord injury (SCI), as reported by the National Spinal Cord Injury Statistical Center [137]. Of those 12,500 people 41% of them are diagnosed with paraplegia, which is the loss of motor and/or sensory function of the lower extremities. This loss of motor and/or sensory function can greatly inhibit the persons ability to perform activities of daily life. Passive devices, such as orthoses or walkers, can be used to help these people regain some of the functionality of their lower extremities; however, because these devices are incapable of generating movement they are limited to static applications such as standing. Restoring functional movement of the lower extremities to these individuals can further increase their quality of life by enabling them to perform tasks such as walking.

One method that has been explored to restore functional movement of the lower extremities to individuals with an SCI is the application of functional electrical stimulation (FES) [8, 51, 58, 78, 80, 97]. FES is the application of low-level electrical stimulation to the nerves that innervate the muscles to produce a muscle contraction. The electrical stimulation can be applied using either transcutaneous (surface) [8], percutaneous [106], or implanted electrodes [65]. FES has been used for many medical applications; such as cochlear implants [53], grasping [111], bladder voiding [15], and drop foot correction [95]. By sequentially stimulating the muscle groups functional movements, such as walking, can be achieved [8, 51, 58, 78, 80, 97]. One example of this is the Parastep system [76] (Therapeutics Inc.), which is an FDA approved gait restoration that uses six channels of transcutaneous stimulation to allow paraplegics to stand and walk [109].

Although FES can be used to restore functional movement and has many health benefits associated with it (e.g., increased muscle mass, bone density, and blood flow [80]) there are still many challenges to using it for gait restoration. The major challenge is the rapid onset of muscle fatigue, which is the decline in the ability of a muscle to produce a force, and typically occurs due to nervous system or metabolic fatigue. There are two theories on how FES recruits the motor units, and both support the rapid muscle fatigue that is observed due to the application of FES. The first theory is that the application of FES violates Henneman's size principle [102], which states that during a volitional contraction the motor units are recruited from smallest (low force, fatigue resistant) to largest (large force, fatigue rapidly). When transcutaneous FES is used the motor units are recruited in the reverse order of the size principle. In other words, FES recruits the rapidly fatiguing motor units first, which causes muscle fatigue to occur more rapidly. The second theory is that FES inherently recruits muscle fibers in a repeated, spatially fixed, and non-selective manner [12]. Since the same motor units are repeatedly stimulated, compared to volitional contractions that recruits many motor units asynchronously, rapid muscle fatigue occurs. Regardless as to which of these theories is correct, rapid muscle fatigue severely limits the duration that FES may be used. FES devices for gait restoration have been shown to be capable of walking approximately 100 feet on average, with some individuals being unable to walk tens of feet [52].

Error-based feedback control of FES [2, 3, 125, 129] can compensate for the reduction in performance that can result due to muscle fatigue by increasing the amount of stimulation used. However, none of these controllers take into consideration muscle fatigue dynamics and increasing the amount of stimulation used only exacerbates the issue by increasing the rate of muscle fatigue. One solution that has been explored to reduce muscle fatigue and increase walking durations in FES-based gait restoration devices is using a passive orthosis [6, 101, 132]. By using a passive orthosis less stimulation may be required, since the brace can support the user in between steps or when standing. The reduction in stimulation required resulted in an increase in walking durations; however, the physical constraints of the orthoses often produce unnatural gait motions. For example, Andrews and Bajd [6] used a passive orthosis that locked that the knee joints in combination with FES. The gait motion was produced

using stimulation of the gastrocnemius muscles to achieve plantarflexion and peroneal nerve stimulation to achieve hip flexion. Using the aforementioned stimulation with an orthosis that does not allow knee motion resulted in a gait motion that was referred to as "tip-toe gait". Although less stimulation may be required by devices like this during standing and in between steps, because they result in inefficient gait motions they may require more stimulation when producing the movement.

An alternative to addressing the challenges of using FES is to use a fully actuated orthosis, also referred to as an exoskeleton. Exoskeleton devices such as the Vanderbilt exoskeleton [36], ReWalk [35], Mina [107], and Ekso [135, 136] are capable of greater walking durations than FES-based walking devices. Since the actuators used in these exoskeleton devices (electric motors and hydraulics) are highly repeatable they are simpler to control than electrically stimulated muscles, which are nonlinear and variable actuators. Also, because they are not using FES these devices are not subject to the rapid onset of muscle fatigue, and therefore are capable of greater walking duration. However, because of the magnitude of the joint torques required to produce a natural gait motion, these devices are heavier and bulkier than FES devices. Also, if the devices wish to achieve longer walking durations they will likely need to use larger battery packs, which will increase the size and weight of the device. In other words, although these devices may be capable of greater walking durations than FES-based systems the duration that they may be used is limited entirely by the capacity of the power source.

To overcome the challenge of rapid muscle fatigue caused by FES systems, and to potentially reduce the size and weight of powered exoskeleton devices, hybrid FES/exoskeleton gait restoration devices have been proposed [23, 55, 72, 112]. However, combining these two methods of gait restoration results in an actuator redundancy. One technique for solving the actuator redundancy would be to switch between using FES and the electric motors as the muscles fatigue and the application of FES becomes insufficient for creating the gait motion. Then, once the muscles have sufficiently recovered the system can switch back to using FES. This method of switching between FES and electric motors would require a measurement or estimate of muscle fatigue for the system to know when to switch, and the appropriate controller must be used to allow for stable switching between the two actuators.

Another technique for solving the actuator redundancy problem would be to allocate control simultaneously to the FES and electric motors. Allocating control simultaneously would allow the FES to produce some of the necessary joint torque, allowing the gait restoration devices to use smaller, lighter, and more efficient actuators. Similarly, the electric motors can reduce the amount of FES required to produce the gait motion, which should inhibit the onset of muscle fatigue and allow for longer walking durations. However, this creates the problem of choosing how much control to allocate to the FES and how much to allocate to the electric motors. There are a number of methods that may be used to solve the control allocation problem [64]; however, the nonlinear dynamics of walking, the nonlinear actuator dynamics of FES induced muscle contractions, and the effects of muscle fatigue make allocating control between FES and electric motors challenging.

In this dissertation a number of control methods are presented to compensate for or inhibit the effects of muscle fatigue that can degrade the control performance of neuroprosthetic devices. The remainder of this Chapter will present previous research that will motivate and facilitate the work presented in this dissertation, followed by a summary of the contributions of this work. Next, because a number of model-based control and estimation techniques will be used in this dissertation Chapter 2 will discuss the models and parameter identification processes that will be used by the subsequently discussed controllers. Chapter 3 will present a new nonlinear controller that uses estimates of muscle activation and fatigue in the control law to compensate for the effects of muscle fatigue. This feedback control law may compensate for the degradation in performance, but it may also induce more muscle fatigue because it increases the stimulation to achieve prolonged performance. To inhibit the effects of muscle fatigue, and prolong the duration that neuroprosthetic devices may be used, a nonlinear model predictive controller (NMPC) was tested. The details of the NMPC algorithm and the results of experiments on three able-bodied subjects are presented in Chapter 4. To further prolong the duration that FES may be used a controller that can perform stable switching between FES and an electric motor based on an estimate of muscle fatigue was developed. The control development and simulations for this switching controller are presented in Chapter 5. Next, in Chapter 6 dynamic control allocation (DCA) is used to optimally allocate control between FES and an electric motor in a hybrid neuroprosthesis.

To explore the benefits of using a hybrid gait restoration device, in terms of duration of use and power consumption, a musculoskeletal gait model with muscle fatigue dynamics was developed and simulated for three different actuation cases: FES only, electric motors only, and hybrid (FES and motors). The results of the simulations of this model are presented and discussed in Chapter 7. Finally, Chapter 8 presents the development and preliminary testing of a finite-state machine controlled hybrid orthosis that may be used for future research to test the controllers developed in this dissertation.

1.1 BACKGROUND AND STATE-OF-THE-ART

This section discusses the present state of gait restoration devices and the background theory that is used in this dissertation. First, the current state of gait restoration technology is presented to illustrate that the research performed in this dissertation and the device that we are developing is the next logical step in gait restoration technology.

1.1.1 Gait Restoration Technology

In 1963 Kantrowitz used FES to restore the walking function to paraplegics [66]. Kantrowitz used continuous stimulation of the glutei and quadriceps muscles to stiffen the lower extremity joints of a paraplegic, enabling them to stand. With the aid of a walker the user was able to stand for a few minutes, and was even able to produce a mode of gait similar to long leg-brace walking. These were the first results presented on the use of FES for gait restoration.

Twenty years later Bajd et al. expanded upon the work of Kantrowitz by using peroneal nerve stimulation to produce a withdraw reflex of the leg (combination of hip flexion, knee flexion, and dorsiflexion), which is an important characteristic of a natural gait motion [8]. To keep the user standing Bajd et al. continually stimulated the quadriceps muscles to keep the knees extended. Then, during the swing phase the peroneal nerve was stimulated to achieve ground clearance and to swing the foot through. This method produced a much more natural
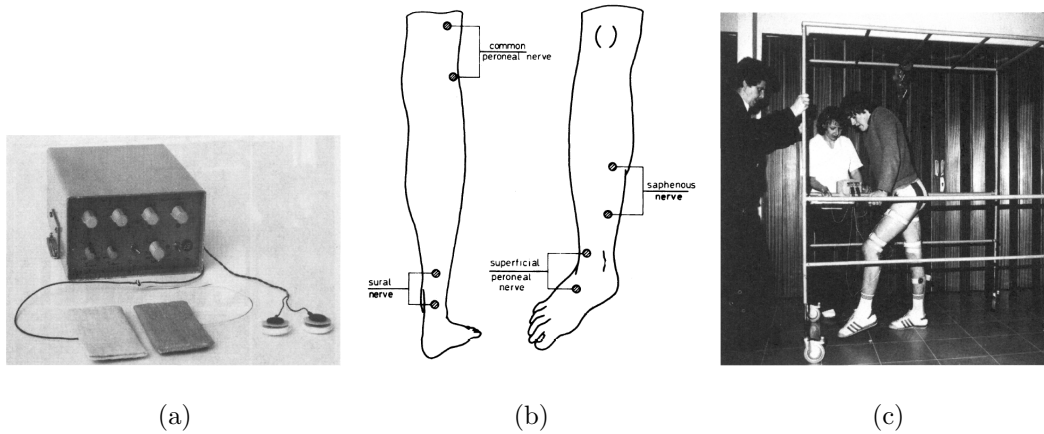
Figure 1.1: A four channel stimulator (a), electrode placements (b), and a paraplegic patient walking using FES (c) (from [8]).

gait motion than the one produced by Kantrowitz in 1963, and is still commonly used in FES gait restoration. In fact, a similar method is used by the Parastep system [76] (Therapeutics Inc.), which is an FDA approved gait restoration device that can be used for standing and walking [109]. Fig. 1.1 shows a paraplegic walking using this method, the electrodes used, and the placement of the electrodes.

Through many years of research the use of FES for gait restoration, as well as other application, has been shown to yield many health benefits for the users, such as [80]:

- Patient uses their own muscles and metabolic energy
- Prevention of muscle atrophy
- Increased blood flow to the muscles and skin
- Prevention of contractures and joint ossification
- Increased bone density

Despite all of these health benefits of using FES, using FES as a means of gait restoration has not yet been widely accepted. This is mostly due to the fact that FES causes the muscles to fatigue more rapidly compared to volitional contractions, which resulted in most

users only being able to walk approximately 100 feet. It has been shown by [80] that cyclic stimulation training can be used to strengthen the muscles and make them more fatigue resistant. However, even after retraining the muscles the walking durations remained limited.

To decrease the amount of stimulation that was needed, passive orthoses were combined with the FES. The passive orthoses provided the user with support while standing or in between steps so that constant stimulation was not required, thus reducing muscle fatigue. This type of hybrid system was proposed as early as 1973 by Tomovic et al. [141], who developed the floor reaction ankle-foot orthosis (FRO). The FRO used a modified, rigid ankle joint that tilted the user forward so that the knee joint was locked in hyperextension while standing. Andrews and Bajd combined FES with an orthosis that was constantly locked at the knee, creating a sort of "tip-toe gait" [6]. Solomonow et al. combined FES with a reciprocating gait orthosis (RGO), which can transfer movement of one leg to the other [133]. In [48], Goldfarb et al. used controlled braking at the knee joints of the passive orthosis to produce a more natural gait by allowing the knee joints to unlock during the swing phase. These devices were able to make a significant improvement to walking duration and/or speed, compared to FES systems that did not use any orthoses. However, the inclusion of the passive orthoses limits the degrees of freedom of the lower extremities, which can cause inefficient gaits or may be unable to produce motions other than gait.

Although combining FES with passive orthoses reduced muscle fatigue, and resulted in greater walking durations, there are still other challenges that result from FES that need to be overcome:

- FES induced muscle contractions are difficult to control because of their nonlinear dynamics

- Day-to-day physiological variability and subject variability can also make FES control challenging

- Withdraw reflex is highly variable and subject to rapid habituation

These challenges have been addressed by developing fully actuated orthoses, also known as exoskeletons, to restore walking to paraplegics [35, 36, 107, 135]. Some of these exoskeleton devices, such as the ones shown in Fig. 1.2, are commercially available. Also, a few of them,

<div align="center">(a)   (b)   (c)</div>
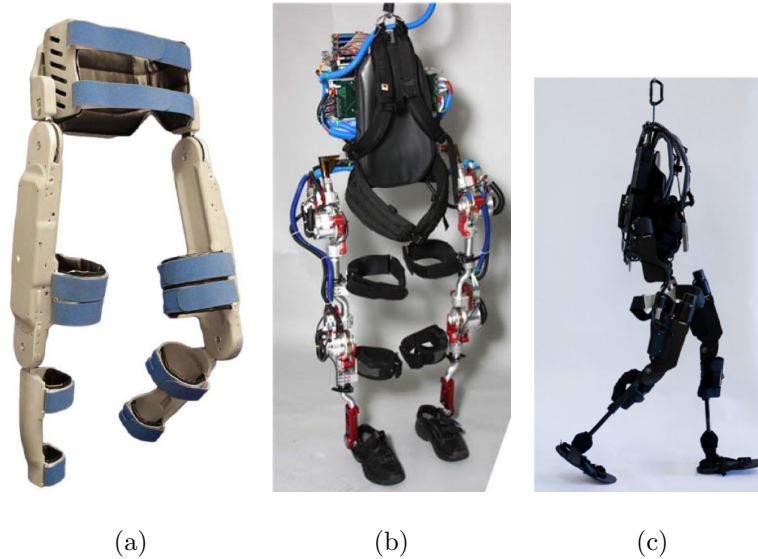
Figure 1.2: Some examples of the fully actuated exoskeletons for gait restoration are the Vanderbilt Exoskeleton (Indego) (a) (from [36]), Mina exoskeleton (b) (from [107]), and Ekso Bionics exoskeleton (c) (from [135]).

such as Ekso [135] and ReWalk [35], have been approved by the FDA. These exoskeleton devices, which are used with crutches or a walker, have allowed paraplegic users to achieve longer walking durations than when using FES or FES/passive orthosis devices. However, because these devices use electric motors, and not the patient's own muscles, they are bulkier and heavier. Also, because these devices do not use FES they do not have the therapeutic benefits that result from the use of FES [80, 98, 114].

Some research has been done to investigate combining FES with actuated orthoses [23, 55, 70, 77, 113] so that lighter devices that are capable of longer walking durations may be developed. By adding FES to an actuated orthosis smaller actuators could be used to produce the required joint torques for walking. Also, the additional work done by the electric motors will reduce the amount of stimulation that is needed, which could decrease the effects of muscle fatigue and increase walking durations. However, combining these two methods of gait restoration results in an actuator redundancy problem.

<div align="center">8</div>

1.1.2 Control Allocation in Hybrid Neuroprosthesis

When multiple actuators influence the same degree of freedom then there is no unique solution as to how much influence each actuator should provide. This is referred to as redundant actuation. Redundant actuation appears in many systems and can either be inherent to the system, as is the case for muscles [138], or an intentional design feature, as is the case in fault-tolerant control [14]. In the case of hybrid neuroprostheses actuator redundancy will be used as an intentional design feature to reduce the weight, size, and power consumption of gait restoration devices so that their walking durations may be increased.

Some research has been done to investigate the advantages of combining FES with an actuated orthosis. In [77], Kobetic et al. combined FES with hydraulic actuators and wrap-spring clutches to facilitate standing, walking, and stair climbing. The device developed and used by Kobetic et al., which is shown in Fig. 1.3, is controlled by a finite-state machine. The finite-state machine uses force-sensing resistors at the bottom of the foot and hip angular velocity (computed from the cylinder position of the hydraulics) to determine when to switch between controlling the stance phase and the swing phase. Although the results indicated that the device was able to achieve the aforementioned motions, no method for the synchronous control of FES and exoskeleton was presented.

Quintero et al. have done preliminary assessment of a cooperative controller that combines FES and electric motors to elicit knee extension movements in a subject while seated [113]. In [113] an adaptive control gain was used to distribute a portion of the control effort to FES from an electric motor. The block diagram of the control system, and the test setup that was used, are shown in Fig. 1.4. In the block diagram in Fig. 1.4 the gain K_s is the adaptive gain that distributes some of the control effort from the motor to the FES of the quadriceps muscles. The control gain was adapted using a gradient descent method that sought to minimize the motor torque used to produce the knee extension movement. The results of this research indicated a 55.9% reduction in mechanical energy from the motor when FES was used in coordination with the knee motor of the exoskeleton.
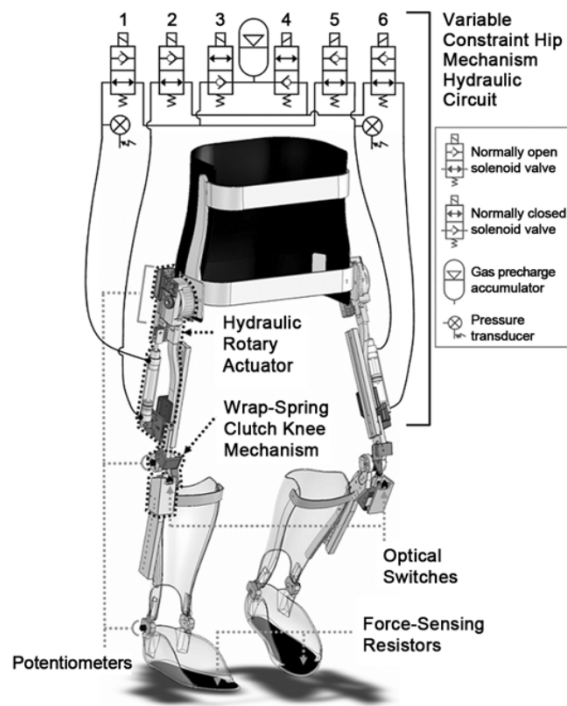
Figure 1.3: This hydraulically actuated exoskeleton device, developed by Kobetic et al. was used in coordination with electrical stimulation to facilitate standing, walking, and stair climbing (from [77]).

(a)   (b)
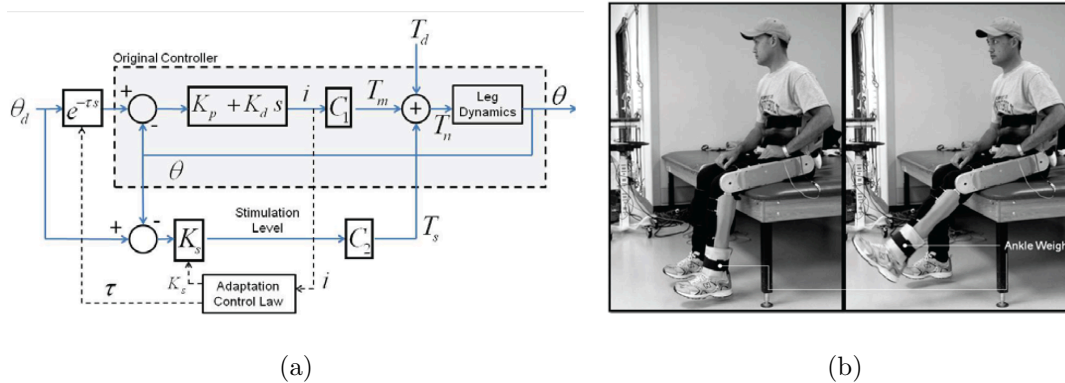
Figure 1.4: The block diagram (a) and the test setup (b) used by Quintero et al. to test control of FES and electric motors to elicit knee extension movements (from [113]).

In [23] and [55] a PID controller was combined with an iterative learning controller to cooperatively control FES and electric motors in hybrid exoskeletons. Like the adaptive cooperative control in [113], iterative learning control is an adaptive control technique. However, the iterative learning controller adapts only at each iteration of a task, which in this case is a step. In [23] the amount of stimulation used was adapted based on the performance achieved in the previous step, while in [55] the stimulation was adapted based on a desired torque profile and the torque profile achieved in the previous step.

As previously mentioned, combining FES with electric motors creates a redundant actuation problem. Therefore, a controller must be developed that can adequately distribute control effort between FES and electric motors. Two novel techniques that will be considered by this research for solving the actuator redundancy problem are switching control and dynamic control allocation. A switching controller may be used to discretely switch between using FES and an electric motor based on how fatigued the muscle is. When the muscles become severely fatigued such that the performance of the neuroprosthesis is affected the controller may switch to using the electric motors. Then, once they recover the controller may switch back to using FES. The primary challenge with developed switched control systems is that switching between two stable systems does not result in a stable switching system [92]. Therefore, a stability analysis must be used to show that stable switching can be achieved.

DCA is the application of model predictive control (MPC) to solve the control allocation problem by choosing how to allocate control to the redundant actuators based on the solution to a finite time optimal control problem [17, 100]. Although some research has simulated the application of MPC for neuroprostheses [11, 34, 104] it has not yet been experimentally validated or considered for control of hybrid neuroprostheses to solve the actuator redundancy problem. The main challenge hindering the real-time implementation of MPC for control of FES and for DCA in hybrid neuroprostheses is that they both require a finite-time optimal control problem to be solved at each time step of the control. These optimizations can be computationally very intensive and require significantly long solve times, especially for high order or relatively fast dynamic systems. However, through using fast optimization solvers, such as the gradient projection method [50, 67, 89], real-time implementation of MPC of

FES and DCA for hybrid neuroprostheses can be achieved. Another necessity to real-time implementation of MPC and DCA is a model of the system. Methods, such as the ones in [30, 110], may be used to identify the necessary model parameters for neuroprostheses and hybrid neuroprostheses so that these control methods may be implemented experimentally.

1.2 CONTRIBUTIONS

This dissertation presents a number of novel control methods to compensate for and/or inhibit the effects of muscle fatigue. The contributions of this dissertation can be summarized as follows:

- Development and experimental validation of a controller for a neuroprosthetic system that uses estimates of muscle activation and fatigue in the control law in order to compensate for their affects (see Chapter 3).

- Methods and experimental validation off nonlinear MPC of FES using a gradient projection algorithm (see Chapter 4).

- Development of a novel switching controller for a hybrid neuroprosthesis that switches between FES and an electric motor based on how fatigued the muscles are (see Chapter 5).

- Methods for the real-time implementation of nonlinear MPC-based DCA of a hybrid neuroprosthesis using a gradient projection algorithm (see Chapter 6).

- Dynamic optimizations of a musculoskeletal model of gait are used to determine optimal control signals for FES, electric motor, and hybrid (FES and electric motor) gait restoration systems. These results illustrate the potential of adding FES to exoskeleton systems to improve efficiency, and increase the duration that gait restoration devices may be used (see Chapter 7).

2.0 MUSCULOSKELETAL MODELING AND SYSTEM IDENTIFICATION OF NEUROPROSTHESES

In this dissertation a number of model-based control and estimation techniques will be used for neuroprostheses and hybrid devices. Therefore, having an accurate model of the response of a musculoskeletal system to the application of FES is essential. This chapter presents a musculoskeletal neuroprosthesis model of leg extension, and the procedures that are used to estimate the parameters of the model. The procedures presented here are modified versions of some of the procedures used in [123, 134, 140] that were used to identify musculoskeletal parameters. Some of the methods were modified due to a lack of appropriate equipment, and some were modified to improve upon or simplify the previous methods.

The passive dynamics of the muscles and tendons at the joints, and the active muscle forces due to the application of FES are modeled in this dissertation using a modified Hill-based muscle model [148]. The Hill-based muscle model is a phenomenological model of the force-length and force-velocity relationships that have been observed in the responses of skeletal muscles.

The response of the muscle activation will be modeled as a first order response [144]. Other phenomena that may affect the time response of muscle activation (such as electromechanical delay [18, 151]) will not be modeled here. However, to a degree these phenomena are captured in the estimated first order response (i.e., the unmodeled delay results in slower time constants than if the delay model were included). The muscle activation model may not be used in the development of all of the controllers in this dissertation; however, it is possible to include the muscle activation dynamics in the control development by using a backstepping method [69].
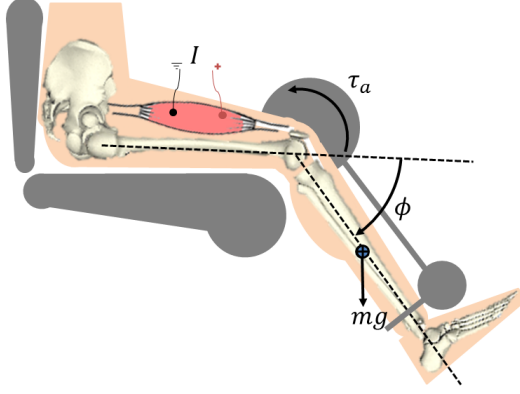
Figure 2.1: This knee extension neuroprosthesis uses electrical stimulation of the quadriceps muscles (I) to elicit a knee extension. The angle ϕ is the anatomical knee joint angle.

The model that will be presented in this chapter is a simple, single joint model of knee extension response due to FES of the quadriceps muscles. However, the modeling of the knee joint and quadriceps muscles can be similarly applied to the other joint of the lower extremities. This simple model will be expanded upon in a later chapter to create a musculoskeletal gait model based on [30, 110].

2.1   LEG EXTENSION NEUROPROSTHESIS MODEL

The rigid body dynamics for a leg extension neuroprosthesis, as depicted in Fig. 2.1, can be expressed as

$$J\ddot{\phi} + G + \tau_p = -\tau_a, \tag{2.1}$$

where $\phi, \dot{\phi}, \ddot{\phi} \in \mathbb{R}$ are the anatomical knee joint angle, angular velocity, and acceleration. In (2.1), J is the moment of inertia of the lower leg (shank and foot), $G = mgl_c \cos(\phi)$ is the gravitational moment, τ_p is the passive torque of the joint, and τ_a is the knee extension torque

produced by stimulation of the quadriceps muscles. In the gravitational moment $m \in \mathbb{R}^+$ is the mass of the lower leg, $g \in \mathbb{R}^+$ is gravitational acceleration, and $l_c \in \mathbb{R}^+$ is the distance from the knee joint to the center of mass of the lower leg.

The passive moment that is generated by the damping and elasticity of the muscles, tendons, and ligaments at the knee joint can be modeled as [110]

$$\tau_p = d_1(\phi - \phi_0) + d_2\dot{\phi} + d_3\mathrm{e}^{d_4\phi} - d_5\mathrm{e}^{d_6\phi}, \tag{2.2}$$

where ϕ_0, the equilibrium angle of the linear stiffness, and d_i, for $i = \{1 - 6\}$, are subject specific parameters. The exponential terms are used to model hyper-flexion and hyper-extension of the knee joint. This function that models the passive joint stiffness and damping at the knee can similarly be used (and will in a later chapter) to model stiffness and damping of the hip and ankle joints.

The moment that is generated by the muscle activation due to FES can be modeled as

$$\tau_a = \psi_l(\phi)\psi_v(\dot{\phi})a(u), \tag{2.3}$$

where $\psi_l(\phi)$ is the torque-length relationship, $\psi_v(\dot{\phi})$ is the torque-velocity relationship, and $a \in [0, 1]$ is the normalized muscle activation. The torque-length relationship can be modeled using a number of functions, but is most simply modeled as the parabolic function [110]

$$\psi_l(\phi) = c_2\phi^2 + c1\phi + c_0. \tag{2.4}$$

The torque-velocity relationship for the quadriceps muscles can be modeled as [110]

$$\psi_v(\dot{\phi}) = \begin{cases} 0, & \dot{\phi} < -1/c_3 \\ 1 + c_3\dot{\phi}, & -1/c_3 \leq \dot{\phi} < (c_4 - 1)/c_3 \\ c_4, & (c_4 - 1)/c_3 \leq \dot{\phi} \end{cases} \tag{2.5}$$

This function models the change in force that results from concentric and eccentric muscle contractions. A slightly different function is used for the torque-velocity relationship of flexor

muscles. This function will be presented in a later chapter where flexor muscles will be modeled. The parameters c_j, for $j = \{0-4\}$ in (2.4) and (2.5) are subject specific parameters. For relatively slow movements (angular velocities approximately in the range $\pm 0.5\,\text{rad/s}$ based on the results of [110])

Modifications to the torque-length and torque-velocity functions in equations (2.4) and (2.5) that will be used to facilitate control development or stability analysis will be discussed in the chapter in which they are used.

The state $a \in [0, 1]$ in (2.3) is the normalized muscle activation, which is a function of the normalized muscle stimulation, $u \in [0, 1]$. This state corresponds to the percentage of muscle fibers recruited. In other words, when $a = 1$ 100% of the muscle fibers are recruited, and the joint torque produced is the maximum torque for that angle and angular velocity. Muscle activation is most simply modeled as a first order differential equation [144]

$$\dot{a} = \frac{u - a}{T_a}, \tag{2.6}$$

where $T_a \in \mathbb{R}^+$ is the activation time constant. The activation time constant in (2.6) corresponds to the time it takes for a muscle to contract and relax, and assumes that muscle activation and de-activation occur at the same rate. The normalized stimulation, u in (2.6), can be computed from the current amplitude of the stimulation as

$$u = \begin{cases} 0, & I < I_t \\ \frac{I_s - I}{I_s - I_t}, & I_t \leq I \leq I_s \\ 1, & I_s < I \end{cases} \tag{2.7}$$

In (2.7) I_t is the threshold current amplitude, which corresponds to the minimum current amplitude required to produce a movement. I_s is the saturation current amplitude, which corresponds to the minimum current amplitude that produces the maximum muscle force.

It should be noted that this model of the muscle's response to electrical stimulation assumes that only current amplitude is varied, and that all other parameters of the electrical stimulation (such as pulse-width and frequency) remain constant. Therefore, the stimulation parameters used must remain constant when estimating the parameters of the model and if the model is used in the control.
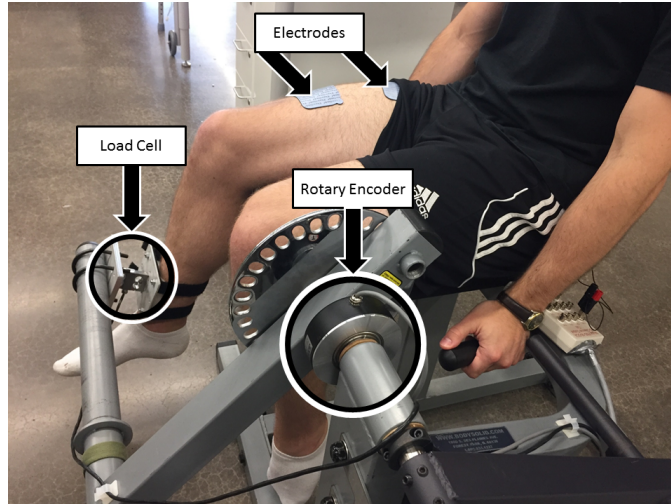
Figure 2.2: Participants were seated in a leg extension machine that has been modified with an encoder and load cell. Electrical stimulation of the quadriceps muscles was used to produced the knee extension motion.

2.2 PARAMETER ESTIMATION PROCEDURES

To develop some of the controllers in this dissertation the structure of the dynamics of a neuroprosthesis system are sufficient. However, for the model-based control techniques developed in this dissertation, such as model predictive control, estimates of the parameters of the model must be determined. This section describes procedures, which are adapted from methods in [117] and [134], for estimating the necessary parameters. The parameter estimation procedure was conducted on three able-bodied male participants between the ages of 25-28 years. Results from each procedure of the process will be shown for one participant (Participant 1) to exemplify the results of each step. The resulting parameters that were estimate and metrics that illustrates the goodness of fit of the model will be given at the end of this section for all three participants.

17

2.2.1 Setup for Parameter Estimation

All parameter estimation procedures were performed using the test setup shown in Fig. 2.2. The leg of the subject is strapped to the arm of a leg extension machine that is fitted with a load cell (HBM Inc., Hesse, Germany) and an incremental rotary encoder (GHH100-35G1024BSP526 Shanghai Qiyi Electrical & Mechanical Equipment Co. Ltd, Shanghai, China). The rotary encoder can be used to measure the knee joint angle of the participant during each part of the parameter estimation procedure. The load cell can be used to measure the force of the participant pushing on the arm of the let extension machine, which can be used to calculate knee joint torque. During each parameter estimation procedure the participants were instructed to remain relaxed and not influence any of the load cell measurements with volitional muscle contractions.

In the subsequently discussed parameter estimation procedures only stimulation of the quadriceps muscle is considered. However, the procedures for identifying the model of FES-induced muscle contractions for other muscles can be performed in a manner similar to the methods used for identification of the quadriceps muscles. The quadriceps muscles were stimulated using an FNS-16 Multi-Channel Stimulator (CWE Inc., USA), which was modified to have a maximum current amplitude of 100 mA. The stimulator was operated in a current amplitude controlled mode, with all other parameters of the stimulation train constant. The stimulation pulses used were bi-phasic, to ensure charge balance of the stimulation, at a frequency of 35 Hz and pulse-width of 400 μs. It is important to note that the estimated parameters are dependent on the stimulation parameters (frequency and pulse-width) used during the parameter estimation procedure. Therefore, a frequency of 35 Hz and pulse-width of 400 μs will be used in all experiments in this dissertation that use the parameters estimated in this chapter.

The electrodes were placed on the quadriceps muscles according to educational videos provided by Axelgaard Manufacturing Co., LTD [9]. With FES, the recruitment of motor units depends heavily on the size of the electrodes used; i.e., larger electrodes distribute the stimulation more and can recruit more motor units. 5"×2.5" electrode pads (as seen

in Fig. 2.2) were found to be sufficiently large for stimulation of the quadriceps muscles. Since electrode size and placement can also affect the estimated parameters the same size electrodes and consistent placements will be used in all experiments in this dissertation.

2.2.2 Test 1

First, so that the current amplitude can be normalized for each participant, the saturation and threshold current amplitudes (I_s and I_t in (2.7)) are determined. With the participant seated in the leg extension machine in an isometric contraction configuration, 2 second long pulse trains of stimulation were administered to induce a muscle contraction. The isometric knee joint torque was then measured by using the load cell attached to the leg extension machine. The current amplitude of the two second long pulse trains was slowly increased from 20 mA to 80 mA, with two seconds in between the pulse trains. Only twenty different current amplitudes, evenly spaced from 20 mA to 80 mA, and 2 second long pulse trains are used instead of a continuous current ramp. This was done so that the muscles were not unnecessarily fatigued. The peak current amplitude was set to 80 mA because participants found current amplitudes above that level to be uncomfortable. The isometric joint torque produced by each 2 second long pulse train was computed by averaging the joint torque measurements for the last second that the pulse train was applied. This was done so that the transient response of the isometric contractions are neglected, and to average out any noise in the measurement.

The threshold current amplitude (I_t) of an individual was taken as the current amplitude that produced the first significant muscle contraction. A significant muscle contraction was defined as a joint torque measurement that exceeded three times the standard deviation of the load cell signal noise. Therefore, the first current amplitude that caused an increase in the joint torque measurement that exceeded three times the standard deviation of the noise is set as the threshold current amplitude for that participant. Increases in the current amplitude that did not produce a significant increase in the torque were considered to be above the saturation limit. Therefore, the current amplitude that produced the last significant change in joint torque was considered to be the saturation current amplitude (I_s) of that individual.

19
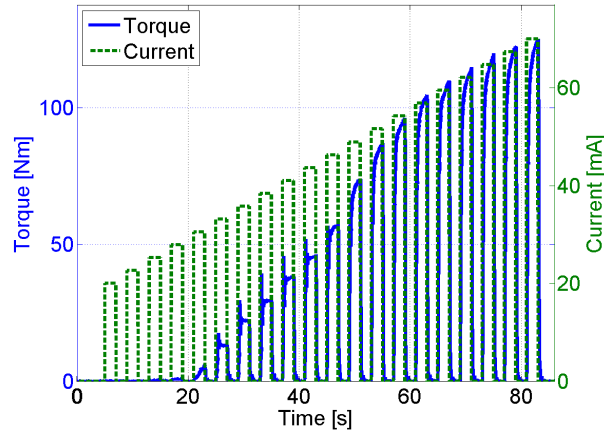
Figure 2.3: Stimulation current amplitude ramp to determine the saturation and threshold of the participant. The threshold is the current amplitude that causes the first significant torque measurement, and the saturation is the current amplitude that produced the last significant change in the torque measurement.

A significant increase in joint torque was defined as a muscle contraction that produced at least 1% more torque than the previous muscle contraction. Therefore, the saturation current amplitude was determined by checking each computed joint torque with respect to the previous one to see if the increase exceeded 1%.

The torque measurements are plotted with the current amplitudes against time in Fig. 2.3 for the demonstrative participant (Participant 1). From this data the threshold was determined to be 23.2 mA (the second current pulse), and the saturation was determined to be 76.8 mA (the second to last current pulse).

2.2.3 Test 2

The passive stiffness parameters (d_i for $i = [1, 3, 4, 5, 6]$ and θ_{eq} in (2.2)) and the mass parameters (m and l_c in (2.1)) were determined by holding the participant's leg at different joint positions. At each of the different joint angles the load cell in the leg extension machine was used to measure the joint torque due to passive elements at the knee (stiffness of the

20
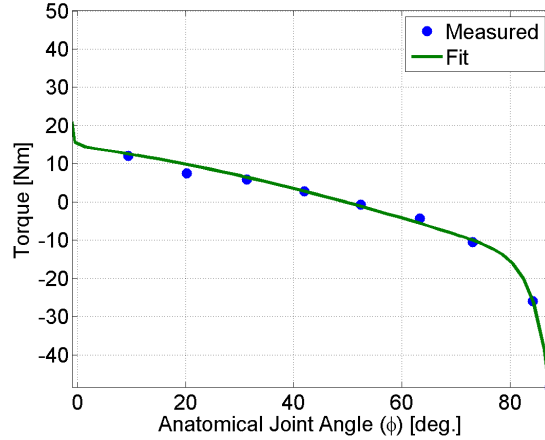
Figure 2.4: Push/pull tests to determine the mass and stiffness parameters of the musculoskeletal system. The exponential terms that model hyperextension and hyperflexion of the anatomical joint angles (ϕ) can be observed around 0° and 80°, respectively.

muscles, ligaments, etc.) and the weight of the lower leg. A nonlinear, least-squares curve fitting algorithm was then used to estimate the parameters that resulted in a best fit between the measured data and the function of the passive knee torque (see (2.2)).

The measured data and the resulting best fit determined by the nonlinear, least-squares curve fitting algorithm for the demonstrative participant are shown in Fig. 2.4. The root-mean square (RMS) of the fit for this participant was $0.264\,\mathrm{N\,m}$. From these results the passive joint torque appears to be approximately linear in the range of 0-80°. The exponential terms that model the hyperextension and hyperflexion of the knee joint can be observed to be the dominant terms outside of that range.

2.2.4 Test 3

From (2.5) it can be shown that during an isometric contraction, when $\dot{\phi} = 0$, then $\psi_v = 1$. Also, by stimulating at the saturation current amplitude and by assuming that the muscle activation is sufficiently fast then $a \approx u = 1$. Therefore, it can be concluded that for an isometric contraction test when stimulating at the saturation $\tau_a = \psi_l$. This means that

21
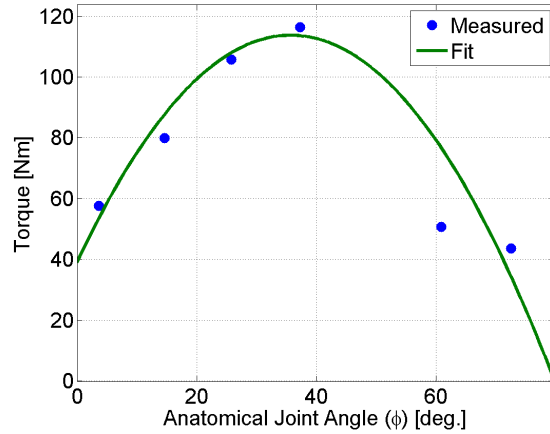
Figure 2.5: Torques produced during isometric contraction tests at different anatomical joint angles (ϕ), and the best fit of the force-length model to the measured data.

when the passive and gravitational torques are subtracted from the load cell measurements during an isometric contraction test, while stimulating at the saturation, the torque-length relationship (ψ_l) can be measured directly.

Given the previous statements, torque-angle relationship parameters (c_i for $i = [0 - 2]$ in (2.3)) were determined from isometric contraction data while stimulating at the saturation level (determined from Test 1) for two seconds at a number of different joint angles. Similar to Test 2, a nonlinear, least squares curve fitting algorithm was used to determine the torque-angle parameters that resulted in a best fit between the measured torque and joint angle at the different positions. The isometric contraction torques were measured at seven different joint angles and the best fit to the measured data are shown for the demonstrative participant in Fig. 2.5. The fit shown in Fig. 2.5 fits the data with an RMS of $7.97\,\mathrm{N\,m}$.

By normalizing the joint torque data from the isometric contraction tests by the previously determined torque-length relationship the muscle activation can be measured. In other words since $\tau_a = \psi_l a$, where psi_l is now known, the muscle activation, a, can be determined as $a = \tau_a/\psi_l$. Using this relationship, because the input (normalized stimulation, u) is known, and using the first order response that models muscle activation (see (2.6)) the

22

muscle activation time constant, T_a, can be determined from one of the isometric contraction tests. Since the input used in the isometric contraction tests was a step input the muscle activation unit step response can be solved to be $a(t) = 1 - \exp(t/T_a)$.

The muscle activation time constant was solved by using a nonlinear, least squares curve fitting algorithm to determine the time constant that gives the activation time response that best fits the normalized torque data from an isometric contraction test. The normalized load cell data from an isometric contraction for the demonstrative participant is shown in Fig. 2.6, where the stimulation begins at one second. The muscle activation time constant of the first order response in (2.6) that best fits the measured data was determined to be 0.18 seconds, which resulted in a fit with an RMS error of 0.0373.

2.2.5   Test 4

The damping and inertial parameters of the system (d_2 in (2.2) and J in (2.1)) were determined using a pendulum test. This was done with the subject seated in the leg extension machine by holding the leg at approximately full extension then releasing it and allowing it to fall. The encoder in the leg extension machine was used to measure the decaying, oscillating response of the leg as it fell. Then an optimization was used to determine the damping and inertial parameters that resulted in a response that best fit the measured data, using the initial conditions as a constraint of the optimization. It is important to note that the pendulum response of the leg is also affected by previously determined parameters, specifically the mass and stiffness parameters determined in Test 2. Although these parameters affect the pendulum response, since the previously determined parameters resulted in an accurate fit they will be considered known and constant during this parameter estimation procedure.

The measured encoder data from the pendulum test for the demonstrative participant and the response from the best fit model are shown together in Fig. 2.7. Some discrepancy between the measured data and fit occur due to keeping the previously determined parameters constant during the estimation. The fit that was determined using an optimization resulted in a fit with an RMS error of 7.78°.
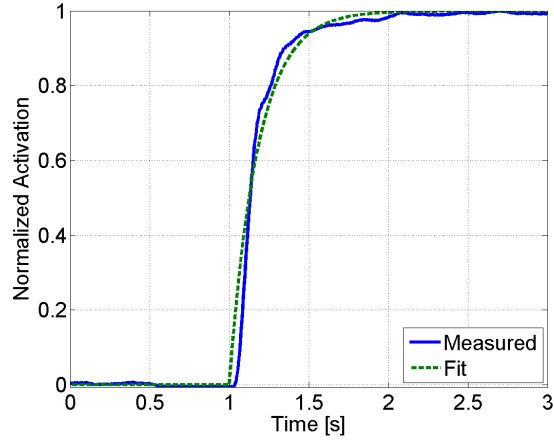
Figure 2.6: For an isometric contraction produced by a stimulation at the saturation current amplitude the normalized joint torque is approximately equal to muscle activation. Therefore, the load cell data can be used to determine the muscle activation time constant by determining the first order system time constant that results in a response that best fits the normalized load cell data.
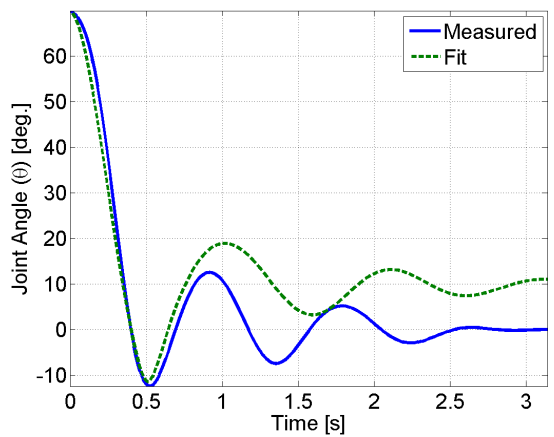
Figure 2.7: Plot of the results of the pendulum test with the response of the model that best fits the measured response.
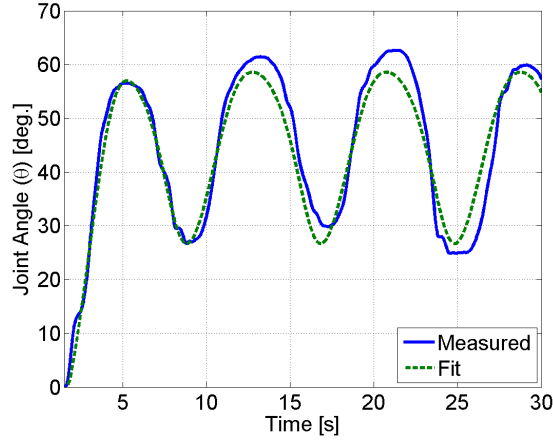
Figure 2.8: A known, sinusoidal stimulation was applied to the quadriceps and the resulting joint angle was measured. This plot shows the measured joint angle and the joint angle predicted by the model with the estimated parameters.

2.2.6 Test 5

A sinusoidal stimulation, with a period of 8 seconds, was applied to the quadriceps muscles of the participant to elicit a movement while the knee joint angle was measured using the encoder on the leg extension machine. The amplitude of the stimulation was selected such that for each participant the joint angle range of motion was within 10-70°. this ensured that the muscles were always in tension and sufficiently far from hyperextension/hyperflexion. The parameters estimated in Tests 1-4 were used to populate a model of knee extension, and then an optimization was performed to identify the force-velocity parameter (c_3 in (2.5)) that makes the model best fit the measured data.

Fig. 2.8 compares the measured knee joint angle to the knee joint angle of the model when given the same input for the demonstrative participant. The output of the model matches the measured joint angle with an RMS error of 3.15°, which illustrates that the model and the estimated parameters are a close match to the actual system.

2.3   RESULTS OF PARAMETER ESTIMATION

As previously mentioned, the parameter estimation procedure was conducted on three able-bodied participants. The resulting estimated parameters for all three participants are shown in Table 2.1. The RMS errors of the fits resulting from the push/pull, isometric contraction, muscle activation, pendulum, and sinusoidal input tests are also given in Table 2.1.

2.4   CONCLUSION

The model of the response of the muscles to FES and the parameters estimated in this chapter are used in model-based FES controllers that are developed and discussed in later chapters. It is important to remember that the the results of the parameter estimation can vary from person-to-person, thus the significant differences in some of the estimated parameters of the three subjects, and can depend on the stimulation parameters used. Therefore, each controller will need to use the subject specific estimated parameters and the same stimulation parameters that were used in the estimation procedure. Although this procedure was only demonstrated for a single muscle group (quadriceps) it can be similarly conducted on other muscle groups to estimate the musculoskeletal parameters.

Errors in the parameter estimation process could have resulted from unmodeled musculoskeletal dynamics, such as electromechanical delay [151] or muscle fatigue dynamics [117]. Although the electromechanical delay in FES systems is somewhat captured in the first order system that models muscle activation (delayed response causes response to occur later and appear slower), it will not be considered here and its affects will be assumed to be negligible. In a later chapter a muscle fatigue model and methods for estimating parameters of the model are presented. The estimated muscle fatigue model is used to estimate the muscle fatigue state, which can then be used to compensate for the effects of muscle fatigue.

Table 2.1: Estimated parameters of each able-bodied participant. These parameters are subject specific, and can change with the stimulation pulse train used. For the parameter estimation 400 μs bi-phasic rectangular pulse trains at 35 Hz were used.

Parameter	Participant 1	Participant 2	Participant 3
α [1/kgm^2]	1.29	1.17	1.31
β [N/kgm^2]	40.3	42.4	40.9
ϕ_0 [rad]	2.81×10^{-14}	9.10×10^{-4}	3.78×10^{-6}
d_1 [N m]	0.863	9.03	6.99
d_2 [N m s]	2.56	5.52	3.52
d_3 [N m]	1×10^{-10}	1×10^{-12}	1.19×10^{-11}
d_4	15.9	16.0	15.9
d_5 [N m]	0.405	3.68	0.0302
d_6	-94.2	-1.72	-45.1
c_0 [N m]	50.9	58.1	41.9
c_1 [N m]	163	68.3	21.1
c_2 [N m]	-125	-47.9	-23.0
c_3	1.28	0.990	0.0400
θ_{eq} [rad]	0.416	0.309	0.264
T_a [s]	0.18	0.24	0.2
I_t [mA]	23.2	26.0	39.0
I_s [mA]	76.8	79.0	80
Test 2 Fit RMS [N m]	0.264	0.928	0.352
Test 3 Isometric Fit RMS [N m]	7.97	2.352	8.53
Test 3 Activation Fit RMS	0.0373	0.0397	0.0431
Test 4 RMS Fit [deg.]	7.78	8.68	7.72
Test 5 RMS Fit [deg.]	3.15	7.94	7.47

3.0 A NONLINEAR CONTROL METHOD TO COMPENSATE FOR MUSCLE FATIGUE DURING NEUROMUSCULAR ELECTRICAL STIMULATION

Effective application of neuromuscular electrical stimulation (NMES) to produce a desired muscle contraction is inhibited by numerous technical challenges, such as nonlinearity associated with muscle force generation, uncertainties in muscle physiology (e.g., calcium dynamics, pH, and muscle architecture), muscle fatigue, time delays etc. To overcome these challenges researchers have explored several control strategies such as linear PID-based pure feedback methods (cf. [1,75,83,84,94] and the references therein), neural network (NN) based controllers (cf. [46,79,124,142,150] and the references therein), and combined feedback and feedforward methods [2,19,21,38,41,42].

Recently, Lyapunov-based techniques were used in [31,33,121,127,129,130] to design NMES controllers that are proven to be asymptotically stable for an uncertain nonlinear muscle model. However, these recently developed nonlinear NMES controllers do not account for the effects of muscle fatigue. Since muscle fatigue is the primary limiting factor in the duration that NMES-based therapy sessions and functional devices may be used, its effects should be considered in the control development.

As briefly discussed in the introduction (see Chapter 1), muscle fatigue is heuristically a decrease in the muscle force output for a given input. Muscle fatigue has been observed to be a complex and multifactorial phenomenon [88,119]. Some of the factors associated with the onset of fatigue are failure of excitation of motor neurons, impairment of action propagation in the muscle membrane, conductivity of the sarcoplasmic reticulum due to Ca^{2+} ion concentration, and the change in concentration of catabolites and metabolites [7]. Other factors such as the stimulation method, muscle fiber composition, state of training of

the muscle, and the duration and task being performed have also been observed to affect fatigue during NMES. Different stimulation strategies have been proposed to delay the onset of fatigue such as choosing different stimulation patterns/parameters, improving fatigue resistance through retraining, and sequential stimulation [13, 31–33, 96].

It is possible to develop controllers with some feedforward knowledge to approximate the fatigue onset, or employ some assumed mathematical model of the fatigue in the control design. However, to use such a control technique a method for estimating fatigue or a model of fatigue is required. In [24, 25, 45, 116, 117], researchers developed various mathematical models for muscle fatigue. A musculotendon model of a quadriceps muscle undergoing isometric contractions during NMES that incorporated a model of fatigue was given in [45]. The muscle fatigue was modeled based on the intracellular pH level, where fatigue parameters for a typical subject were found through metabolic information, experimentation, and curve fitting. A more general mathematical dynamic model for muscle fatigue, defined as a function of the Ca^{2+} dynamics, was proposed in [117] and [116]. Fatigue was introduced in the musculoskeletal dynamics as a fitness variable that varies as electrically stimulated muscles fatigue or recover. The parameters of this fatigue model were estimated from stimulation experiments. The models in [25] and [24] predict force due to the effect of stimulation patterns and resting times with changing physiological conditions, where model parametrization required investigating experimental forces generated from a standardized stimulation protocol.

Although many mathematical models for muscle fatigue are available, few researchers have used such models for closed-loop NMES control. Results in [116] and [63] use the fatigue model proposed in [117] and [116] for NMES controllers, where patient specific parameters (e.g., fatigue time constants) are assumed to be known. The challenge in using the calcium dynamics, or pH level, in the control design is that these states cannot be measured for real-time control. One ad-hoc method to obtain states, such as the calcium dynamics of pH level, for real-time would be to estimate the states from a differential equation that acts as a phenomenological model of muscle fatigue (cf., [45, 63, 116]), where the parameters of the model are estimated from experimentation or are based on data from previous studies.

In this chapter a nonlinear NMES controller is developed that incorporates a model-based estimate of the muscle fatigue state from the model developed in [117]. This work extends upon the preliminary results presented in [128] by addition of muscle fatigue and activation model estimation, and experimental validation of the new controller. The developed controller uses constant estimates of fatigue time constants and natural frequency of the calcium dynamics, which were identified through experimentation. The identified model parameters are then used in a model-based state estimation control scheme so that the muscle activation and fatigue states may be used in the developed NMES controller. The mismatch between the estimated parameters and actual parameters is included in the stability analysis. The fatigue model that is used is defined as a function of the normalized muscle activation state, which denotes the calcium dynamics that are an intermediate variable between the contractile machinery and external stimulus. The calcium dynamics are modeled as a first order differential equation based on [121] and [63].

An open-loop error system for an uncertain nonlinear muscle model is developed that includes the state estimates of fatigue and calcium dynamics. A virtual control input is designed using a nonlinear backstepping technique [29,40] that is composed of a neural network (NN)-based feedforward signal and an error-based feedback signal. The NN-based control structure is used to provide a feedforward estimate of the unknown/uncertain muscle dynamics, and also to approximate the error generated due to parametric uncertainties in the approximated fatigue and activation models. The control-input (current amplitude modulated stimulation pulse trains) is designed based on the backstepping error. Through this error system development, the continuous NN-based controller is proven through a Lyapunov-based stability analysis to yield a globally uniformly ultimately bounded stability result despite the uncertain nonlinear muscle model and the presence of bounded disturbances (e.g., muscle spasticity, changing loads in functional tasks, and delays). The developed controller was evaluated on the right and left leg of three able-bodied subjects, and its performance was shown to be a statistically significant improvement compared to a proportional-derivative controller. Partial knowledge of the muscle dynamics were required to implement this controller, specifically the parameters of the muscle activation and muscle fatigue dynamics needed to be estimated. The muscle activation time constant was estimated using the method that was

presented in Chapter 2. A model of muscle fatigue that was used to estimate the fatigue state, and the procedure to identify the parameters of the model, are presented in this chapter. The results of the estimation procedures and controller validation experiments on both legs of the participants are presented and discussed.

3.1   MUSCLE ACTIVATION AND LIMB MODEL

The following will re-present the musculoskeletal model of the knee extension neuroprosthesis that was presented in Chapter 2, such that it can be used in a Lyapunov-based stability analysis of the proposed controller. Some changes and additions are made to the model that further elaborate the previously presented model, such as pennation angle of muscle fibers, to validate the use of assumptions that are necessary in the stability analysis. The total model can be categorized into body segmental dynamics and muscle activation/contraction dynamics. The body segmental dynamics considers the active and passive joint moments acting at the knee joint, and the muscle activation/contraction dynamics model the force generation in the muscle.

3.1.1   Contraction and Activation Dynamics

The forces, due to the application of NMES, acting on the upper and lower leg that result in a torque at the knee joint are a result of the tendon force $F_T \in \mathbb{R}$, defined as [149]

$$F_T \triangleq F \cos a, \tag{3.1}$$

where $a \in \mathbb{R}$ is defined as the pennation angle between the tendon and the direction of the muscle fibers. The pennation angle of the human quadriceps muscle changes monotonically during a contraction of the quadriceps, is continuously differentiable, positive, and a bounded function of muscle length with a bounded first time derivative [120]. The muscle force $F \in \mathbb{R}$ in (3.1) is derived as [116]

$$F \triangleq \mu F_m \eta_l \eta_v x, \tag{3.2}$$

31

where $F_m \in \mathbb{R}$ is the constant maximum isometric force generated by the muscle and μ is the muscle fatigue state. The uncertain and nonlinear functions $\eta_l : \mathbb{R} \to \mathbb{R}$ and $\eta_v : \mathbb{R} \to \mathbb{R}$ in (3.2) are force-length and force-velocity relationships, respectively. These functions are similar to the torque-length and torque-velocity relationships presented in Chapter 2; however, they assume that the joint angle dependent moment arm of the quadriceps muscle may be lumped into the force-length relationship. The force-length and force-velocity relationships presented here are defined as [57, 59, 116]

$$\eta_l \triangleq \exp\left(-\left(\frac{\bar{l}-1}{b}\right)^2\right), \tag{3.3}$$

$$\eta_v \triangleq c_1 \arctan(c_2\bar{v} + c_3) + c_4,$$

where $b \in \mathbb{R}$ is a constant that denotes the unknown shape factor, $\bar{l} \in \mathbb{R}$ denotes the unknown normalized muscle length with respect to the optimal muscle length, $\bar{v} \in \mathbb{R}$ is an unknown non-negative normalized velocity with respect to the maximal contraction velocity of the muscle, and $c_1, c_2, c_3, c_4 \in \mathbb{R}^+$ are unknown constants.

It was assumed that the muscle tension is considerably reduced when fully shortened or lengthened, but does not drop to zero [146]. Therefore, the force-length relationship can be lower bounded as $\varepsilon_l \leq \eta_l$ where $\varepsilon_l \in \mathbb{R}^+$ is a known constant. Similarly, the force-velocity function is lower bounded $\varepsilon_v \leq \eta_v$, where $\varepsilon_v \in \mathbb{R}^+$ is a known constant. This bound is reasonable because $\eta_v \to 0$ only occurs during a concentric muscle contraction when the muscle shortening velocity approaches infinity.

The definitions of the force-length and force-velocity functions in (3.3) are not directly used in the control development. However, the structure of the relationships and the previously discussed bounds are used to conclude that η_l and η_v are continuously differentiable, non-zero, positive, and bounded functions. These properties of these relationships will be used in the stability analysis of the developed controller.

The muscle force in (3.2) is coupled to the stimulation control input, $v \in \mathbb{R}$, through an intermediate normalized muscle activation variable $x \in \mathbb{R}$. The muscle activation is governed by the following differential equation [45, 149]

$$2\dot{x} = -wx + wsat[v], \tag{3.4}$$

where $w \in \mathbb{R}$ is the natural frequency of the calcium dynamics, which is constant and unknown. The function $sat[v] \in \mathbb{R}$ models the motor unit recruitment curve and is modeled by a piecewise linear function as

$$sat[v] \triangleq \begin{cases} 0 & v < v_{\min} \\ \frac{v - v_{\min}}{v_{\max} - v_{\min}} & v_{\min} \leq v \leq v_{\max} \\ 1 & v > v_{\max}, \end{cases} \tag{3.5}$$

where $v_{\min} \in \mathbb{R}$ is the minimum stimulation required to produce a noticeable movement or force in a muscle, and $v_{\max} \in \mathbb{R}$ is the stimulation input to the muscle where no considerable increase in force or movement is observed (refer to threshold and saturation in Chapter 2). From (3.4) and (3.5), a linear differential inequality can be developed to show that $x \in [0, 1]$.

Muscle fatigue, μ in (3.2), can be modeled as a first order differential equation that is a function of the muscle activation as [116, 117]

$$\dot{\mu} = \frac{1}{T_f}(\mu_{\min} - \mu)x + \frac{1}{T_r}(1 - \mu)(1 - x), \tag{3.6}$$

where $\mu_{\min} \in (0, 1]$ is the unknown fatigue constant, and T_f, $T_r \in \mathbb{R}^+$ are unknown time constants for fatigue and recovery of the muscle, respectively. Because $x \in [0, 1]$, it can be shown that $\mu \in [\mu_{\min}, 1]$, where $\mu = 1$ when the muscle is fully rested, and $\mu = \mu_{\min}$ when the muscle is fully fatigued.

3.1.2 Body Segmental Dynamics (Knee Dynamics)

The rigid body dynamics of the lower leg can be modeled as

$$M_I + M_e + M_g + M_v + \tau_d = \tau, \tag{3.7}$$

where $M_I \in \mathbb{R}$ is the inertial effects of the lower leg, $M_e \in \mathbb{R}$ is the elastic effects due to joint stiffness, $M_g \in \mathbb{R}$ is the moment due to gravity, $M_v \in \mathbb{R}$ is the viscous moment due to musculotendon damping [39], $\tau_d \in \mathbb{R}$ is an unknown and bounded exogenous disturbance that represents an unmodeled reflex activation of the muscle (e.g., muscle spasticity) and other unknown unmodeled phenomena (e.g., changing loads), and $\tau \in \mathbb{R}$ denotes the torque produced at the knee joint due to NMES.
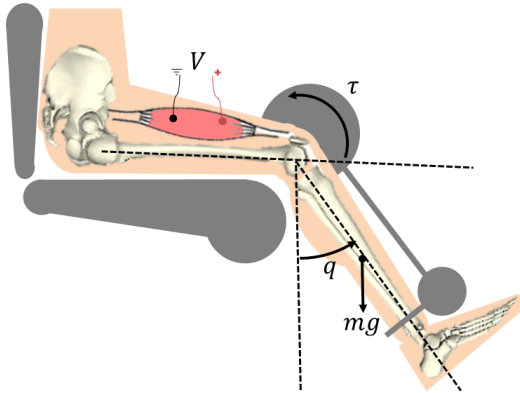
Figure 3.1: Electrical stimulation of the quadriceps causes the muscle to contract and shorten. This creates a torque at the knee joint, causing a knee extension motion.

The inertial and gravitational effects in (3.7) can be modeled as

$$M_I \triangleq J\ddot{q}, \qquad M_g \triangleq mgl\sin(q), \tag{3.8}$$

where $\ddot{q}, \dot{q}, q \in \mathbb{R}$ denote the angular acceleration, angular velocity, and angle of the shank relative to vertical (illustrated in Fig. 3.1), respectively. Although the inertial and gravitational parameters, $J, m, l, g \in \mathbb{R}^+$, were estimated in Chapter 2, for the controller developed in this chapter the will assume to be unknown constants. These parameters, as they will be referred to in this chapter, are defined as follows: J is the inertia of the lower leg, m is the mass of the lower leg, l is the distance from the knee joint to the center of mass of the lower leg, and g is the gravitational acceleration.

The musculotendon elastic moment in (3.7) is model, based on empirical findings by Ferrarin and Pedotti in [39], as

$$M_e \triangleq k_1(q - k_3)\exp(-k_2 q), \tag{3.9}$$

where k_1, k_2, $k_3 \in \mathbb{R}^+$ are unknown positive coefficients. As shown in [121], the viscous moment in (3.7) can be modeled as

$$M_v \triangleq B_1\dot{q} - B_2\tanh(-B_3\dot{q}), \tag{3.10}$$

where B_1, B_2, $B_3 \in \mathbb{R}$ are unknown positive constants.

The torque produced at the knee joint due to NMES can be modeled as

$$\tau \triangleq \varsigma F_T, \tag{3.11}$$

where $\varsigma \in \mathbb{R}$ denotes the moment arm of the muscle, which is a function of the joint angle. The moment arm function is assumed to be an unknown, strictly positive, continuously differentiable, and bounded function with a bounded first time derivative. These assumptions are shown to be valid in [16, 81, 116].

It should be noted that the parameters discussed in this subsection (rigid body and viscoelastic parameters) are assumed to be unknown in the control development in this chapter. It is important to note this distinction because this chapter uses some estimated parameters in the control development (calcium dynamics time constant and fatigue model parameters), and because future chapters will assume that all the parameters of the model are known.

3.2 CONTROL DEVELOPMENT

The objective of the controller developed in this chapter is to develop an NMES controller to produce a knee trajectory that track's a desired trajectory, denoted by $q_d \in \mathbb{R}$, despite an uncertain musculoskeletal model and an uncertain estimate of muscle fatigue. Without loss of generality, the developed controller is applicable to different stimulation protocols (i.e., voltage, frequency, or pulse width modulation). To quantify the objective, a position tracking error, denoted by $e \in \mathbb{R}$, is defined as

$$e = q_d - q, \tag{3.12}$$

where q_d is designed such that $q_d^i \in \mathcal{L}_\infty$, where $q_d^{(i)}$ denotes the ith derivative for $i = 0, 1, 2, 3, 4$. To facilitate the subsequent analysis, a filtered tracking error, denoted by $r \in \mathbb{R}$, is defined as

$$r = \dot{e}(t) + \alpha e(t), \tag{3.13}$$

where $\alpha \in \mathbb{R}$ denotes a positive constant.

3.2.1 Feedforward Neural Network Estimation

Neural network (NN)-based estimation methods are well suited for control of NMES because the musculoskeletal model contains unstructured (i.e., not linearly parameterizable) nonlinear disturbances, as described in (3.7)-(3.11). Due to the universal approximation property, NN-based estimation methods can be used to represent the unknown nonlinear musculoskeletal model by using a three-layer NN as [91]

$$f = W^T \sigma(U^T y) + \epsilon(y), \tag{3.14}$$

for some input $y \in \mathbb{R}^{N_1+1}$. In (3.14), $U \in \mathbb{R}^{(N_1+1) \times N_2}$, and $W \in \mathbb{R}^{(N_2+1) \times n}$ are bounded constant ideal weight matrices for the first-to-second and second-to-third layers, respectively. N_1 is the number of neurons in the input layer, N_2 is the number of neurons in the hidden layer, and n is the number of neurons in the output layer. The sigmoid activation function is denoted by $\sigma : \mathbb{R}^{N_2} \to \mathbb{R}^{N_2+1}$ in (3.14), and $\epsilon \in \mathbb{R}^n$ is the functional reconstruction error. The

additional term "1" in the dimension of the input vector y and activation term σ enables the activation function thresholds to be included as the first columns of the weight matrices [91]. Thus, any tuning of W and U also includes tuning the thresholds. Based on (3.14), the typical three layer NN approximation for f is given by [91]

$$\hat{f} \triangleq \hat{W}^T \sigma(\hat{U}^T y), \tag{3.15}$$

where $\hat{U} \in \mathbb{R}^{(N_1+1)\times N_2}$ and $\hat{W} \in \mathbb{R}^{(N_2+1)\times n}$ are estimates of the ideal weight matrices. The estimation errors of the NN weight matrices, denoted by $\tilde{U} \in \mathbb{R}^{(N_1+1)\times N_2}$ and $\tilde{W} \in \mathbb{R}^{(N_2+1)\times n}$, are defined as

$$\tilde{U} = U - \hat{U}, \qquad \tilde{W} = W - \hat{W}, \tag{3.16}$$

and the mismatch for the hidden-layer output error, denoted by $\tilde{\sigma} : \mathbb{R}^{N_2} \to \mathbb{R}^{N_2+1}$, for a given y is defined as

$$\tilde{\sigma} = \sigma - \hat{\sigma} = \sigma(U^T y) - \sigma(\hat{U}^T y). \tag{3.17}$$

The NN estimate has several properties that will facilitate the subsequent control development. **Property 1:** (Taylor Series Approximation) The Taylor series expansion for $\sigma(U^T y)$ for a given y is [91]

$$\sigma(U^T y) = \sigma(\hat{U}^T y) + \sigma'(\hat{U}^T y)\tilde{U}^T y + O(\tilde{U}^T y)^2, \tag{3.18}$$

where $\sigma'(\hat{U}^T y) = d\sigma(U^T y)/d(U^T y)\big|_{U^T y = \hat{U}^T y}$, and $O(\tilde{U}^T y)^2$ denotes the higher order terms. After substituting (3.18) into (3.17) the following expression can be obtained:

$$\tilde{\sigma} = \hat{\sigma}'\tilde{U}^T y + O(\tilde{U}^T y)^2, \tag{3.19}$$

where $\hat{\sigma}' = \sigma'(\hat{U}^T y)$.

Property 2: (Boundedness of the Ideal Weights) The ideal weights are assumed to exist and be bounded by known positive values so that

$$\|U\|_F^2 = tr(U^T U) \leq \bar{U}_B, \tag{3.20}$$
$$\|W\|_F^2 = tr(W^T W) \leq \bar{W}_B,$$

where $\|\cdot\|_F$ is the Frobenius norm of a matrix, and $tr(\cdot)$ is the trace of a matrix.

3.2.2 Open-Loop Error System

The open-loop error dynamics can be derived by taking the time derivative of (3.13), multiplying by J, and then using the expressions in (3.1), (3.2), (3.7), (3.11), and (3.12) to get

$$J\dot{r} = J(\alpha\dot{e} + \ddot{q}_d) + M_e + M_g + M_v + \tau_d - \rho\mu x, \tag{3.21}$$

where the auxiliary term $\rho \in \mathbb{R}$ is defined as

$$\rho \triangleq \varsigma \cos(a) F_m \eta_l \eta_v. \tag{3.22}$$

After multiplying (3.21) by ρ^{-1}, the following expression is obtained:

$$J_\rho \dot{r} = J_\rho(\alpha\dot{e} + \ddot{q}_d) + L_\rho + \tau_{d\rho} - \mu x, \tag{3.23}$$

where J_ρ, $\tau_{d\rho}$, $L_\rho \in \mathbb{R}$ are defined as

$$J_\rho \triangleq \frac{J}{\rho}, \qquad \tau_{d\rho} \triangleq \frac{\tau_d}{\rho}, \qquad L_\rho \triangleq \frac{(M_e + M_g + M_v)}{\rho}. \tag{3.24}$$

Property 3: Based on the assumptions and properties in Section 3.1, it can be concluded that the auxiliary function ρ is continuously differentiable, positive, and bounded. Also, the first time derivatives of ρ and $\frac{1}{\rho}$ exist and are bounded. Therefore, the inertia function J_ρ is positive definite and can be upper and lower bounded as

$$a_1 \|\gamma\|^2 \le \gamma^T J_\rho \gamma \le a_2 \|\gamma\|^2 \quad \forall \gamma \in \mathbb{R}^n, \tag{3.25}$$

where $a_1, a_2 \in \mathbb{R}^+$ are some known positive constants.

Based on the boundedness of ρ, $\dot{\rho}$, and $\frac{1}{\rho}$, it can be concluded that

$$\left| \dot{J}_\rho \right| \le \xi_j \quad |\tau_{d\rho}| \le \xi_\tau, \tag{3.26}$$

where $\xi_j, \xi_\tau \in \mathbb{R}^+$ are some known positive constants.

Based on (3.6) an estimate of μ, defined as $\hat{\mu}$, is generated as

$$\dot{\hat{\mu}} = \frac{1}{\hat{T}_f}(\hat{\mu}_{\min} - \hat{\mu})\hat{x} + \frac{1}{\hat{T}_r}(1 - \hat{\mu})(1 - \hat{x}), \tag{3.27}$$
$$1 \geq \hat{\mu}(0) > 0,$$

where $\hat{T}_f$, $\hat{T}_r \in \mathbb{R}^+$ denote constant estimates of the time constants T_f and T_r, respectively. $\hat{\mu}_{\min} \in (0, 1]$ is a non-zero known positive constant that is an estimate of μ_{min}, and $\hat{x} \in [0, 1]$ is the estimated normalized muscle activation variable. The estimate of the normalized muscle activation is generated based on the first order differential equation that models the calcium dynamics (see (3.4)) as

$$2\dot{\hat{x}} = -\hat{w}\hat{x} + \hat{w}sat[v], \tag{3.28}$$

where $\hat{w} \in \mathbb{R}^+$ is the estimate of the natural frequency of the calcium dynamics, w.

The estimate of the fatigue state can be upper bounded by a positive constant as $\bar{\mu} \in \mathbb{R}^+$, where $\bar{\mu}$ can be determined as

$$\bar{\mu} = \hat{\mu}(0) + 1 + \frac{\hat{T}_r}{\hat{T}_f}\hat{\mu}_{\min}.$$

The differential equation in (3.27) ensures that $\hat{\mu}$ remains strictly positive. Also, based on (3.5) and (3.28), a linear differential inequality can be developed to show that $\hat{x} \in [0, 1]$. Defining these bounds will become relevant during the stability analysis of the developed controller.

After some algebraic manipulation, the open loop dynamics in (3.23) can be expressed as

$$J_\rho \dot{r} = S + \tau_{d\rho} - e - \mu\tilde{x} - \mu_e\hat{x} - \hat{\mu}\hat{x} - \frac{1}{2}\xi_j r, \tag{3.29}$$

where the auxiliary function $S \in \mathbb{R}$ is defined as

$$S = J_\rho(\ddot{q}_d + \alpha\dot{e}) + L_\rho + e - \tilde{\mu}\hat{x} + \frac{1}{2}\xi_j r, \tag{3.30}$$

and the error functions $\mu_e, \tilde{\mu}, \tilde{x} \in \mathbb{R}$ are defined as

$$\tilde{\mu}(\hat{x}) \triangleq \mu(\hat{x}) - \hat{\mu}(\hat{x}), \quad \mu_e(x, \hat{x}) \triangleq \mu(x) - \mu(\hat{x}), \tag{3.31}$$
$$\tilde{x} \triangleq x - \hat{x}.$$

Since μ and $\hat{\mu}$ have been shown to be bounded functions, the error function μ_e can be upper bounded as

$$|\mu_e| \le \xi_\mu, \tag{3.32}$$

where $\xi_\mu \in \mathbb{R}^+$ is some known positive constant.

As previously discussed, the unknown/uncertain dynamics in the auxiliary function S can be represented by a three-layer NN as

$$S = W^T \sigma(U^T y) + \epsilon(y),$$

where the input to the NN, $y \in \mathbb{R}^7$, is defined as

$$y = \begin{bmatrix} 1 & q & \dot{q} & \ddot{q}_d & \hat{x} & e & r \end{bmatrix}. \tag{3.33}$$

From the aforementioned properties of the NN, the functional reconstruction error ϵ can be upper bounded as

$$|\epsilon(y)| \le \varepsilon, \tag{3.34}$$

where $\varepsilon \in \mathbb{R}^+$ is some known positive constant.

3.2.3 Closed-Loop Error System

Since the open-loop system in (3.29) is not explicitly a function of the control input (normalized stimulation amplitude v), a backstepping-based approach is used to inject a virtual control input $x_d \in \mathbb{R}$ (i.e., desired muscle activation) as

$$J_\rho \dot{r} = S + \tau_{d\rho} - \frac{1}{2} \xi_j r - e - \mu \tilde{x} - \mu_e \hat{x} - \hat{\mu}\hat{x} + \hat{\mu}x_d - \hat{\mu}x_d. \tag{3.35}$$

Based on (3.35), the virtual control input is designed as a three-layer NN feedforward term plus a feedback term as

$$x_d = \hat{\mu}^{-1}(\hat{S} + k_s r), \tag{3.36}$$

where $k_s = k_{s_1} + k_{s_2}$ and $k_{s_1}, k_{s_2} \in \mathbb{R}^+$ are positive constant gains. The feedforward NN component in (3.36), denoted by $\hat{S}(t) \in \mathbb{R}$ is generated as

$$\hat{S} = \hat{W}^T \sigma(\hat{U}^T y), \tag{3.37}$$

where estimates for the NN weights in (3.37) are generated on-line using a projection algorithm [82] as

$$\dot{\hat{W}} = proj(\Gamma_1 \hat{\sigma} r), \qquad \dot{\hat{U}} = proj(\Gamma_2 y (\hat{\sigma}'^T \hat{W} r)^T), \tag{3.38}$$

where $\Gamma_1 \in \mathbb{R}^{(N_2+1)\times(N_2+1)}$ and $\Gamma_2 \in \mathbb{R}^{(N_1+1)\times(N_1+1)}$ are constant, positive definite, symmetric gain matrices. The closed-loop tracking error system can be developed by substituting (3.36) into (3.35) as

$$J_\rho \dot{r} = -\frac{1}{2}\xi_j r - e + \tilde{S} + \tau_{d\rho} - \mu \tilde{x} - \mu_e \hat{x} - k_s r - \hat{\mu} e_x,$$

where $\tilde{S} \in \mathbb{R}$ is defined as

$$\tilde{S} = S - \hat{S}, \tag{3.39}$$

and $e_x \in \mathbb{R}$ is the backstepping error defined as

$$e_x = \hat{x} - x_d. \tag{3.40}$$

The closed-loop system can be expressed as

$$J_\rho \dot{r} = -\frac{1}{2}\xi_j r - e + \tilde{W}^T \hat{\sigma} + \hat{W}^T \tilde{\sigma} + \tilde{W}^T \tilde{\sigma} + \epsilon(y)e_x, \tag{3.41}$$
$$+ \tau_{d\rho} - \mu \tilde{x} - \mu_e \hat{x} - k_s r - \hat{\mu}$$

where $\hat{\sigma}$ and $\tilde{\sigma}$ are introduced in (3.17). The Taylor series approximation described in (3.18) and (3.19) can now be used to rewrite (3.41) as

$$J_\rho \dot{r} = -\frac{1}{2}\xi_j r - e + N + \tilde{W}^T \hat{\sigma} \tag{3.42}$$
$$+ \hat{W}^T \hat{\sigma}' \tilde{U}^T y - k_s r - \hat{\mu} e_x.$$

The unmeasurable auxiliary term $N \in \mathbb{R}$ is defined as

$$N = \tilde{W}^T \hat{\sigma}' \tilde{U}^T y + W^T O(\tilde{U}^T y)^2 + \epsilon + \tau_{d\rho} - \mu \tilde{x} - \mu_e \hat{x}.$$

Based on (3.26), (3.32), (3.34), (3.38), the fact that $x, \hat{x} \in [0, 1]$, and the assumption that desired trajectories are bounded, the following inequality can be developed [90]:

$$|N| \leq \zeta_1 + \zeta_2 \|z\|, \tag{3.43}$$

where $\zeta_i \in \mathbb{R}^+$ for $(i = 1, 2)$ are known positive constants, and $z \in \mathbb{R}^2$ is defined as

$$z \triangleq \begin{bmatrix} e^T & r^T \end{bmatrix}^T.$$

3.2.4 Backstepping Error System

To facilitate the subsequent stability analysis, the time derivative of the backstepping error (3.40) can be determined by using (3.28) as

$$\dot{e}_x = -\frac{\hat{w}}{2}\hat{x} + \frac{\hat{w}}{2}sat[v(t)] - \dot{x}_d. \tag{3.44}$$

Based on (3.5) and (3.44) the stimulation control input $v \in \mathbb{R}$ is designed as

$$v(t) = (v_{\max} - v_{\min}) \left[\left(\frac{\hat{w}}{2} \right)^{-1} \left(\dot{x}_d + \frac{\hat{w}}{2}\hat{x} + \hat{\mu}r - ke_x \right) \right] + v_{\min} \tag{3.45}$$

where $k \in \mathbb{R}^+$ denotes a positive, constant adjustable control gain. Substituting (3.45) into (3.44), yields

$$\dot{e}_x = \hat{\mu}r - ke_x, \tag{3.46}$$

which is the time derivative of the backstepping error that is defined in (3.40).

3.3   STABILITY ANALYSIS

Theorem 1. *The controller defined by (3.36) and (3.45) ensures that all signals are bounded under closed-loop operation, and that the position tracking error is uniformly ultimately bounded in the sense that*

$$|e| \leq \epsilon_0 \exp(-\epsilon_1 t) + \epsilon_2,$$

provided the control gain α, introduced in (3.13), and the subsequently introduced control gain, k_{s_1}, are selected according to the following sufficient condition:

$$\min(\alpha_1, k_{s_1}) > \zeta_2, \tag{3.47}$$

where $\epsilon_0, \epsilon_1, \epsilon_2 \in \mathbb{R}^+$ denote positive constants, and ζ_2 is a known positive constant introduced in (3.43).

Proof. Let $V \in \mathbb{R}$ denote a continuously differentiable, non-negative, radially unbounded function defined as

$$V(t) \triangleq \frac{1}{2}e^2 + \frac{1}{2}J_\rho r^2 + \frac{1}{2}e_x^2 + \frac{1}{2}tr(\tilde{W}^T\Gamma_1^{-1}\tilde{W}) + \frac{1}{2}tr(\tilde{U}^T\Gamma_2^{-1}\tilde{U}). \tag{3.48}$$

Using (3.25) and the aforementioned NN properties [91], V can be upper and lower bounded as

$$\lambda_1 \|X\|^2 \le V(t) \le \lambda_2 \|X\|^2 + \theta, \tag{3.49}$$

where $\lambda_1, \lambda_2, \theta \in \mathbb{R}^+$ are known positive constants, and $X \in \mathbb{R}^3$ is defined as

$$X \triangleq \begin{bmatrix} z^T & e_x \end{bmatrix}^T. \tag{3.50}$$

Taking the time derivative of (3.48), then using (3.13), (3.42), (3.46), the definition of k_s, and canceling similar terms yields

$$\begin{aligned}
\dot{V} = &-\alpha e^2 + rN - (k_{s_1} + k_{s_2})r^2 + \\
&r\tilde{W}^T\hat{\sigma} + r\hat{W}^T\hat{\sigma}'\tilde{U}^Ty - ke_x^2 - tr(\tilde{W}^T\Gamma_1^{-1}\dot{\hat{W}}) \\
&- tr(\tilde{U}^T\Gamma_2^{-1}\dot{\hat{U}}) + \frac{1}{2}\dot{J_\rho}r^2 - \frac{1}{2}\xi_j r^2.
\end{aligned} \tag{3.51}$$

Using (3.26), (3.38) and (3.43), the expression in (3.51) can be upper bounded as

$$\dot{V} \le -\alpha e^2 - k_{s_1}r^2 + \zeta_2 \|z\| |r| + \left[(|r|\zeta_1 - k_{s_2}r^2) \right] - ke_x^2. \tag{3.52}$$

Completing the squares for the bracketed term in (3.52) and further bounding the expression yields

$$\dot{V} \le -[\min(\alpha, k_{s_1}) - \zeta_2] \|z\|^2 - ke_x^2 + \frac{\zeta_1^2}{4k_{s_2}}. \tag{3.53}$$

The inequality in (3.49) can be used to rewrite (3.53) as

$$\dot{V} \le -\frac{\beta}{\lambda_2}V + \delta, \tag{3.54}$$

where $\delta \in \mathbb{R}^+$ is a positive constant defined as

$$\delta = \frac{\zeta_1^2}{4k_{s_2}} + \frac{\beta}{\lambda_2}\theta,$$

43

and $\beta \in \mathbb{R}$ is defined as

$$\beta = \min[(\min(\alpha_1, k_{s_1}) - \zeta_2), k].$$

The linear differential inequality in (3.54) can be solved as

$$V \le V(0)e^{-\frac{\beta}{\lambda_2}t} + \delta\frac{\lambda_2}{\beta}\left[1 - e^{-\frac{\beta}{\lambda_2}t}\right]. \tag{3.55}$$

Provided the sufficient condition in (3.47) is satisfied, the expressions in (3.48) and (3.55) indicate that e, r, e_x, $\tilde{W}$, $\tilde{U} \in \mathcal{L}_\infty$. Given that e, r, q_d, $\dot{q}_d \in \mathcal{L}_\infty$, (3.12) and (3.13) indicate that q, $\dot{q} \in \mathcal{L}_\infty$. Since $\tilde{W}$, $\tilde{U} \in \mathcal{L}_\infty$, (3.16) and Property 2 can be used to conclude that $\hat{W}$, $\hat{U} \in \mathcal{L}_\infty$. Based on (3.4), it can be shown that $\hat{x} \in [0,1]$. Given that $\ddot{q}_d$, e, r, q, $\dot{q}$, $\hat{x} \in \mathcal{L}_\infty$, the NN input vector $y \in \mathcal{L}_\infty$ from (3.33). Since e_x, $\hat{x} \in \mathcal{L}_\infty$, (3.40) can be used to show that $x_d \in \mathcal{L}_\infty$. Given that r, $\hat{W}$, $\hat{U}$, $x_d \in \mathcal{L}_\infty$, (3.36) and (3.37) indicate that $\hat{S}$, $\hat{\mu}^{-1} \in \mathcal{L}_\infty$. Since e, r, $\hat{W}$, $\tilde{W}$, $\tilde{U}$, e_x $\hat{\mu} \in \mathcal{L}_\infty$, (3.42) and (3.43) indicate that $\dot{r} \in \mathcal{L}_\infty$. As r, y, $\hat{W} \in \mathcal{L}_\infty$, the update laws $\dot{\hat{W}}$, $\dot{\hat{U}} \in \mathcal{L}_\infty$. Since $\hat{\mu}$, $\hat{x} \in \mathcal{L}_\infty$, it can be shown that $\dot{\hat{\mu}} \in \mathcal{L}_\infty$. Given that the $\hat{\mu}$, $\hat{\mu}^{-1}$, $\dot{r}$, r, $\hat{W}$, $\hat{U}$, $\dot{\hat{W}}$, $\dot{\hat{U}} \in \mathcal{L}_\infty$, it can be shown that $\dot{x}_d \in \mathcal{L}_\infty$. Because $\hat{\mu}$, $\dot{x}_d$, r, $\hat{x}$, $e_x \in \mathcal{L}_\infty$, it can be concluded that the stimulation control input v is bounded. $\qquad\square$

3.4 PARAMETER ESTIMATION

To implement the controller given in (3.45) estimates of the threshold $(v_{\min})$, saturation $(v_{\max})$, natural frequency of the calcium dynamics (w), muscle fatigue state (μ), and the muscle activation (x) are required. Because the fatigue and activation states cannot be measured they were estimated using model of their dynamics, which means that estimates of the parameters of their dynamics are necessary. Methods for determining estimates of the natural frequency of the calcium dynamics, the threshold, and the saturation were presented in Chapter 2 (see Tests 1 and 3 in Chapter 2). Therefore, only the resulting estimated parameters for each participant will be presented here. However, this section will present a procedure for estimating the parameters of the muscle fatigue model (see (3.27)).

The parameter estimation was performed on the right and left legs of three able-bodied subjects [1]. During the parameter estimation procedures the participants were asked to relax and avoid any voluntary contractions that might influence the results during electrical stimulation. Similar to the parameter estimation procedures in Chapter 2, all of the procedures discussed in this section were performed in a leg extension machine fitted with a load cell, as illustrated in Fig. 3.2. The isometric joint torque was computed from the force measured by the load cell (Omega Engineering Inc., USA) and the moment arm of the leg extension machine. Isometric tests were used because it can be shown that in an isometric contraction the joint torque normalized by the maximum torque that can be produced at that joint angle is equal to the product of the muscle activation and the fatigue state (i.e. for isometric contraction $\eta_v = 1$ and $\frac{F}{F_m \eta_l} = \mu x$ from (3.2)). The quadriceps muscles were stimulated using an FNS-16 Multi-Channel Stimulator (CWE Inc., USA). A current amplitude controlled 35 Hz pulse train with a pulse width of 400 µs was used. Because the estimated parameters are dependent on the stimulation parameters, it should be noted that the stimulation parameters used in this chapter are consistent with the procedures in Chapter 2. The results of the parameter estimation for Subject 1 are presented in this section to demonstrate the procedure and accuracy of the parameter estimation. The parameters estimated for all participants can be found in the following section.

3.4.1   Estimation of Fatigue Model Parameters

To generate an estimate of the fatigue state, an estimated model of the fatigue dynamics, described in (3.27), was used. To implement this model-based estimation the parameters T_f, T_r, and $\mu_{\min}$ of the fatigue dynamics were estimated using a procedure similar to the methods in [117]. This procedure was conducted on a separate day from when the procedures to estimate the other required parameters to ensure that the muscle was fully rested. This validates the assumption that the fatigue state has the initial condition $\mu = 1$, which will be used in the estimation process. The fatigue model estimation procedure consists of three

---

[1]Prior to any experimentation, approval from the Institutional Review Board at the University of Pittsburgh was obtained.
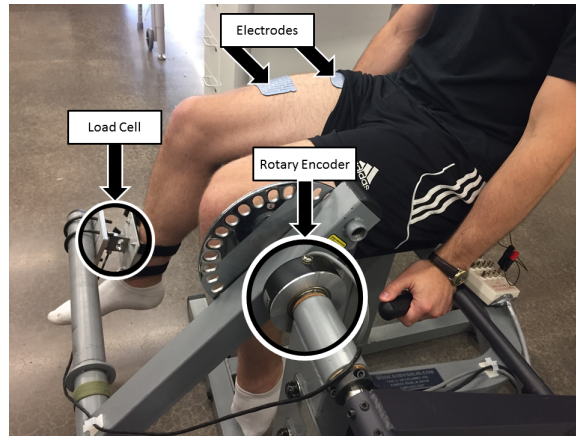
Figure 3.2: Test setup for estimating fatigue and activation dynamics of quadriceps muscle. The isometric joint torque, produced by stimulation of the quadriceps muscles, was measured by keeping the arm of the leg extension machine fixed and holding the subject's leg in place with a load cell. The test setup was also used to validate the developed controller for NMES knee extension tracking experiments. A rotary encoder was used to measure the knee joint angle.

phases: potentiation, fatigue, and recovery. During all three phases the leg of the participant was placed in an isometric contraction configuration, and the saturation for each participant was used as the current amplitude.

First, during the potentiation phase, the muscle was potentiated using 10, 1-second long pulse trains with ten seconds between the trains. This was done to warmup the quadriceps muscles to electrical stimulation, and the duration of the stimulation used during the potentiation was short to prevent the muscles from fatiguing. After the potentiation sequence, a constant stimulation train was used for three minutes. This was done such that the quadriceps muscles would become fatigued, causing an observable decrease in joint torque produced by the quadriceps. The long duration of this phase ensures that the participant's muscles fatigue approximately to their minimum level, $\mu_{\min}$. Immediately after the fatiguing protocol, one-second long pulse trains of stimulation were used every ten seconds. This was done so that the rate of recovery of the joint torque production of the quadriceps can be observed. Because the purpose of this procedure was to observe fatigue and recovery, the participants were not given any breaks in between each phase of the procedure.

The measured load cell data during the potentiation, fatigue and recovery processes can be seen in Fig. 3.3. The steady decrease in the measured joint torque during the fatigue process and the steady increase in the joint torque produced during the recovery process illustrate that fatigue and recovery are occurring as expected. These measurements were then used to estimate the parameters of muscle fatigue dynamics in (3.27).

To estimate the fatigue model parameters from the data in Fig. 3.3, it was assumed that the muscle was fully rested at the beginning of the fatigue process. Therefore, the initial condition of the fatigue state was assumed as $\hat{\mu}(0) = 1$. Also, because the participant was being stimulated at the saturation amplitude for the duration of the fatigue procedure, the muscle activation variable was assumed to be 1 throughout the fatigue process. This is because the duration of the procedure is significantly longer than the muscle activation time constants that were previously determined (see Chapter 2. Using these assumptions the equation of the muscle fatigue dynamics (see (3.27)) can be reduced to $\dot{\hat{\mu}} = \frac{1}{\hat{T}_f}(\hat{\mu}_{\min} - \hat{\mu})$ whose solution, given the previously stated initial condition, is $\hat{\mu}(t) = \hat{\mu}_{\min} - (\hat{\mu}_{\min} - 1)e^{-t/\hat{T}_f}$. A least-squares nonlinear curve fitting algorithm was then used to solve for the parameters
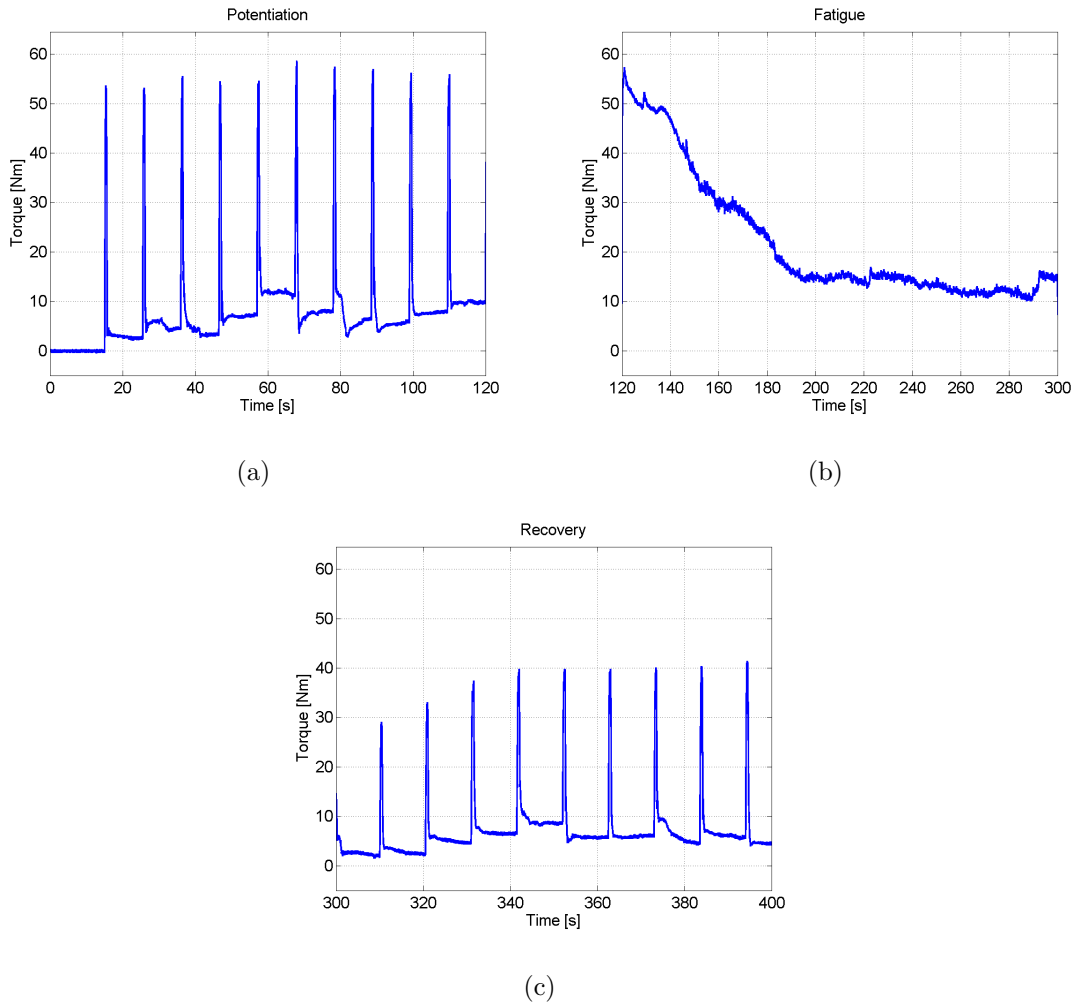
Figure 3.3: Results of the experiments to determine the parameters of the muscle fatigue parameters. These three plots show the torque measured during the potentiation, fatigue, and recovery segments of the procedure.

$\hat{T}_f$ and $\hat{\mu}_{\min}$ that best fit the time response of the fatigue state to the normalized load cell measurement from the fatigue process. The normalized load cell data and the plot of the fatigue state that best fits the measured data are shown in Fig. 3.4 (a). The resulting fit has an RMS error of 0.0373, and the parameters that were determined from this fit are $\hat{T}_f = 43.3s$ and $\hat{\mu}_{\min} = 0.188$.

During the recovery procedure, it was assumed that the pulses of stimulation were sufficiently short such that the muscle activation variable was essentially zero throughout the duration of the procedure. Therefore the equation of the muscle fatigue dynamics can be reduced to $\dot{\hat{\mu}} = \frac{1}{\hat{T}_r}(1 - \hat{\mu})$, whose solution is $\hat{\mu}(t) = 1 + (\hat{\mu}_{r0} - 1)e^{-t/\hat{T}_r}$, where $\hat{\mu}_{r0}$ is the initial condition that was measured from the first isometric contraction during the recovery procedure. The normalized load cell data and the plot of the fatigue state that best fits the measured data are shown in Fig. 3.4 (b). For the demonstrative participant whose results are shown in Fig. 3.4, the initial condition of the recovery (initial condition of the curve fit) was measured to be $\hat{\mu}_{r0} = 0.493$. The resulting fit has an RMS error of 0.0031, and the recovery time constant determined from the fit is $\hat{T}_r = 72.0 \, \text{s}$. The estimated parameters of all of the participants are given in Table 3.1.

3.5 EXPERIMENTAL RESULTS

The controller developed in (3.45) was validated on the right and left leg of three able-bodied subjects. The participants were seated in the leg extension machine that was used for the parameter estimation procedures, which is fitted with a CALT GHH100 rotary encoder (Shanghai Qiyi Electrical & Mechanical Equipment Co. Ltd) to measure the knee angle, and were asked to remain completely relaxed and to avoid any volitional contractions that might influence the control. A desired sinusoidal trajectory with a minimum of 0°, a maximum of 45° and a period of two seconds was used for all experiments. The controller modulated the current amplitude while the pulse train's frequency was fixed at 35 Hz with a pulse width of 400 µs, which are the same stimulation parameters as the ones used in the parameter estimation procedures. Because the new controller is a proportional-derivative

(a)   (b)
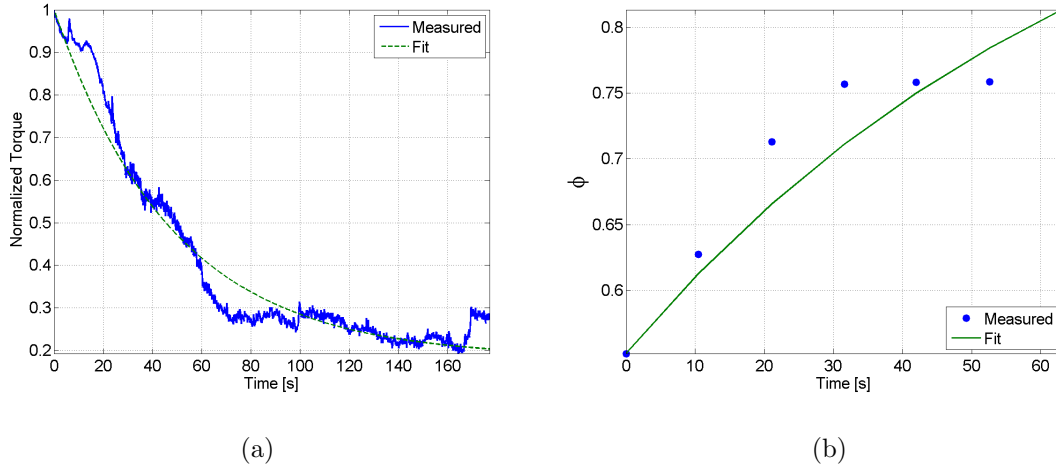
Figure 3.4: (a) The fatigue time constant and minimum fatigue states were determined by fitting the solution of the differential equation of the fatigue state to the normalized load cell data. From this fit, which has an RMS error of 0.0373, the fatigue time constant and minimum fatigue state were determined to be $\hat{T}_f =43.3\,\mathrm{s}$ and $\hat{\mu}_{\min} = 0.188$, respectively. (b) The recovery time constant can be determined by fitting the solution of the differential equation of the fatigue state during recovery to the normalized load cell data. From this fit, which has an RMS error of 0.0031, the recovery time constant was determined to be $\hat{T}_r =72.0\,\mathrm{s}$.

(PD) type controller, tracking experiments using a PD controller were also conducted so that the performance of the new controller could be compared to a similar linear controller. The estimated model parameters, the control gains for the fatigue compensation controller, and the control gains for the PD controller are shown in Table 3.1. The control gains of the fatigue compensation controller (i.e., K_s, α, and K) were introduced in (3.13) and (3.45), and The control gains K_p and K_d are the proportional and derivative gains of the PD controller, respectively. The model parameters used in the control (i.e., $v_{\min}$, $v_{\max}$, $\hat{w}$, $\hat{T}_f$, $\hat{T}_r$, and $\hat{\mu}_{\min}$) were introduced in (3.27), (3.28), and (3.45).

After tuning the controller parameters, five 30 second long tracking experiment trials were performed on each leg of each participant for both controllers. The root mean square (RMS) errors were computed for each trial, and then averaged over the five trials. The averaged RMS errors for the full duration of the experiments (0-30s), the steady-state RMS (SSRMS) errors (ignores the first two periods of the desired trajectory), and the RMS of the current amplitude of the stimulation are shown in Tables 3.2 and 3.3. Representative trials of the results of the fatigue compensation (FC) controller and the PD controller are shown in Fig. 3.5.

A Shapiro-Wilk test was used to determine the normality of the RMS and SSRMS data sets. From the results of the Shapiro-Wilk test it was concluded that the RMS and SSRMS PD controller data sets are not normal distributions. Therefore, a two-tailed Wilcoxon signed rank test with a 95% confidence level was used to determine if there was a difference between the FC and PD data sets. From the results of the Wilcoxon signed rank test [2] it was concluded that the FC and PD controllers are statistically different. Therefore, since the FC controller has a lower mean RMS and SSRMS error and because the data sets are significantly different it can be concluded that the FC controller yielded significantly better performance.

---

[2]The critical test statistic value for a sample size of 30 and a 95% confidence level is 137, and the test statistic from the results of the Wilcoxon test was determined to be 4. Since the calculated test statistic is less than the critical test statistic it was concluded that the RMS and SSRMS data for the FC and PD controllers are significantly different.

Table 3.1: Values of the estimated parameters and control gains used in the experiments for the right leg (RL) and left leg (LL) of each subject.

	Subject 1		Subject 2		Subject 3	
	RL	LL	RL	LL	RL	LL
$\hat{w}$ [Hz]	12.5	10.5	6.67	7.69	8.33	10.53
$\hat{T}_f$ [s]	43.3	26.6	19.7	20.0	101.7	26.0
$\hat{T}_r$ [s]	72.0	110	126	183	119	124
$\hat{\mu}_{\min}$	0.188	0.383	0.138	0.125	4.17×10^{-10}	0.144
$v_{\min}$ [mA]	30	23	25	26	23	26
$v_{\max}$ [mA]	80	74	70	70	80	77
K_s	0.1	0.1	0.07	0.09	0.1	0.09
α	10	10	4	5	6	6
K	6.25	5.3	3.33	3.85	4.17	5.26
K_p	1.9	1.8	1.8	2.05	1.6	3
K_d	0.5	0.5	0.4	0.8	0.2	0.9
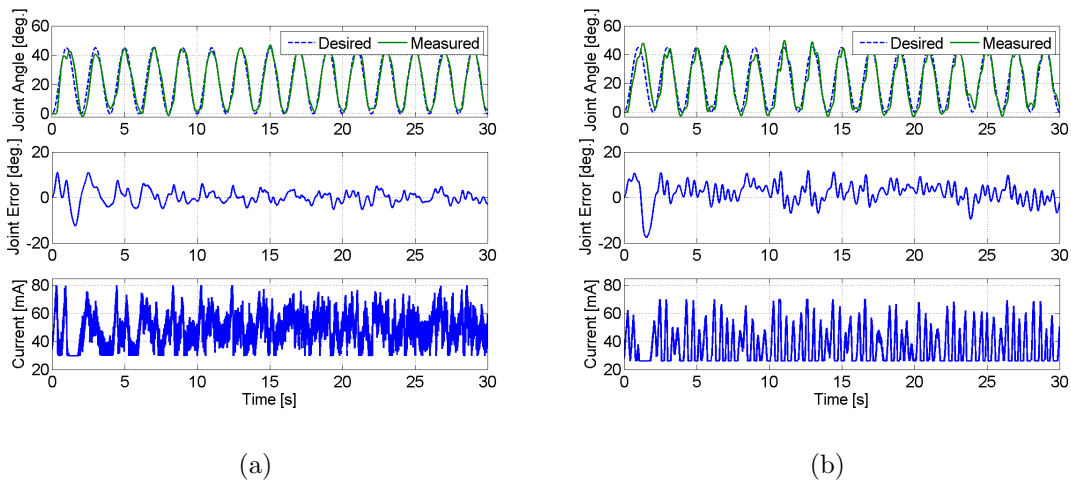
Figure 3.5: The trials that resulted in the lowest steady-state RMS errors for the fatigue compensation and PD controllers are shown in (a) and (b), respectively. The trial for the fatigue compensation controller was taken from one of Subject 1's trials, which had a steady-state RMS error of $2.44°$. The trial for the PD controller was taken from one of Subject 2's trials, which had a steady-state RMS error of $4.23°$.

Table 3.2: Root mean square errors (RMS) for the full 30 second long trajectory tracking experiments and steady-state (4-30 seconds) RMS (SSRMS) errors averaged over five trials for the right leg (RL) and left leg (LL) of each subject for both the fatigue compensation (FC) and PD controllers. These results were evaluated with a Wilcoxon signed rank test, which concluded that the FC controller performed significantly better than the PD controller.

Subject ID	Leg	FC Controller		PD Controller	
		RMS Error [deg.]	SSRMS Error [deg.]	RMS Error [deg.]	SSRMS Error [deg.]
1	RL	3.72	3.43	5.40	5.25
	LL	3.48	3.37	5.40	5.25
2	RL	4.33	4.29	8.30	8.49
	LL	4.15	4.05	5.25	5.08
3	RL	5.00	4.96	8.85	8.92
	LL	2.93	2.85	5.61	5.65
Mean		3.93	3.82	6.73	6.73
Standard Deviation		0.721	0.758	1.56	1.68

Table 3.3: Root mean square (RMS) of the stimulation current amplitude for the full 30 second long trajectory tracking experiments over five trials for the right leg (RL) and left leg (LL) of each subject for both the fatigue compensation (FC) and PD controllers.

		FC Controller	PD Controller
Subject ID	Leg	RMS Current[mA]	RMS Current [mA]
1	RL	46.2	33.6
	LL	44.3	36.2
2	RL	34.7	36.6
	LL	40.9	39.3
3	RL	34.8	36.2
	LL	47.4	46.2
Mean		41.4	38.0
Standard Deviation		6.26	4.39
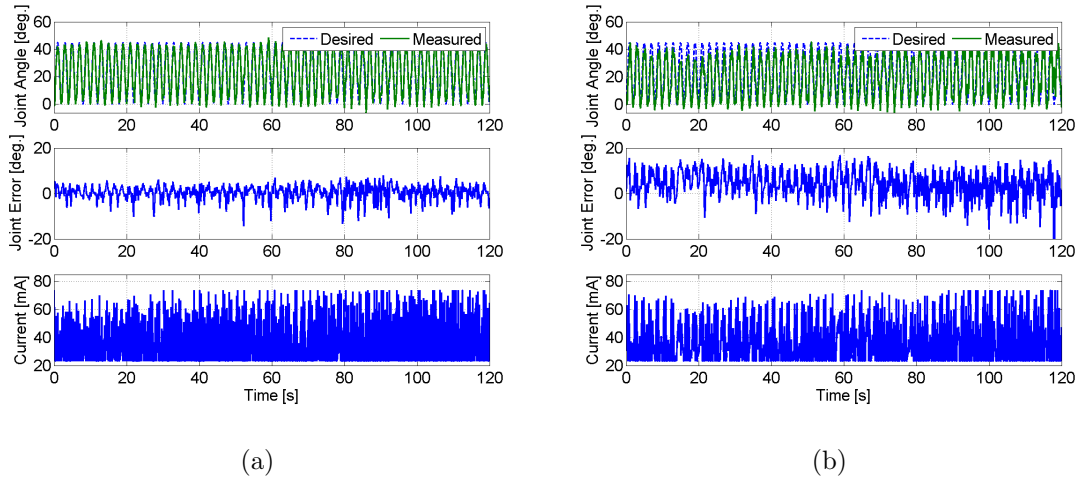
Figure 3.6: The two minute long trials that resulted in the lowest RMS errors for the FC and PD controllers are shown in (a) and (b), respectively. Both trials were taken from the results of Subject 1's left leg. The results of the FC controller in (a) had an RMS error of 3.24°, and the results of the PD controller in (b) had an RMS error of 6.96°.

To determine how well the newly developed controller performed over long durations, where muscle fatigue should have a greater effect on performance, two minute long tracking experiments were performed for one trial on each leg of each subject. The two minute long experiments used the same desired trajectory and control parameters as were used in the thirty second long experiments (see Table 3.1). Representative trials of the two minute long experiments using the FC controller and the PD controller are shown in Fig. 3.6, and the RMS errors computed from these trials are shown in Table 3.4.

Table 3.4: RMS errors for two minute long trials with PD and FC controllers for the right leg (RL) and left leg (LL) of each subject. These results were evaluated with a Wilcoxon signed rank test, which concluded that the FC controller performed significantly better.

Subject ID	Leg	FC Controller		PD Controller	
		RMS Error [deg.]	SSRMS Current [mA]	RMS Error [deg.]	SSRMS Current [mA]
1	RL	3.26	51.6	7.66	37.2
	LL	3.24	37.2	6.96	37.9
2	RL	4.11	35.4	7.28	37.9
	LL	3.92	40.1	7.71	41.3
3	RL	4.08	37.9	12.8	36.4
	LL	4.08	37.2	11.9	41.0
Mean		3.78	39.9	9.0	38.6
Standard Deviation		0.418	5.92	2.57	2.06

The results of a Shapiro-Wilk test indicated that the RMS data from the two minute long trials are not normally distributed. Therefore, a two-tailed Wilcoxon signed rank test was used [3], which concluded that there was a statistical difference between the FC and PD RMS data sets. Therefore, since the mean RMS error of the FC trials is lower than the mean RMS error of the PD trials it can be concluded that the FC controller also yielded significantly better performance over two minute long trials.

The estimated muscle fatigue state, which was estimated using the model in (3.27) and model parameters in Table 3.1, from the two minute long trials are plotted in Fig. 3.7 to illustrate the effect that each controller had on the estimated muscle fatigue. Although the FC controller performed significantly better than the PD controller, it can be observed from Fig. 3.7 that there is little difference in the muscle fatigue induced by both controllers. However, this was not the case for all subjects though. This can be seen in Table 3.5, which shows the estimate of the fatigue states at the end of the two minute long tracking trials. It was concluded from a Shapiro-Wilk normality test that the data sets of the terminal fatigue state estimates for the FC and PD controllers were not normally distributed. Since the data sets were not normally distributed a two-tailed Wilcoxon signed rank test was used [4], which concluded that there is no statistical difference between the two data sets. Therefore, because there is no statistical difference in the terminal fatigue estimate data it can be concluded that the FC controller does not cause any significant increase or decrease in muscle fatigue compared to a PD controller.

---

[3]The critical test statistic value for a sample size of 6 and a 95% confidence level is 0, and the test statistic from the results of the Wilcoxon test was determined to be 0. Since the calculated test statistic is equal to the critical test statistic it was concluded that the RMS and SSRMS data for the FC and PD controllers are significantly different.

[4]The critical test statistic value for a sample size of 30 and a 95% confidence level is 0, and the test statistic from the results of the Wilcoxon test was determined to be 9. Since the calculated test statistic is greater than the critical test statistic it was concluded that there is no statistical difference between the two data sets.
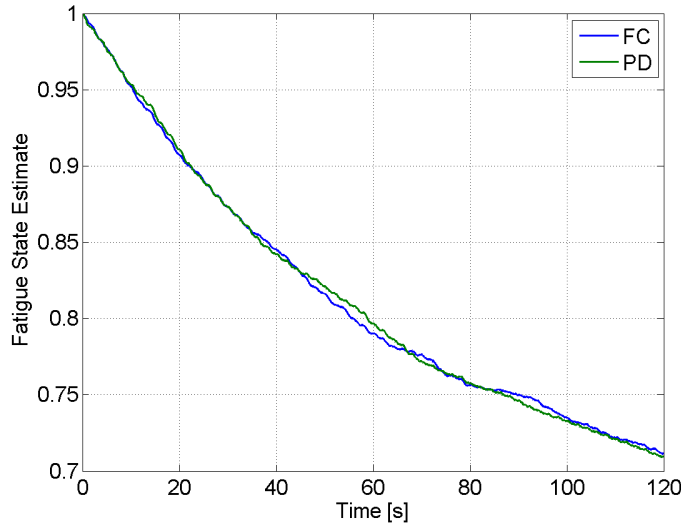
Figure 3.7: Estimate of the fatigue state from the two minute trials of Subject 1 for the FC and PD controllers.

3.6 DISCUSSION

The statistical analysis of the thirty second and two minute long trials illustrated that the developed controller performs significantly better than a PD controller. For the 30 second trials, the mean steady-state RMS errors for the PD controller and the FC controller were 6.73° and 3.93°, respectively. For the two minute long trials the FC controller was shown to have a mean RMS error of 3.78°, while the PD controller was shown to have a mean RMS error of 9.04°. Because of none of the data sets were normal, according to a Shapiro-Wilk normality test, a two-tailed Wilcoxon signed rank test was used to show that the differences in performance were significant. Although the results indicated that the new controller performed significantly better than a PD controller, the estimated muscle fatigue states indicated that the new controller did not fatigue the muscles any more or less than the PD controller. This was concluded from a Wilcoxon signed rank test, whose results indicated that the muscle fatigue states at the end of the two minute long trials for the developed controller and the PD controller were not statistically different. However, it should be noted

Table 3.5: The estimate of the fatigue states at the end of the two minute long tracking trials for the right leg (RL) and left leg (LL) of each subject. From the results of a Wilcoxon signed rank test it was concluded that there is no statistical difference in the fatigue states at the end of the two minute long trials.

		Fatigue State Estimate		
Subject ID	Leg	FC Controller	PD Controller	Difference
1	RL	0.617	0.719	-0.101
	LL	0.705	0.704	0.001
2	RL	0.549	0.579	-0.030
	LL	0.406	0.408	-0.002
3	RL	0.919	0.860	0.058
	LL	0.614	0.605	0.646
Mean		0.635	0.605	-0.011
Standard Deviation		0.171	0.153	0.053

that this is an estimate of the muscle fatigue state and not the actual muscle fatigue state. Also, the controller is only compensating for the muscle fatigue to maintain the tracking performance. In the next chapter an optimal control technique will be presented that may decrease muscle fatigue by minimizing the amount of stimulation used to produce a desired motion.

3.7 CONCLUSION

In this chapter, an NMES controller that incorporates model-based estimates of muscle activation and fatigue dynamics to compensate for the effects of muscle fatigue was developed. Through a Lyapunov-based stability analysis, the developed controller was shown to yield globally uniformly ultimately bounded tracking, provided that the sufficient conditions are met. The experimental results illustrated the feasibility of the controller to enable the lower leg to track a desired trajectory through stimulation of the quadriceps muscles. Although the controller was only demonstrated on single joint knee extension experiments the control development may also be used for the synthesis of other controllers for NMES assistive and rehabilitative devices (e.g. NMES gait restoration and NMES cycling). Given the differences in people with different diseases or injuries, longitudinal clinical trials will have to be performed in specific patient populations to gain further insight into the potential outcomes of the developed controller during functional tasks.

4.0 NONLINEAR MODEL PREDICTIVE CONTROL OF FUNCTIONAL ELECTRICAL STIMULATION

Through the application of functional electrical stimulation (FES) limb function may be restored to individuals with an upper motor neuron disease or disorder. For example, by stimulating specific muscle groups in an appropriate sequential manner a walking motion can be achieved [8, 51, 58, 78, 80, 97]. Most FES-based devices, such as the Parastep system [76] (Therapeutics Inc.), use electrodes placed on the surface of the skin (transcutaneous electrodes) to enable paraplegics to achieve standing and walking. However, as discussed in Chapter 1, due to the manner in which transcutaneous stimulation recruits motor units rapid muscle fatigue occurs. This can greatly limit the duration that FES-based devices can be used.

As was shown in the previous chapter, error-based feedback control of FES can compensate for the effects of muscle fatigue. However, increasing the amplitude or frequency of stimulation can further aggravate the rate at which the muscle fatigue occurs. Recent advances in hybrid powered walking orthoses [36, 37], or the use of an orthosis or exoskeleton in general [28], can reduce stimulation duty cycle of FES by using the orthosis to share the necessary control effort. However, stimulation induced muscle fatigue, or even during shared control between the FES and electric motors [23, 55, 56, 112, 113], is still a significant problem. To overcome this challenge, optimal control techniques may be used to control the stimulation in a manner such that the minimum amount of stimulation that is required to produce the desired movement is used, thus reducing muscle fatigue. In [110, 126] optimizations of musculoskeletal gait models were used to compute the minimum amount of stimulation required to produce a gait motion. The stimulation computed by these optimizations may be applied in open-loop control to reproduce the desired gait. However, due

to the lack of feedback open-loop optimal control techniques are not robust to disturbances or modeling errors. In [145] a PD controller with an adaptive inverse optimal controller was used to control knee extension through stimulation of the quadriceps muscle. This technique coordinates an error-based feedback controller with a neural network that compensates for uncertainties in the musculoskeletal dynamics to robustify the inverse optimal controller. However, the inverse optimal control technique does not solve the optimal control problem of an *a priori* cost function.

Unlike the inverse optimal controller used in [145], model predictive control (MPC) can solve the optimal control problem given an *a priori* cost function. MPC (also referred to as receding horizon control) uses a mathematical model of the dynamics of the system to predict how it will behave over a finite time horizon. Then, the control signals that minimize a user-defined cost function over the finite time horizon are numerically computed. In MPC, at each discrete time step of the control the states of the system are measured, and then used as the initial condition constraint of the optimal control problem for the next horizon. These initial conditions act as feedback for the control, making it more robust to disturbances and uncertainties than open-loop optimal control.

MPC has been proposed for the control of FES for FES-assisted standing in [34] and for drop foot correction in [11]. In [34] MPC was simulated on a musculoskeletal model of the lower extremities and torso to track trajectories that minimize joint torque and jerk, enabling the model to make a smooth and efficient sit-to-stand transfer. In [11] MPC was used in simulations on a musculoskeletal model to compute stimulation to the tibialis anterior muscle that minimizes stimulation and ground clearance of the foot during a step, which in theory would decrease the effects of muscle fatigue and increase the duration that such devices may be used. The nonlinear dynamics of the musculoskeletal system and time-varying muscular response to FES makes MPC of a musculoskeletal system challenging. To overcome this challenge, in [104] MPC was coupled with an input-output feedback linearization controller and simulated on FES-controlled knee extension. The input-output feedback linearization controller was used to cancel out the nonlinear dynamics of the musculoskeletal system, thus linearizing the system. Then, the MPC only needs to solve the optimal control problem for the linear system, which reduces the complexity of the optimal control problem and makes

it easier to implement. In simulations this method was able to compute the solution to the optimal control problem with computation times less than 20 ms. These results indicate that the controller developed in [104] can potentially be applied for real-time MPC of FES with a control frequency of no more than 50 Hz. However, its experimental verification remains to be seen.

In this chapter, a gradient projection-based nonlinear MPC (NMPC) algorithm is used to implement NMPC on a nonlinear musculoskeletal system driven via FES in both simulations and experiments. This work is an expansion on the results presented in [73], which only presented preliminary results for one participant. The solution to the optimal control problem was computed using a gradient projection method, presented in [49, 67], which was found to have sufficiently fast computation times to allow for real-time implementation of NMPC. Experimental results were obtained from the three able-bodied participants whose musculoskeletal parameters were estimated in Chapter 2. The estimated parameters for each subject are used by the MPC and to estimate the muscle activation, which cannot be measured. The results presented in this chapter will illustrate that the developed NMPC method can be used to control knee extension via FES in real time with approximately 2° of steady-state RMS error. This chapter will also present results to illustrate that the NMPC algorithm is robust to impulsive disturbances during knee regulation. Potentially, the proposed NMPC method may benefit FES-based devices by reducing the stimulation required to produce the desired motion, which indirectly decreases the effects of muscle fatigue and increases the durations that such devices may be used.

4.1 LEG EXTENSION NEUROPROSTHESIS MODEL

The NMPC used in this chapter will require that the nonlinear dynamics of the system are expressed in a state-space formulation with the equilibrium at the origin. Therefore, this section will modify the leg extension model from [110] that was presented in Chapter 2 such that it may be used in the gradient projection-based NMPC.
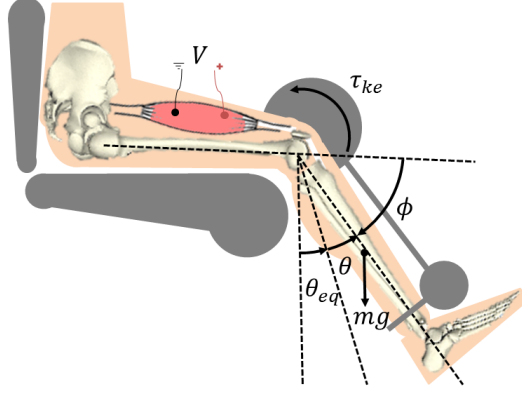
Figure 4.1: This knee extension neuroprosthesis uses electrical stimulation of the quadriceps muscles to elicit a knee extension. The angle θ is the angle of the lower leg relative to the equilibrium position of the lower leg, and the angle ϕ is the anatomical knee joint angle.

The dynamics of a lower leg, with FES as the input, can be described as

$$J\ddot{\theta} + G - \tau_p = \tau_{ke}, \tag{4.1}$$

where $\theta, \dot{\theta}, \ddot{\theta} \in \mathbb{R}$ are the angular position, velocity, and acceleration of the lower leg relative to equilibrium as illustrated in Fig. 4.1, J is the moment of inertia of the lower leg, and $G(\theta) = mgl_c \sin(\theta + \theta_{eq})$ is the gravitational torque. In the gravitational torque m is the mass of the lower leg, g is gravitational acceleration, l_c is the distance from the knee joint to the center of mass, and θ_{eq} is the equilibrium position of the lower leg relative to full extension as illustrated in Fig. 4.1. Since the anatomical knee joint angle is defined as full extension being $0°$ and flexion being positive, the anatomical knee joint angle can be written as a function of the joint angle θ as $\phi = \frac{\pi}{2} - \theta - \theta_{eq}$. Subsequently, the angular velocities and accelerations are related as $\dot{\phi} = -\dot{\theta}$ and $\ddot{\phi} = -\ddot{\theta}$.

The passive musculoskeletal torque of the knee joint, $\tau_p(\theta, \dot{\theta})$ in (4.1), is modeled as

$$\tau_p = d_1(\phi - \phi_0) + d_2\dot{\phi} + d_3 e^{d_4\phi} - d_5 e^{d_6\phi}, \tag{4.2}$$

as was presented in Chapter 2. The torque produced by the muscles due to an FES induced muscle contraction will also be modeled as presented in Chapter 2. However, it will be assumed that the angular velocity of the knee joint is relatively slow, and the torque-velocity relationship can be modeled as $\psi_v = 1 + c_3\dot{\phi}$. Therefore, for the NMPC controller the joint torque produced by the muscles due to the application of FES was modeled as

$$\tau_{ke} = (c_2\phi^2 + c_1\phi + c_0)(1 + c_3\dot{\phi})a_{ke}, \tag{4.3}$$

where $a_{ke} \in [0, 1]$ is the activation of the quadriceps muscles. The NMPC will also include the dynamics of muscle activation, which as presented in Chapter 2 can be modeled as

$$\dot{a}_{ke} = \frac{u_{ke} - a_{ke}}{T_a}, \tag{4.4}$$

where $u_{ke} \in [0, 1]$ is the normalized electrical stimulation amplitude and $T_a \in \mathbb{R}^+$ is the time constant of muscle activation. The normalized stimulation amplitude was defined as the input to the model of the system that the NMPC uses. This is then mapped to the current amplitude of the electrical stimulation as

$$I = I_t + u_{ke}(I_s - I_t), \tag{4.5}$$

where I_t and I_s are the threshold and saturation current amplitudes, respectively, as defined in Chapter 2. It should be noted that a similar relationship can be found for stimulation voltage amplitude and pulse width control of FES.

The differential equations in (4.1) and (4.4) can be expressed in a state-space formulation as

$$
\begin{aligned}
\dot{x} &= f(x, u) \\
&= \begin{bmatrix} x_2 \\ -\beta \sin(x_1 + \theta_{eq}) + \alpha(\tau_p + \tau_{ke}) \\ \frac{u - x_3}{T_a} \end{bmatrix},
\end{aligned}
\tag{4.6}
$$

where $x = \left[\theta, \dot{\theta}, a_{ke}\right]^T$, $u = u_{ke}$, $\alpha = 1/J$, $\beta = mgl_c\alpha$, and $\tau_{ke}(x)$ can be determined from (4.3) and the relationship $\phi = \frac{\pi}{2} - x_1 - \theta_{eq}$. To implement the gradient projection algorithm it is necessary that the state-space dynamics are differentiable so that the gradient of the Hamiltonian may be computed. From (4.6), it is clear that $f(x, u)$ is in fact differentiable. Note that this model assumes that the dynamics of the system are time-invariant. This assumption may become invalid when the effects of muscle fatigue become more prominent, and the muscle fatigue affects the muscle recruitment curve. In this chapter time-invariance will be assumed; however, later chapters will include muscle fatigue dynamics as modeled in [117] and presented in Chapter 3 to make the MPC more robust to fatigue.

4.2 GRADIENT PROJECTION MODEL PREDICTIVE CONTROL

Due to the nonlinearities present in the musculoskeletal system, an NMPC algorithm was used to achieve greater accuracy in the control. Because the system dynamics (see (4.6)) are differentiable, a gradient projection algorithm may be used [93]. It will be shown here that the gradient projection algorithm will provide sufficiently fast computation times to allow real time implementation of the NMPC. Gradient projection MPC, or GRAMPC as it is referred to in [49, 67, 68], uses the gradient of the Hamiltonian to solve the optimal control problem and a projection algorithm to ensure that the solutions remain bounded within some constant box constraint. The projection algorithm helps facilitates faster computation times and makes the solver well suited for our problem, since the normalized stimulation must be bounded box constraints as $u_{ke} \in [0, 1]$. The gradient projection algorithm can also

use an early termination condition to ensure that the algorithm can be implemented in real time. However, this results in a suboptimal solution, which may affect the control. This section will define the optimal control problem and present a brief summary of the gradient projection algorithm, and discuss its stability in the optimal and sub-optimal cases.

4.2.1 Optimal Control Problem

The general, finite-time optimal control problem that can be solved using the gradient projection algorithm is stated as

$$\min_{u} \quad J(x, u) = V(x(T)) + \int_{t_0}^{T} l(x(\tau), u(\tau))d\tau \tag{4.7}$$

$$\text{subject to:} \qquad \dot{x}(t) = f(x, u)$$

$$x(t_0) = x_0$$

$$u \in \mathcal{U}$$

where $x_0 \in \mathbb{R}^3$ is the initial condition of the states at each time step of the control, $\mathcal{U} = [u^-, u^+]$ are the bounds on u, t_0 is the initial time of the horizon, and T is the final time of the horizon. The initial condition equality constraint will be inherently true, because the initial conditions are necessary for the solver to integrate the dynamics, and a projection function will be used to enforce the box constraints on u. The cost function, $J(x, u) \in \mathbb{R}$, is separated into two parts: the terminal cost function $V(x(T))$ and the integral cost function $l(x, u)$. Both of these functions may be defined by the user; however, because a gradient algorithm will be used it is necessary that they are both differentiable functions. Also, although the terminal cost may be freely defined by the user it will be illustrated here how it may be used to stabilize the control.

The objective of the optimal control problem is to solve for the control trajectory, u, that minimizes the cost function $J(x, u)$ over a finite time horizon $t \in [t_0, T]$ while satisfying the aforementioned constraints. For this study, the only control input to the system is the normalized stimulation, which we desire to be bounded as $u_{ke} \in [0, 1]$. Therefore, the constraint on the control trajectory is defined as $u \in [0, 1]$, which means that $u^- = 0$ and $u^+ = 1$.

Let the integral cost function, $l(x, u)$, and the terminal cost, $V(x(T))$, in (4.7) be quadratic functions defined as

$$l(x,u) = \Delta x^T Q \Delta x + \Delta u^T R \Delta u$$
$$V(x(T)) = \Delta x(T)^T P \Delta x(T) \qquad ,$$

(4.8)

where $\Delta x = x - x_{des}$, $\Delta u = u - u_{des}$, $x_{des} \in \mathbb{R}^3$ is the desired state, and $u_{des} \in \mathcal{U}$ is the desired control trajectory. The weight matrices $Q \in \mathbb{R}^{3\times3}$, $R \in \mathbb{R}$, and $P \in \mathbb{R}^{3\times3}$ must be at least positive semi-definite and can be tuned to achieve the desired performance.

Pontryagin's Minimum Principle states that $u^*(t)$ for $t \in [0, T)$ solves the optimal control problem if it minimizes the Hamiltonian [118], where the Hamiltonian for the optimal control problem is defined as

$$H(x, \lambda, u) = l(x, u) + \lambda^T f(x, u),$$

(4.9)

where $\lambda(t) \in \mathbb{R}^n$ is the costate vector. In other words, the constrained optimal control problem in (4.7) can be solved by solving the unconstrained optimal control problem

$$\min_u H(x, \lambda, u) = l(x, u) + \lambda^T f(x, u).$$

(4.10)

If the integral cost function and the dynamics function are differentiable, the gradient of the Hamiltonian can be used to iteratively solve for the optimal control trajectory, $u^*(t)$, using a gradient decent method.

4.2.2 Gradient Projection Algorithm

Detailed steps of the gradient projection algorithm can be found in [49], but will be summarized here for completion. During the iterative solution process the gradient projection algorithm uses a projection function, defined as

$$\psi(u) = \begin{cases} u^- & u < u^- \\ u, & u^- \le u \le u^+ \\ u^+ & u^+ < u \end{cases} ,$$

(4.11)

which ensures that all values in the control trajectory remain in the set $\mathcal{U}$.

The gradient projection algorithm can be summarized as follows for each discrete time step of the control, k:

1. Initialization: $j = 0$

    a. Set the convergence tolerance ε_j.

    b. Choose initial control trajectory $u_k^{(0)} \in \mathcal{U}_{[0,T]}$.

    c. Integrate the system dynamics forward in time to solve for $x_k^{(0)}$ given $u_k^{(0)}$.

2. Gradient Step: While $\left| J(x_k^{(j+1)}, u_k^{(j+1)}) - J(x_k^{(j)}, u_k^{(j)}) \right| > \varepsilon_j$ or $j \leq N$

    a. Integrate $\dot{\lambda} = -\frac{\partial H(x, \lambda, u)}{\partial x}\Big|_{x=x_k^{(j)}, \ u=u_k^{(j)}}$ backward in time to solve for the costates, where $\lambda_k^{(j)}(T) = \frac{\partial V(x_k^{(j)}(T))}{\partial x(T)}$ is the terminal condition.

    b. Compute the search direction, $s_k^{(j)} \in \mathbb{R}$, from the Hamiltonian as $s_k^{(j)} = -\frac{\partial H(x, \lambda, u)}{\partial u}\Big|_{x=x_k^{(j)}, \ u=u_k^{(j)}, \ \lambda_k^{(j)}}$.

    c. Compute the step size, $\alpha_k^{(j)} \in \mathbb{R}^+$, by solving the line search problem $\alpha_k^{(j)} = \underset{\alpha > 0}{\arg\min} \, J(x_k^{(j)}, \psi(u_k^{(j)} + \alpha s_k^{(j)}))$ (this can be approximately solved to decrease computation time using a number of methods [49]).

    d. Compute the new control trajectory $u_k^{(j+1)} = \psi(u_k^{(j)} + \alpha_k^{(j)} s_k^{(j)})$, where $\psi(\cdot)$ is the projection function in (4.11).

    e. Integrate the system dynamics forward in time to solve for $x_k^{(j+1)}$ given $u_k^{(j+1)}$ and evaluate the cost function $J(x_k^{(j+1)}, u_k^{(j+1)})$.

    f. Quit if $\left| J(x_k^{(j+1)}, u_k^{(j+1)}) - J(x_k^{(j)}, u_k^{(j)}) \right| \leq \varepsilon_j$ or if j has exceeded the max iteration limit, N. Otherwise set $j = j + 1$ and reiterate gradient step.

When the iterative loop of the algorithm terminates due to the change in the cost being within the convergence tolerance, ε_j, the resulting control trajectory is said to be optimal. If the loop terminates due to exceeding the max iteration limit (i.e., if $j > N$, where N is specified by the user), then the result is said to be suboptimal. It is always desirable to converge to the optimal solution; however, the max iteration termination condition is necessary to ensure that the algorithm may be implemented in real time.

To increase the convergence rate of this algorithm, and to improve upon previously computed suboptimal solutions, the solution from the previous time step is sued to initialize the control trajectory at the next time step. In other words, if u_k^* is the computed control

trajectory at the kth time step then at the next time step $u_{k+1}^{(0)} = u_k^*$ is used as the initial guess. This is called giving the gradient algorithm a warm-start, and can improve the convergence rate at each time step of the control by reducing the number of iterations required to compute the solution. Therefore, this technique can help improve suboptimal solution at each time step of the control, eventually resulting in them converging to optimal solutions.

A common technique to ensure the stability of MPC is to use a terminal equality constraint on the states (such as $x(T) = x_{des}$) in the definition of the optimal control problem [20]. However, the addition of such a constraint can make the optimal control problem more difficult to solve, resulting in an increase in computation time.

A preferable method to ensure stability that does not affect computation time is to use the terminal cost, $V(x(T))$, as a control Lyapunov function [62]. This can be used to stabilize the MPC for the optimal and suboptimal case, given that the set (x_{des}, u_{des}) are an equilibrium of $f(x, u)$. For the leg extension neuroprosthesis system presented, given a desired joint angle the remaining elements of x_{des} and u_{des} can be solved from (4.6) as $f(x_{des}, u_{des}) = 0$. The control Lyapunov condition is approximately satisfied by solving the algebraic Riccati equation [49, 50]

$$PA + A^T P - PBR^{-1}B^T P + Q = 0 \tag{4.12}$$

for the gain matrix P, where the matrices A and B are the matrices of the linearized state-space system that can be computed using Jacobian linearization of the nonlinear dynamics about the point (x_{des}, u_{des}) as

$$
\begin{aligned}
A &= \left. \frac{\partial f(x, u)}{\partial x} \right|_{x=x_{des},\ u=u_{des}} \\
&= \begin{bmatrix} 0 & 1 & 0 \\ A_{21} & A_{22} & A_{23} \\ 0 & 0 & -\frac{1}{T_a} \end{bmatrix} \\
B &= \left. \frac{\partial f(x, u)}{\partial u} \right|_{x=x_{des},\ u=u_{des}} \\
&= \begin{bmatrix} 0 \\ 0 \\ \frac{1}{T_a} \end{bmatrix}
\end{aligned} \tag{4.13}
$$

where

$$A_{21} = - \beta \cos(x_{des}^{(1)} + \theta_{eq})$$
$$- \alpha \left[d_1 + d_3 d_4 e^{d_4(\frac{\pi}{2} - x_{des}^{(1)} - \theta_{eq})} \right.$$
$$- d_5 d_6 e^{d_6(\frac{\pi}{2} - x_{des}^{(1)} - \theta_{eq})}$$
$$+ \left(2c_2 \left(\frac{\pi}{2} - x_{des}^{(1)} - \theta_{eq} \right) \right.$$
$$\left. +c_1 \right) \left(1 - c_3 x_{des}^{(2)} \right) x_{des}^{(3)} \Bigg] , \tag{4.14}$$

$$A_{22} = - \alpha \left[d_2 + (c_2(\frac{\pi}{2} - x_{des}^{(1)} - \theta_{eq})^2 \right.$$
$$\left. +c_1(\frac{\pi}{2} - x_{des}^{(1)} - \theta_{eq}) + c_0)c_3 x_{des}^{(3)} \right] , \tag{4.15}$$

$$A_{23} = \alpha \left[\left(c_2(\frac{\pi}{2} - x_{des}^{(1)} - \theta_{eq})^2 \right. \right.$$
$$+ c_1 \left(\frac{\pi}{2} - x_{des}^{(1)} - \theta_{eq} \right)$$
$$\left. \left. +c_0 \right) \left(1 - c_3 x_{des}^{(2)} \right) \right] , \tag{4.16}$$

and $x_{des}^{(j)}$ for $j = \{1, 2, 3\}$ is the jth element of x_{des}. It should be noted that the control Lyapunov condition is only approximately satisfied by this condition because the Jacobian linearization process is an approximation of the dynamics of the system. However, assuming that the system's dynamics are time-invariant, and for small displacements from (x_{des}, u_{des}), the control Lyapunov condition is satisfied.

4.3   RESULTS

The gradient projection algorithm based NMPC was tested in simulations and in experiments on the same three able-bodied participants that participated in the parameter estimation procedures in Chapter 2 [1]. The parameters that were estimated for each participant (see 2.1 in Chapter 2) are used to populate the models that are used by the NMPC. The participants were seated in a leg extension machine with a CALT GH100 rotary encoder (Shanghai Qiyi Electrical & Mechanical Equipment Co. Ltd) mounted to the arm of the leg extension machine to measure the joint angle. Position is the only measurable state, so the remaining states, angular velocity and muscle activation, are estimated using different methods. The angular velocity was estimated from the joint angle measurement by using a discrete time derivative. The muscle activation was estimated using the normalized stimulation and the differential equation that models muscle activation, as was done for the fatigue compensation controller in Chapter 3. The participants were all asked to relax and avoid any voluntary muscle contractions during the experiments. The simulation results are plotted with the experimental results so that the experimental performance of the controller can be compared with the performance of the controller for an exact model knowledge case (i.e., model of the system in the simulations is identical to the model given to the NMPC).

The NMPC was implemented in Simulink (MathWorks, Inc.) using a QPIDe data acquisition board (Quanser, Inc.) to collect data from the encoder, and an FNS-16 Multi-Channel Stimulator (CWE, Inc.) to generate the electrical stimulation. A sampling frequency of 100 Hz was used for the control, the horizon of the NMPC was set at 0.5 second, and an adaptive line search method was used to compute the step size. The NMPC used Heun's method, a second order numerical method, to integrate the dynamics function and trapezoidal integration was used to integrate the cost function. The aforementioned numerical methods were used because they were found to be sufficiently accurate and resulted in the fastest computation time. This was validated through simulations using different numerical methods.

---

[1]Prior to any experimentation, approval from the Institutional Review Board at the University of Pittsburgh was obtained.

The desired states and input for the first set of experiments were defined as

$$x_{des} = \begin{cases} \begin{bmatrix} 0 \\ 0 \\ 0 \end{bmatrix}, & t \leq 5 \\ \begin{bmatrix} 40° \\ 0 \\ a_{eq} \end{bmatrix}, & t > 5 \end{cases} \qquad u_{des} = \begin{cases} 0, & t \leq 5 \\ u_{eq}, & t > 5 \end{cases}, \tag{4.17}$$

where a_{eq} and u_{eq} are the muscle activation and normalized stimulation amplitude that make 40° the equilibrium position. These values can be different for each person, but are determined by solving for the equilibrium of the dynamics (see (4.6)) for the given desired knee angle of 40° given the parameters of that participant.

The weight matrices of the integral cost function, Q and R, were tuned to achieve good steady-state performance for each participant. As an example of weights that were found to be appropriate for this controller, the values that were used in experiments and simulations for Participant 1 are

$$Q = \begin{bmatrix} 10 & 0 & 0 \\ 0 & 5 & 0 \\ 0 & 0 & 1 \end{bmatrix} \quad \text{and} \quad R = 1 \ . \tag{4.18}$$

Because Q is a diagonal matrix with all positive elements and R is a positive scalar it is clear that both Q and R are positive definite.

The algebraic Riccati equation was solved using the weight matrices Q and R, and the linearized matrices A and B that resulted from using the subject specific parameters for each participant. For Participant 1, whose model parameter values can be found in Table 2.1, the matrices of the linearized dynamics were computed to be

$$A = \begin{bmatrix} 0 & 1 & 0 \\ -41.95 & -32.04 & -121.46 \\ 0 & 0 & -6.25 \end{bmatrix} \quad \text{and } B = \begin{bmatrix} 0 \\ 0 \\ 6.25 \end{bmatrix}. \tag{4.19}$$

Using these A and B matrices and the selected Q and R weight matrices in (4.18), the solution to the algebraic Riccati equation was computed to be

$$P = \begin{bmatrix} 7.22 & 0.102 & -0.193 \\ 0.102 & 0.0710 & -0.129 \\ -0.193 & -0.129 & 0.765 \end{bmatrix}. \tag{4.20}$$

Although it is not apparent, because P is a Hermitian matrix with all positive eigenvalues it can be shown that the matrix is positive definite. Since Q, R, and P are all positive definite it can be concluded that the quadratic cost function is strictly positive.

The experimental and simulation results of the NMPC for regulation at a knee angle of $40°$ are shown in Fig. 4.2, and the steady-state root mean square (SSRMS) (10-30 seconds) errors are given in Table 4.1. For each participant the simulations and experiments each used the same weight matrices and model parameters. The results of the simulations and experiments are plotted together to illustrate how the controller is expected to perform in the ideal case (exact model knowledge). One notable difference between the experimental and simulation results is oscillations that occur shortly after the onset of the step, which likely a result of errors in the estimation of the parameters or unmodeled dynamics.

Although the terminal cost gain matrix that stabilizes the system is specific to a knee angle of $40°$, regulation of the knee angle to different reference positions was also tested through simulations and experiments. Fig. 4.3 shows the results of simulations and experiments when the reference position is varied. The controller was given a reference of $40°$ for ten seconds, followed by a reference of $20°$ for ten seconds, and then a reference of $60°$ for ten seconds. It took approximately five seconds for the transient response to decay, so SSRMS errors were calculated using the last five seconds that the lower limb was regulated at each of the three reference positions. This corresponds to experiment times of 10-15 seconds for $40°$, 20-25 seconds at $20°$, and 30-35 seconds at $60°$. The SSRMS errors for these times are given in Table 4.2. To determine the robustness of the NMPC to external and unmodeled disturbances an impulse was applied during regulation experiments for each of the three participants. This was accomplished by tapping the arm of the leg extension machine during the steady-state response of a regulation experiment. The results of these experiments for
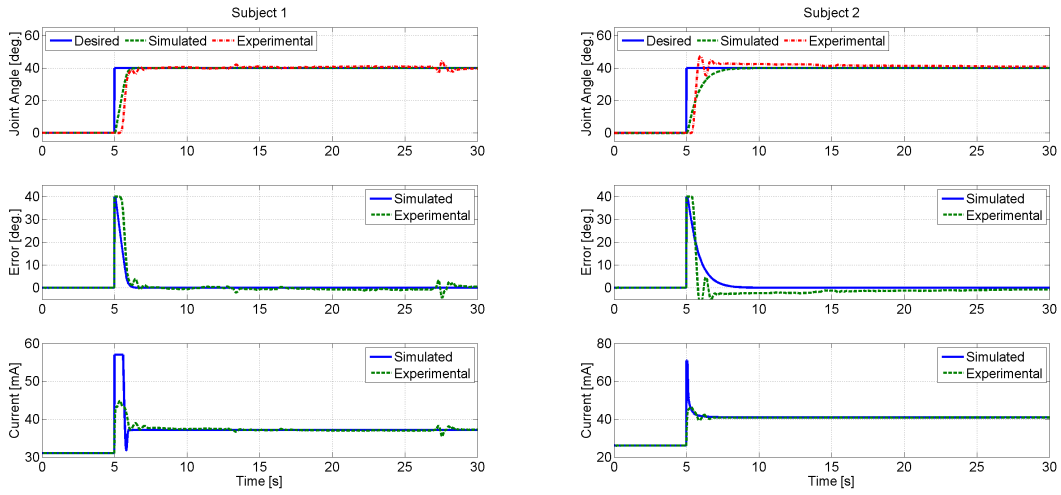
(a)

(b)
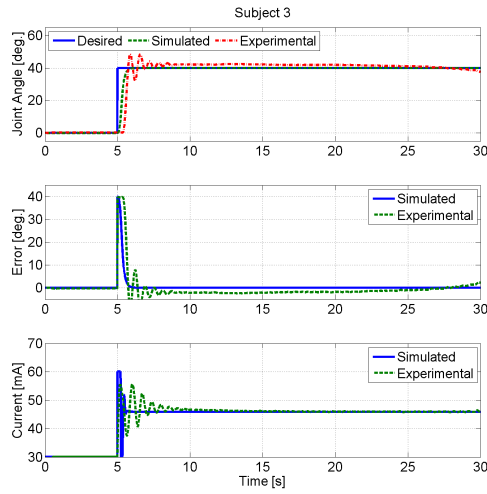
(c)

Figure 4.2: Results of NMPC of FES on three able-bodied participants. The experimental results were plotted with the simulation results, both using the same cost functions and subject parameters, to illustrate how the controller would perform in the ideal case of exact model knowledge.

Table 4.1: Transient (5-10 seconds) and steady-state (10-30 seconds) RMS errors from experimental trials of the NMPC for all three participants.

Participant ID	1	2	3
Transient RMS Error [deg.]	14.4	13.5	13.4
SSRMS Error [deg.]	0.841	1.45	1.71

all three participants are shown in Fig. 4.4. The individual conducting the experiments applied the disturbances at approximately 15 and 25 seconds during the experiments, and the disturbance torque was measured using the load cell that attaches the leg of the participant to the arm of the leg extension machine. It can be observed from Fig. 4.4 that the impulsive disturbances had a magnitude of approximately $10\,N\,m$, and the measured joint angles deviated only slightly from the desired joint angle at the instances that the disturbances were applied. The steady-state RMS errors during these experiments for all three participants are given in Table 4.3.

To determine if the NMPC was causing less muscle fatigue than typical feedback controllers by allocating the optimal stimulation, regulation experiments were performed with the NMPC and a PID controller on separate days. Since it can be shown that muscle fatigue can be approximately measured using normalized joint torques from isometric contractions (see Chapter 3), thirty second long isometric contraction tests were used immediately after each regulation experiment as a measurement of how much the muscles were fatigued. Since day-to-day variation in muscle force produced during an isometric contraction can occur a two second long isometric contraction test was used before each regulation experiment. The peak torques measured during the first isometric contraction tests were then used to normalize the joint torques measured during the isometric contraction tests that were performed after the regulation experiments. To ensure that muscle fatigue occurred during the experiments a 15lbs. weight was added to the arm of the leg extension machine and the experiments were conducted for one minute. To ensure that the added weight would not change the performance of the NMPC the mass and inertia parameters in the model of the
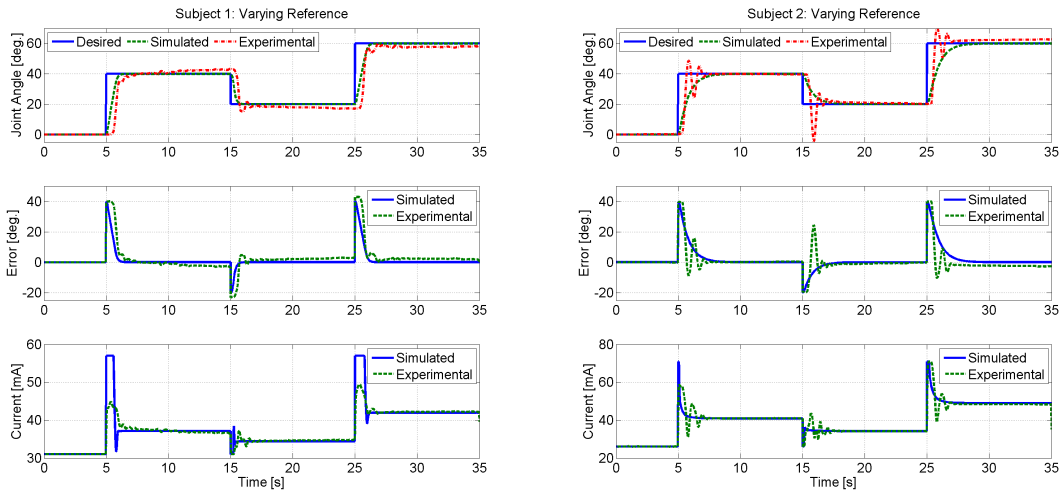
(a)

(b)
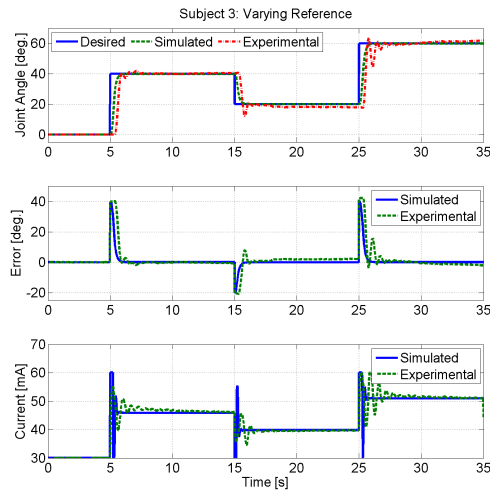
(c)

Figure 4.3: Simulations and experiments of the NMPC regulating the knee angle to different reference positions for three participants. The controller was given a reference of 40° for 5-15 seconds, followed by a reference of 20° for 15-25 seconds, and then a reference of 60° for 25-35 seconds.

Table 4.2: Transient and steady-state (SS) RMS errors calculated for the knee regulation experiments where the reference positions was varied.

Participant ID	1	2	3
Transient RMS Error (5-10s) [deg.]	15.0	13.0	13.6
SSRMS Error (10-15s) [deg.]	1.15	0.920	1.00
Transient RMS Error (15-20s)	10.8	8.40	6.72
SSRMS Error (20-25s) [deg.]	2.34	1.89	2.70
Transient RMS Error (25-30s) [deg.]	15.0	12.7	13.6
SSRMS Error (30-35s) [deg.]	3.44	2.51	1.38

controller were adjusted. The initial normalized isometric contraction, regulation experiment (NMPC and PID), and the final normalized isometric contraction for one of the participants are shown in Fig. 4.5.

The peak torque values of the isometric contractions before the regulation experiments were 69.6 N m and 73.9 N m for the NMPC and PID, respectively. The steady-state RMS values from the regulation experiments, shown in Fig. 4.5(b), were computed to be 3.70° for the PID controller and 6.17° for the NMPC. The RMS error of the NMPC in these experiments is approximately three times greater than the average RMS error of the first set of regulation experiments. This is clearly a result of the onset of muscle fatigue, whose effects become evident around approximately 30 s into the experiment. The RMS values of the current were computed to be 51 mA for the NMPC and 55 mA for the PID controller. These results illustrate that the PID controller was able to achieve better performance than the NMPC controller by increasing the current amplitude as fatigue occurred. Immediately after each regulation experiment an isometric contraction test was used to measure how much the muscles had fatigued. These are shown in Fig. 4.5(c). Since variation in muscle force can occur, the second isometric contraction test was conducted for 30 s and the integral of the normalized torque measurements were used as a metric for how much the muscles had fatigued. The normalized torque integral for the NMPC was computed to be 19.1 s, and the
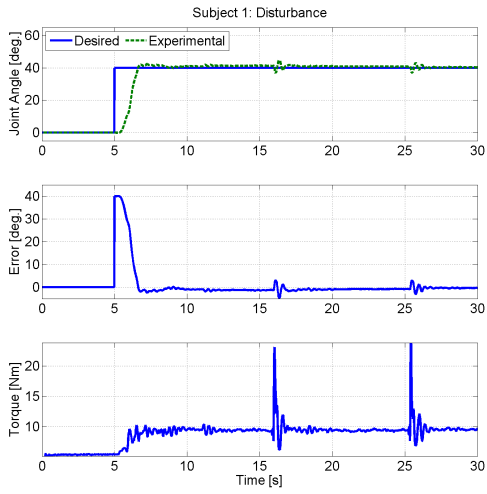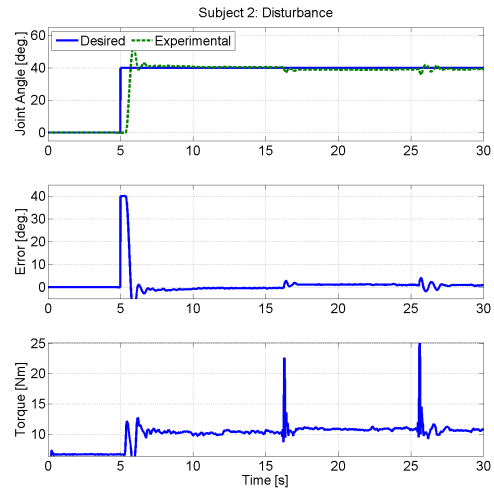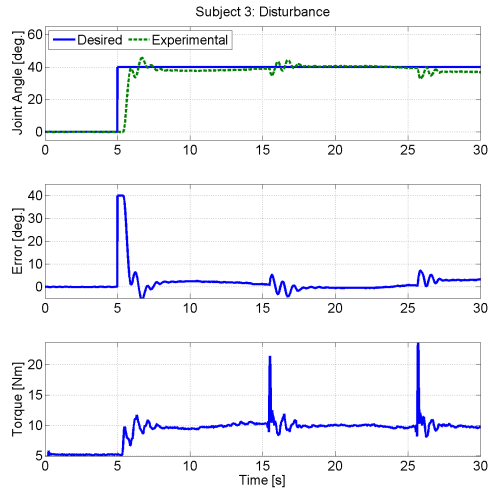
Figure 4.4: Results from disturbance rejection experiments. Impulse disturbances were applied by tapping the arm of the leg extension machine at approximately 15 and 25 seconds during a regulation experiment.

Table 4.3: Transient (5-10 seconds) and steady-state(SS) RMS (10-30 seconds) errors from experimental trials of the NMPC with impulse disturbances with a magnitude of approximately 10 N m at approximately 15 and 25 seconds during the experiments.

Participant ID	1	2	3
Transient RMS Error [deg.]	17.07	13.2	13.9
SSRMS Error [deg.]	1.12	1.03	2.05

normalized torque integral for the NMPC was computed to be 14.2 s. This demonstrates that the muscles were more fatigued after the PID regulation experiment than after the NMPC regulation experiment.

4.4   DISCUSSION

The results presented in this chapter illustrated that the NMPC can be implemented despite external disturbances and uncertainties in the identified muscle model. The settings used in the implementation of the NMPC algorithm resulted in an average computation time of 2.0 ms at each time step, which is faster than the sampling period of 10 ms that was used in the control. Modifications to the settings may be made to further decrease the computation time; however, the settings that were used were chosen because they yielded a sufficient computational precision and solve time. Although we were able to adjust the algorithm to allow for sufficiently fast computations time for this system, as the order and complexity of the system increases (more muscles and/or more degrees of freedom) other methods or modifications may need to be used to achieve a sufficiently fast computation time.

The muscle model used by the NMPC algorithm in this chapter is a Hill-type muscle model. However, other muscle models that may be simpler to identify or yield a more accurate model may be used instead. For example, other phenomenological muscle models, such as a Hill/Huxley type muscle model, may be used [25–27]. Also, non-phenomenological

81
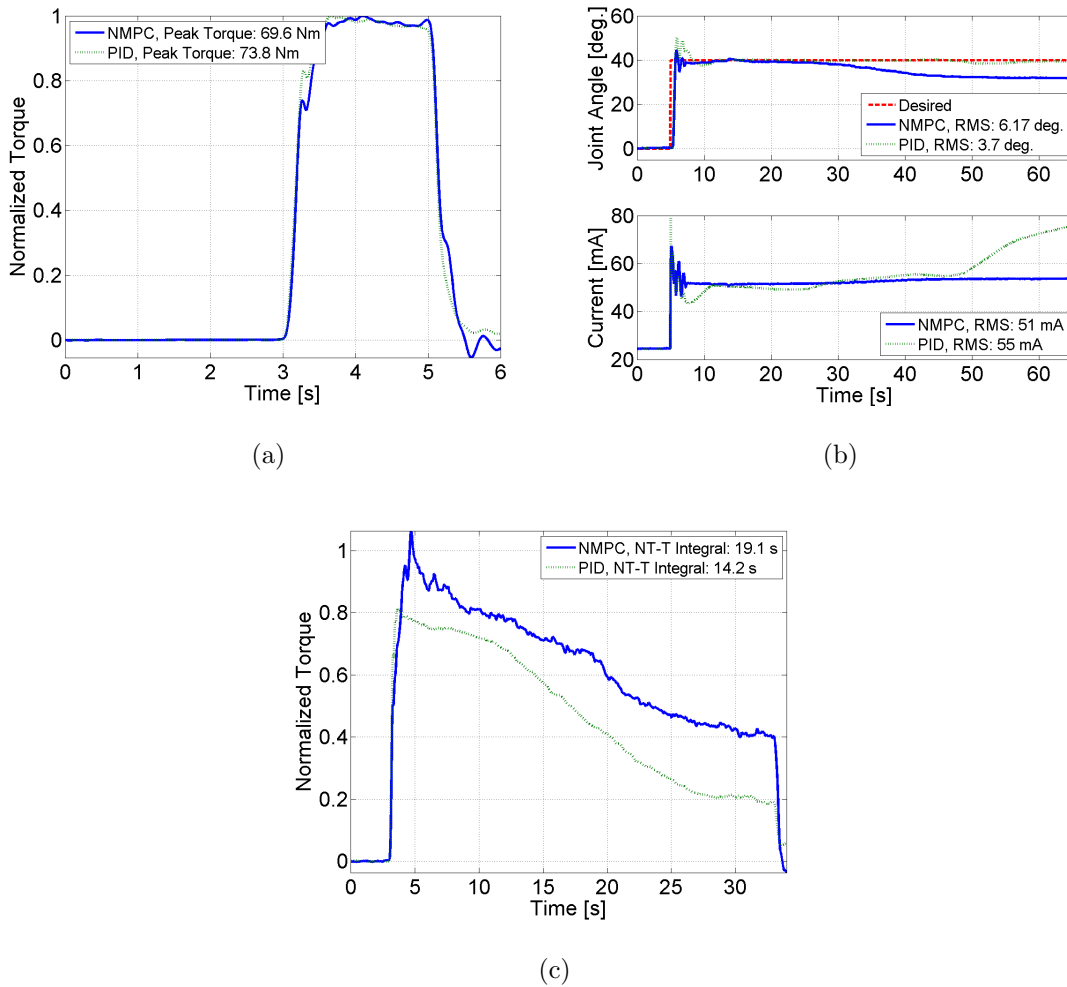
Figure 4.5: To determine if the NMPC controller reduces muscle fatigue, compared to traditional feedback controllers, a regulation test was performed with the NMPC controller and with a PID controller. The NMPC test and PID test were performed on separate days so that muscle fatigue during one test would not affect the other. Since muscle force can vary from day-to-day first an isometric contraction test is performed (a) so that the load cell measurement can be normalized. Then a 60 second long regulation test was performed (b). To determine how fatigued the leg was after the regulation experiment another isometric contraction test was performed (c). The load cell measurements from the second isometric contraction test is normalized by the peak torque from the first isometric contraction, and then the integral of the normalized force is used to determine how fatigued the muscle is. A lower normalized torque-time (NT-T) integral indicates more fatigue.

models, such as a Hammerstein model [42, 86], sigmoid functions [122], and neural networks [22], that have previously been used to model the muscles response to FES may be used by the NMPC algorithm.

This work can be extended to a complete gait system by using the models developed in [30, 110] that include models of hip, knee, and ankle flexors/extensors. Although the model used in this chapter is not immediately valid for walking many of the elements that were identified may remain valid. For example, the force-length and force-velocity relationships of the quadriceps muscles remain valid because they are independent of hip and ankle joint angles. If the ankle joints are fixed (perhaps by an orthosis) then the shank mass/inertial parameters would also remain valid. However, if the user wishes to use stimulation of the gastrocnemius and tibialis anterior to elicit dorsi/plantar flexion of the ankle joint then the mass/inertial parameters of the lower leg and foot would need to be estimated separately.

Although further results with a larger population size are necessary to determine statistical significance, these preliminary results indicated that NMPC may cause less muscle fatigue than feedback-based FES controllers. However, this comes at the cost of a decrease in performance. In the results presented in this chapter the isometric contractions after the NMPC experiment had a normalized torque-time integral of 19.1 s, while the isometric contraction after the PID experiment had a normalized torque-time integral of 14.2 s. This indicated that the muscle was more fatigued after the PID experiment than the NMPC experiment. Although the torque-time integral of the NMPC experiment was higher there was a noticeable drop in performance after 30 s in the regulation experiment while the performance of the PID controller remained approximately the same. The steady-state RMS error for the NMPC was computed to be 6.17°, while the steady-state RMS error of the PID controller was computed to be 3.70°. These results were somewhat expected, since the NMPC is minimizing a cost function that contains both performance (minimize error) and effort (minimize control). In this case performance and effort are conflicting terms (reducing error requires an increase in effort), and the NMPC solves for the control effort that achieves a balance between the two to minimize the overall cost function.

4.5 CONCLUSION

A gradient projection based NMPC was presented in this for regulating the knee joint angle through stimulation of the quadriceps muscles. The NMPC was validated through knee extension experiments on three able-bodied persons, whose musculoskeletal parameters had been identified in Chapter 2. The presented experimental results showed that the NMPC was capable of controlling stimulation of the quadriceps muscles to regulate the knee joint angle with a steady-state RMS error of approximately $2°$, even in the presence of an external disturbance and modeling uncertainties. These results also indicated that gradient projection based NMPC of FES can be implemented in real time with a sampling frequency of $100\,\mathrm{Hz}$.

In a later chapter the muscle fatigue model, which was used in Chapter 3, will be added to this model. This may allow the NMPC to increase the stimulation as muscle fatigue occurs, as the PID controller was able to do, since the muscle fatigue state can be included in the cost function. However, since increasing the amount of stimulation to maintain a desired position only exacerbate the effects of muscle fatigue an electric motor will also be added to the model and to the leg extension machine. The addition of the motor not only decreases the amount of stimulation required by performing some of the control effort, but it also be used to maintain performance as muscle fatigue occurs. Potentially, the NMPC algorithm can be used to determine the minimum amount of stimulation and motor torque necessary to create the gait motion in existing hybrid walking exoskeletons [23,37], and [55]. The results of this research will be used to inform the control of a hybrid (FES and electric motor) walking exoskeleton being developed in our laboratory [72].

Some future work, which is not presented in this dissertation, will explore robustifying techniques for MPC, such as tube-based MPC [99]. These techniques will make the MPC more robust to modeling errors/uncertainties and unmodeled dynamics, such as the electromechanical delay that has been observed in musculoskeletal systems [3, 125, 151]. Also, the feedback linearization technique used in [104] will be explored to allow for tracking control and to reduce computation time.

5.0 FATIGUE-BASED SWITCHING OF FUNCTIONAL ELECTRICAL STIMULATION AND AN ELECTRIC MOTOR

The major technical barrier to the successful implementation of FES-based rehabilitation systems is the rapid onset of muscle fatigue that results from the transcutaneous application of functional electrical stimulation (FES). Muscle fatigue is a decrease in the ability of a muscle to produce or sustain a force, which can be a result of many factors such as accumulation of metabolites within the muscle fibers or the limitations of the nerve's ability to sustain a muscle contraction. Few FES controllers, such as the one presented in Chapter 3, have been developed to maintain performance in the presence of muscle fatigue [74, 128]. These control designs, which model fatigue dynamics as a decreasing control gain, may delay the onset of muscle fatigue by using the fatigue dynamics in the feedforward control structure; however, pure reactionary based feedback control may further aggravate the muscle fatigue. The impending onset of muscle fatigue, which would decrease the control effectiveness, cannot be completely compensated by these controllers. Passive orthoses have been combined with FES-based systems to decrease the requirement for stimulation during standing and walking [61, 126, 139]; however, the duration that such devices may be used still remains limited.

Motorized lower extremity exoskeleton devices have recently been developed [35, 36, 107, 135, 136]. These devices may be capable of longer walking durations compared to systems that strictly use FES due to reliable torque generation at the powered joint. However, because of the duration of the use of such devices depends strictly on the capacity of the power source, these devices would need to use larger batteries to further increase their duration of use.

To overcome the muscle fatigue problem that greatly limits FES-based systems, and also to potentially reduce the size and weight of powered exoskeleton devices, hybrid gait restoration devices that use both FES and electric motors have been proposed [23, 55, 70, 112].

One challenge in controlling these hybrid devices is that the FES and motors are redundant actuators, and there is no unique solution as to choose how to allocate control between the FES and motors. In [113], an adaptive control scheme was used to allocate a portion of the control to FES, while the remainder of the control effort was allocated to the electric motors. In [23] and [55] a combination of PID and iterative learning control was used to control the FES, while the motors were controlled using joint angle feedback.

An alternative to using cooperative control of FES and electric motors is to switch between the two actuators. This technique is becoming increasingly popular in FES cycling to eliminate kinematic dead zones where the application of FES produces little or no torque to the crank of the cycle [60]. However, stabilization of such systems can be difficult, and it cannot be assumed that switching between two stable systems will result in a stable switching system [92]. In [10] a switching, first order sliding mode controller was used to switch stimulation on and off during FES cycling based on kinematic dead zones. This state dependent switching controller decreases muscle fatigue by switching stimulation off in domains where the application of FES has minimal contribution to generating the motion. A switching controller that switches based muscle fatigue, by using an estimate of fatigue from a phenomenological model as was done in Chapter 3, could be used for hybrid exoskeleton or FES-based stroke rehabilitation devices to switch from FES to electric motors. This would allow such systems to switch to motors when the muscle fatigue severely affects the users' ability to continue using the device, and switch back to FES once they have recovered.

In this chapter an asymptotically stable control system for a hybrid neuroprosthesis that switches between FES and an electric motor is presented. The developed controller uses feedback linearization to compensate for the nonlinear musculoskeletal dynamics, then a second order sliding mode controller is used to make the control robust to disturbances and uncertainties in the nonlinear system. The feedback linearization is also used to make the nonlinear tracking system a linear and time-invariant system to facilitate the stability analysis. Second order sliding mode control is used instead of first order to eliminate chattering, which can occur in first order sliding when due to the discontinuity in the control signal on the sliding surface [131]. To achieve second order sliding the variable-gain super twisting algorithm (VGSTA) is used. Through a Lyapunov stability analysis it is shown

that the switched system is asymptotically stable regardless of when the controller switched from using FES to the motor, or vice versa. The developed controller is simulated on a modified version of the leg extension neuroprosthesis model that was presented in Chapter 2. The modifications to the model include the addition of an electric motor at the knee joint, switched actuator dynamics, and the muscle fatigue model that was presented in Chapter 3. The switching between FES and motor will be determined using the estimate of the muscle fatigue state.

5.1 DYNAMIC MODEL OF SWITCHED SYSTEM

A hybrid neuroprosthesis that uses FES and an electric motor to produce knee extension movements, as is illustrated in Fig. 5.1, can be modeled as

$$J\ddot{q} + G - \tau_p + \tau_d = \tau, \tag{5.1}$$

where $q, \dot{q}, \ddot{q} \in \mathbb{R}$ are the angular position, velocity, and acceleration of the lower leg (shank and foot) relative to equilibrium, $J \in \mathbb{R}$ is the moment of inertia of the lower leg, and $G(q) \in \mathbb{R} = mgl_c \sin(q + q_{eq})$ is the gravitational torque. In the gravitational torque term $m \in \mathbb{R}$ is the mass of the lower leg, $g \in \mathbb{R}$ is gravitational acceleration, $l_c \in \mathbb{R}$ is the distance from the knee joint to the center of mass, and $q_{eq} \in \mathbb{R}$ is the equilibrium position of the lower leg relative to vertical as illustrated in Fig. 5.1. The torque acting on the knee joint, $\tau \in \mathbb{R}$, can be produced through the application of electrical stimulation of the quadriceps or the motor at the knee joint. Any unmodeled effects or disturbances, which are assumed to be bounded, are modeled in the dynamics as $\tau_d \in \mathbb{R}$

As previously presented in Chapter 2, the passive musculoskeletal torque of the knee joint, $\tau_p(q, \dot{q}) \in \mathbb{R}$, can be modeled as [110]

$$\tau_p = d_1(\phi - \phi_0) + d_2\dot{\phi} + d_3\mathrm{e}^{d_4\phi} - d_5\mathrm{e}^{d_6\phi}, \tag{5.2}$$

where the anatomical knee joint angle and angular velocity, $\phi, \dot{\phi} \in \mathbb{R}$, are defined as $\phi = \frac{\pi}{2} - q - q_{eq}$, $\dot{\phi} = -\dot{q}$. The parameters d_i, for $i = [1 - 6]$), and $\phi_0 \in \mathbb{R}$ are subject specific
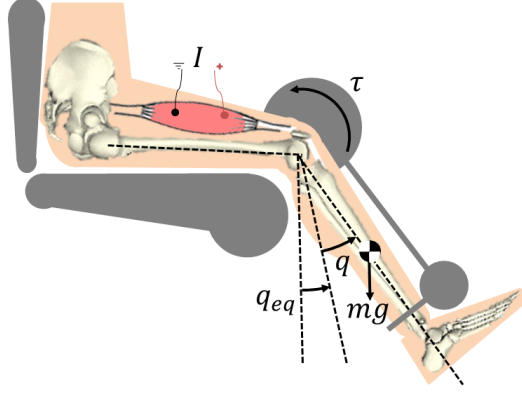
Figure 5.1: Illustration of a knee extension musculoskeletal model where q is the position of the shank relative to equilibrium. Movement of the shank can be actuated through the use of an electric motor torque, τ, or by applying a current, I, to the quadriceps muscles.

parameters that model the stiffness and damping of the knee joint. The exponential terms in τ_p model the resistivity of the leg to hyper-extension/flexion motions of the knee joint. Further details of these parameters, and how they may be estimated, can be found in Chapter 2.

The torque acting on the lower leg due to the application of FES or a torque at the knee joint produced by the motor can be expressed as

$$\tau = B_p u, \quad p \in \mathcal{P}, \tag{5.3}$$

where $B_p \in \mathbb{R}^{1 \times 2}$ for $p \in \mathcal{P}$ denotes the switched actuation dynamics and $\mathcal{P} = \{1, 2\}$ represents the set of switched control signals, and $u \in \mathbb{R}^2$ is the vector of inputs. Therefore, the dynamics of the switched system may be expressed as

$$J\ddot{q} + G - \tau_p + \tau_d = B_p u, \quad p \in \mathcal{P}. \tag{5.4}$$

For this system the vector of control inputs is defined as

$$u = \begin{bmatrix} u_k \\ u_m \end{bmatrix}, \tag{5.5}$$

where $u_k \in \mathbb{R}$ is the normalized stimulation of the quadriceps muscles, which assumes that muscle activation (see Chapter 2) is not present, and $u_m \in \mathbb{R}$ is the current amplitude to the electric motor. The switched actuation dynamics are

$$B_1 = \begin{bmatrix} \psi_l(\phi)\psi_v(\dot{\phi})\mu & 0 \end{bmatrix}, \; B_2 = \begin{bmatrix} 0 & K_m \end{bmatrix}, \tag{5.6}$$

where $K_m \in \mathbb{R}^+$ is the electric motor torque constant, $\psi_l(\phi) \in \mathbb{R}^+$ and $\psi_v(\dot{\phi}) \in \mathbb{R}^+$ model the torque-length and torque-velocity relationships of the quadriceps muscles, and μ models the muscle fatigue. The torque-length and torque-velocity relationships can be modeled as [57, 59, 116]

$$
\begin{aligned}
\psi_l(\phi) &= c_1 e^{-\frac{(\phi - c_2)^2}{2c_3}} \\
\psi_v(\dot{\phi}) &= c_4 \left[1 + \tanh\left(c_5 \dot{\phi} + \frac{1}{c_4} \right) \right],
\end{aligned}
$$

where the parameters $c_1, c_3, c_4, c_5 > 0$ and $c_2 \geq 0$ ensure that $\psi_l \psi_v > 0 \; \forall (\phi, \dot{\phi})$. Note that although these relationships differ from the ones presented in Chapter 2 they are still acceptable phenomenological models. The physical interpretation of these new relationships is that is that the muscles can only ever generate a positive (contractile) force. These new relationships satisfy this physical phenomenon, and are continuously differentiable.

The muscle fatigue dynamics can be modeled as [117]

$$\dot{\mu} = \frac{1}{T_f}(\mu_{\min} - \mu)u_k + \frac{1}{T_r}(1 - \mu)(1 - u_k), \tag{5.7}$$

where $\mu \in [\mu_{\min}, 1]$, and $\mu_{\min} \in (0, 1)$ is the minimum amount that the muscles can fatigue. Because the torque-length and torque-velocity relationships are greater than zero for all ϕ and $\dot{\phi}$, and the fatigue state is non-zero, it can be concluded that $\psi_l \psi_v \mu > 0 \; \forall (\phi, \dot{\phi})$. Therefore, it can be concluded that $B_p > 0 \; \forall p \in \mathcal{P}$. This relationship will be important when deriving the feedback linearization controller.

To switch between the FES and electric motor a switching signal, σ, is used. This allows the switched dynamics in (5.4) to be expressed as

$$J\ddot{q} + G - \tau_p + \tau_d = B_\sigma u_1, \tag{5.8}$$

where $u_1 \in \mathbb{R}$ is a scalar control signal and $B_\sigma \in \mathbb{R}$ is the switched actuation dynamics that are defined as

$$B_\sigma = \psi_l(\phi)\psi_v(\dot{\phi})\mu\kappa_k\sigma_k + K_m\kappa_m\sigma_m. \tag{5.9}$$

In the switched actuation dynamics $k_k \in \mathbb{R}^+$ and $k_m \in \mathbb{R}^+$ are positive control gains that proportionally scale the control signal for the FES and motors. The variables σ_k and σ_m are the switching signals for the stimulation and motors, respectively, which are defined as

$$\sigma_k = \begin{cases} 1, & \mu \notin \mathcal{F} \\ 0, & \mu \in \mathcal{F} \end{cases}, \quad \sigma_m = \begin{cases} 0, & \mu \notin \mathcal{F} \\ 1, & \mu \in \mathcal{F} \end{cases}. \tag{5.10}$$

In (5.10) the domain $\mathcal{F}$ is a region of muscle fatigue that defines when to switch from using FES to the electric motor, or vice versa. In other words, $\mathcal{F}$ can be defined such that when the muscles are considered to be too fatigued the controller will switch from using FES to using the motor. Note that due to how the switching signals are defined the FES and motor will never be used simultaneously. The subsequent stability analysis will show that the developed controller stabilizes the switched system regardless of the choice of the domain $\mathcal{F}$. Since $\mathcal{F}$ may be arbitrarily selected, to avoid the Zeno behavior that may occur from using a domain that is strictly defined by μ (e.g. for $\mathcal{F} = \{\mu \in [0, 0.5]\}$ infinitely fast switching may occur at $\mu = 0.5$) a domain defined by some switching logic will be used.
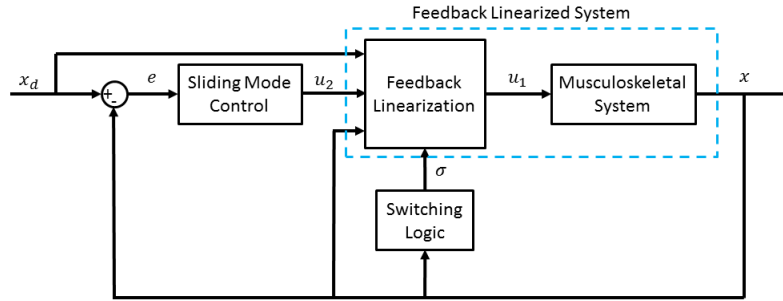
Figure 5.2: This block diagram illustrates the cascaded feedback linearization and sliding mode controller that is used to achieve stable switching between electrical stimulation and electric motors.

5.2   CONTROL DEVELOPMENT

The controller that is subsequently developed in this chapter will first use a feedback linearization to compensate for the nonlinear musculoskeletal dynamics, then a second order sliding mode controller will be used to stabilize the open-loop error dynamics and make the system robust to modeling uncertainties and disturbances. This cascaded control system is illustrated in Fig. 5.2. The feedback linearization is used to transform the nonlinear and time-varying tracking system into a linear and time-invariant system, which will facilitate the stability analysis. Second order sliding mode is achieved through the use of the VGSTA [131], which will yield exponential stability of the system when there is no switching. The exponential stability achieved by the cascaded control system will allow us to show that the switching control system has a common Lyapunov function [92]. From this we can conclude that the switched system is asymptotically stable.

5.2.1 Feedback Linearization

Let the error signals be defined as $e_1 = q_d - q$ and $e_2 = \dot{e}_1 = \dot{q}_d - \dot{q}$ where $q_d, \dot{q}_d \in \mathbb{R}$ are the desired position and velocity of the shank, respectively. Letting $e = [e_1 \; e_2]^T$ be defined as the states of the system and using the dynamics of the switched system in (5.8), the open-loop error dynamics can be expressed in state-space form as

$$
\begin{aligned}
\dot{e} &= f(e) + g_\sigma(e)u_1 + T_d, & (5.11)\\
y &= h(e) = e_1,
\end{aligned}
$$

where $\ddot{q}_d \in \mathbb{R}$ is the desired acceleration and $f(e) \in \mathbb{R}^2$, $g_\sigma(e) \in \mathbb{R}^2$, and $T_d \in \mathbb{R}^2$ are defined as

$$
f(e) = \begin{bmatrix} e_2 \\ \ddot{q}_d - \frac{1}{J}\left(\tau_p - G\right) \end{bmatrix}, \quad g_\sigma(e) = \begin{bmatrix} 0 \\ -\frac{1}{J}B_\sigma \end{bmatrix}, \tag{5.12}
$$

$$
T_d = \begin{bmatrix} 0 \\ \frac{\tau_d}{J} \end{bmatrix}. \tag{5.13}
$$

Because the relative degree of this system is of order two, the control signal that linearizes the system can be computed using Lie derivatives [69] as

$$
\begin{aligned}
u_1 &= \frac{1}{L_g L_f h(e)}\left[-L_f^2 h(e) + u_2\right] \\
&= -\frac{J}{B_\sigma}\left[-\ddot{q}_d + \frac{1}{J}\left(\tau_p - G\right) + u_2\right], \tag{5.14}
\end{aligned}
$$

where $u_2 \in \mathbb{R}$ is the control input to the feedback linearized system, as can be seen in Fig. 5.2. Note that if B_σ can be equal to zero then the control signal, u_1, becomes undefined. From the definition of B_σ in (5.9) it can be shown that $B_\sigma > 0$ for all joint angles and angular velocities. Therefore, the feedback linearization control signal is always defined.

The feedback linearization control signal in (5.14) reduces the nonlinear error dynamics in (5.11) to

$$
\dot{e} = Ae + B\left(u_2 + \frac{\tau_d}{J}\right), \tag{5.15}
$$

where

$$
A = \begin{bmatrix} 0 & 1 \\ 0 & 0 \end{bmatrix}, \quad B = \begin{bmatrix} 0 \\ 1 \end{bmatrix}. \tag{5.16}
$$

As can be observed from (5.15), after the feedback linearization the resulting system is linear, time-invariant. The modeling and system identification that is performed in Chapter 2 can be used to implement the feedback linearization control law. Note that any uncertainties or unmodeled dynamics are modeled included here as the disturbance torque, τ_d.

5.2.2 Variable-Gain Super-Twisting Sliding Mode Control

Let the sliding surface be defined as $s = e_2 + \alpha e_1 = 0$, where $\alpha \in \mathbb{R}^+$. When the motion is restricted to the sliding surface manifold the reduced order system will have dynamics $\dot{e}_1 = -\alpha e_1$, which results in exponential convergence of e_1 to zero when on the sliding surface.

Let the input to the linearized system be

$$u_2 = -\alpha e_2 + u_3, \tag{5.17}$$

where u_3 will be a sliding mode control law that will force the system to the sliding surface in finite time. By using (e_1, s) as the new state variables, the system in (5.15) becomes

$$\begin{align} \dot{e}_1 &= -\alpha e_1 + s \tag{5.18} \\ \dot{s} &= u_3 + \frac{\tau_d}{J} \end{align}$$

First order sliding mode control uses a discontinuous control signal, which allows the controller to respond quickly and makes it robust to disturbances. However, this discontinuous control signal results in a phenomenon that is referred to as chattering. To avoid the chattering phenomenon second order sliding mode control can be used instead of first order sliding mode control. To achieve second order sliding mode control in a system or relative degree two a VGSTA may be used. Let u_3 be the control signal from a VGSTA [131], which can be expressed as

$$\begin{align} u_3 &= -k_1(t,e)\phi_1(s) - \int_0^t k_2(\theta, e)\phi_2(s)d\theta, \tag{5.19} \\ \phi_1(s) &= |s|^{\frac{1}{2}}\text{sign}(s) + k_3 s, \\ \phi_2(s) &= \frac{1}{2}\text{sign}(s) + \frac{3}{2}k_3|s|^{\frac{1}{2}}\text{sign}(s) + k_3^2 s, \end{align}$$

93

where $k_1 \in \mathbb{R}^+$ and $k_2 \in \mathbb{R}^+$ are variable gain functions and $k_3 \in \mathbb{R}^+$ is a constant gain. Let $\phi_1' = \frac{\partial \phi_1}{\partial s}$ and note that

$$\phi_1 \phi_1' = \left(|s|^{\frac{1}{2}} \text{sign}(s) + k_3 s \right) \left(\frac{1}{2|s|^{\frac{1}{2}}} + k_3 \right) = \phi_2. \tag{5.20}$$

The variable gain functions, k_1 and k_2, can make the control robust to perturbations that grow without bounds and the constant gain k_3 allows the controller to deal with perturbations that grow linearly outside of the sliding surface. Because the VGSTA uses the integral of the discontinuous control signal instead of directly using the sign function the chattering phenomenon, which is present in first order sliding mode control, is attenuated.

Assume that the uncertainty/disturbance term, τ_d, can be expressed as

$$\frac{\tau_d(e_1, s - \alpha e_1, t)}{J} = g_1(e_1, s, t) + g_2(e_1, t) \tag{5.21}$$

where it is assumed that g_1 and g_2 can be written as [131]

$$g_1 = \alpha_1(t, e)\phi_1(s), \tag{5.22}$$
$$\dot{g}_2 = \alpha_2(t, e)\phi_2(s). \tag{5.23}$$

Then the linear system in (5.18) driven by the VGSTA in (5.19) can be expressed as

$$\begin{aligned} \dot{e}_1 &= -\alpha e_1 + s, \\ \dot{s} &= -k_1 \phi_1 + e_0 + g_1, \\ \dot{e}_0 &= -k_2 \phi_2 + \dot{g}_2, \end{aligned} \tag{5.24}$$

which is the closed-loop error dynamics of the linearized system. The new state, e_0, that is introduced in (5.24) results from the dynamics that are present in the VGSTA.

94

5.3 STABILITY ANALYSIS

Theorem 2. *The switched dynamic system is asymptotically stable for an arbitrary switching time given that the following variable gain functions of the variable-gain super-twisting algorithm, $k_1(e, t)$ and $k_2(e, t)$, are selected such that:*

$$k_2(e, t) > \alpha_2(e, t)$$

$$(k_1(e, t) - \alpha_1(e, t))^2 > k_2(e, t) - \alpha_2(e, t)$$

for all states e and time t, where α_1 and α_2 are defined in (5.22) *and* (5.23).

Proof. Let

$$V = \zeta^T P \zeta \tag{5.25}$$

which can be bounded as

$$\lambda_1 ||\zeta||^2 \leq V \leq \lambda_2 ||\zeta||^2 \tag{5.26}$$

be a positive definite and radially unbounded Lyapunov candidate, where $\zeta = \left[|s|^{\frac{1}{2}} \text{sign}(s) + \kappa_1 s \quad e_0 \right]^T$. $P \in \mathbb{R}^{2 \times 2}$ is a symmetric matrix, which is can be chosen as

$$P = \begin{bmatrix} 4p & 0 \\ 0 & p \end{bmatrix}, \tag{5.27}$$

where $p \in \mathbb{R}^+$. It can be shown that $\lambda_1, \lambda_2 \in \mathbb{R}^+$ in (5.26) are the minimum and maximum eigenvalues of P, respectively. Due to the symmetry of the matrix P, the derivative of V can be derived as

$$\dot{V} = 2\zeta^T P \dot{\zeta}. \tag{5.28}$$

Using (5.20)-(5.23) it can be shown that

$$\dot{\zeta} = \phi_1' \mathcal{A}(t, e) \zeta, \tag{5.29}$$

where

$$\mathcal{A}(t, e) = \begin{bmatrix} -(k_1 - \alpha_1) & 1 \\ -(k_2 - \alpha_2) & 0 \end{bmatrix}. \tag{5.30}$$

Therefore, (5.28) can be expressed as

$$\dot{V} = 2\phi_1' \zeta^T P \mathcal{A} \zeta = -\phi_1' \zeta^T Q \zeta \tag{5.31}$$

where $Q \in \mathbb{R}^{2 \times 2}$ is

$$Q = -2P\mathcal{A} = \begin{bmatrix} 8p(k_1 - \alpha_1) & -8p \\ 2p(k_2 - \alpha_2) & 0 \end{bmatrix}. \tag{5.32}$$

It can be shown that if the k_1 and k_2 functions are selected such that $k_2 > \alpha_2 \ \forall(e, t)$ and $(k_1 - \alpha_1)^2 > k_2 - \alpha_2 \ \forall(e, t)$, then both of the eigenvalues are always positive and $\epsilon_1 ||\zeta||^2 \le \zeta^T Q \zeta \le \epsilon_2 ||\zeta||^2$ where ϵ_1 and ϵ_2 are the minimum and maximum eigenvalues of Q, respectively. Using the bound on Q the time derivative of the Lyapunov function can be bounded as

$$\dot{V} = -\phi_1' \zeta^T Q \zeta \le -\epsilon_1 \phi_1' ||\zeta||^2 = -\epsilon_1 \left(\frac{1}{2|s|^{\frac{1}{2}}} + k_3 \right) ||\zeta||^2 \tag{5.33}$$

From the bounds on the Lyapunov candidate, given in (5.26), it can be shown that

$$\dot{V} \le -\frac{\epsilon_1 \lambda_1^{\frac{1}{2}}}{2\lambda_2} V^{\frac{1}{2}} - \frac{\epsilon_1 k_3}{\lambda_2} V, \tag{5.34}$$

For the sake of simplicity, let $a = \frac{\epsilon_1 \lambda_1^{\frac{1}{2}}}{2\lambda_2}$ and $b = \frac{\epsilon_1 k_3}{\lambda_2}$ in (5.34). Therefore, equation (5.34) can be written as

$$\dot{V} \le -aV^{\frac{1}{2}} - bV.$$

This differential equation can be solved using separation of variables as

$$\frac{dV}{dt} \le -aV^{\frac{1}{2}} - bV$$

$$-\frac{1}{aV^{\frac{1}{2}} + bV} dV \ge dt$$

$$-\int \frac{1}{aV^{\frac{1}{2}} + bV} dV \ge \int dt = t + C, \tag{5.35}$$

where C is the constant of integration.

To integrate the left hand side of (5.35) let $w_1 = V^{\frac{1}{2}}$ and $dw_1 = \frac{1}{2V^{\frac{1}{2}}}dV$, which results in

$$-2\int \frac{w_1}{aw_1 + bw_1^2}dw_1 = -2\int \frac{1}{a + bw_1}dw_1.$$

Using another change of variables, where $w_2 = a + bw_1$ and $dw_2 = bdw_1$, results in

$$-\frac{2}{b}\int \frac{1}{w_2}dw_2 = -\frac{2}{b}log(w_2). \tag{5.36}$$

From the definitions of the change of variables the right hand side of (5.36) can be written as a function of V as

$$-\frac{2}{b}log(w_2) = -\frac{2}{b}log(a + bw_1) = -\frac{2}{b}log\left(a + bV^{\frac{1}{2}}\right). \tag{5.37}$$

Putting (5.37) back into (5.35) results in

$$-\frac{2}{b}log\left(a + bV^{\frac{1}{2}}\right) \geq t + C. \tag{5.38}$$

From this equation, solving for V results in

$$V \leq \frac{1}{b^2}e^{-bt}\left[d - ae^{\frac{b}{2}t}\right]^2 \tag{5.39}$$

If we solve $V = \frac{1}{b^2}e^{-bt}\left[d - ae^{\frac{b}{2}t}\right]^2$ at $t = 0$ with the initial condition $V(0)$ then we get that $V(0) = \frac{d^2}{b^2}$. Therefore we can let $d = bV(0)^{\frac{1}{2}}$ and the inequality becomes

$$V \leq e^{-bt}\left[V(0)^{\frac{1}{2}} - \frac{a}{b}e^{\frac{b}{2}t}\right]^2 \tag{5.40}$$

By using the definitions of the variables a and b, the final solution of the differential inequality in (5.34) is

$$V(t) \leq e^{-\frac{\epsilon_1 k_3}{\lambda_2}t}\left[V(0)^{\frac{1}{2}} - \frac{\lambda_1^{\frac{1}{2}}}{2k_3}e^{\frac{\epsilon_1 k_3}{2\lambda_2}t}\right]^2. \tag{5.41}$$

Since $V(t)$ converges to zero in finite time it can be concluded that s and e_0 also converge to zero in finite time. Once the sliding surface has been reached the dynamic system (5.24) reduces to a single differential equation, $\dot{e}_1 = -\alpha e_1$, which has the solution $e_1(t) = e_1(0)e^{-\alpha t}$. Therefore, it can be concluded that the states of the system (s, e_0, e_1) exponentially decay to zero. Because this stability analysis bounds the switched system for any arbitrary switching it can be concluded that (5.25) is a common Lyapunov function for the family of switched

systems in (5.4). Therefore, because the system in the family (5.4) share a radially unbounded common Lyapunov function then from Theorem 2.1 in [92] it can be concluded that the switched system in (5.8) is globally uniformly asymptotically stable. It should also be noted that the common Lyapunov function determined in this stability analysis is not explicitly a function of any switching time or the switching dynamics. This means that switching of the system can be performed at any arbitrary time without invalidating the preceding stability analysis.

$\square$

5.4   SIMULATION RESULTS

The cascaded, switched control system presented in this chapter was simulated on a model of a musculoskeletal system with passive and activation muscle parameters that were estimated by [110] for a female participant with an SCI at the T10 level whose height and weight are $1.61 \, \text{m}$ and $52 \, \text{kg}$. The mass and inertial parameters were estimated using anthropometric data from [146] with the aforementioned height and weight. The muscle fatigue parameters used in the simulations were estimated by [117] for five persons with paraplegia.

In [110] a parabolic function was used to model the torque-length relationship, and a piece-wise continuous function was used to model the torque-velocity relationship. These were the relationships that were defined in Chapter 2, and used in the nonlinear model predictive control of FES in Chapter 4. However, for this controller an exponential function was used to model the torque-length relationship, and a hyperbolic tangent function was used to model the torque-velocity relationship. This was done so that the feedback linearization control signal, u_1, is always defined. A nonlinear least-squares curve fitting method was used to determine parameters for the new torque-length/velocity relationships. The new and old torque-length/velocity relationships are shown together in Fig. 5.3. The exponential torque-length relationship fit the parabolic torque-length relationship with a root mean square (RMS) error of $13.4 \, \text{N m}$, and the hyperbolic tangent torque-velocity relationship fit the piece-wise torque relationship with an RMS error of 0.0822.
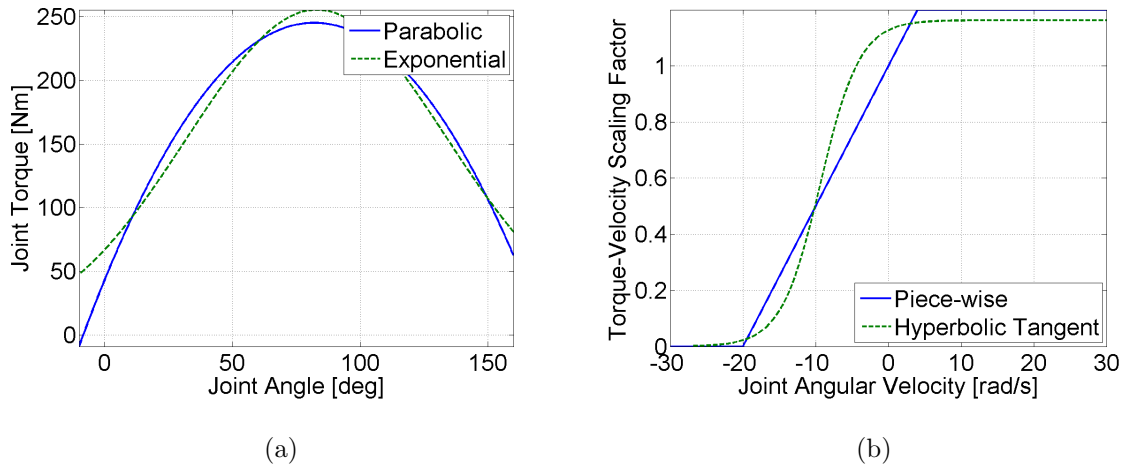
Figure 5.3: Nonlinear least-squares curve fitting was used to find the parameters of the exponential torque-length relationship from the parabolic torque-length relationship, and the parameters of the hyperbolic tangent torque-velocity relationship from the piece-wise torque-velocity relationship.

All of the parameters used in the simulation are given in Table 5.1. The control gains used in the cascaded control system are given in Table 5.2. To simplify tuning the controller, and because the disturbance torque does not grow without bounds, the variable gain functions, $k_1(e,t)$ and $k_2(e,t)$, were chosen to be constants.

The developed control was simulated on a musculoskeletal knee extension model to track a sinusoidal trajectory with a period of 4 seconds, a minimum and maximum shank angle of 10° and 50°, respectively. The switching fatigue domain, $\mathcal{F}$, is defined such that when the fatigue drops below 0.5 the control switches from the FES to the motor, and once the fatigue recovers to 0.9 it switches back to FES. This logic-based domain was selected to avoid a Zeno behavior that would occur if the domain was strictly defined by the fatigue state. The results of the simulation, using the control gains in Table 5.2, are shown in Fig. 5.4. The control was able to track the desired trajectory with an RMS error of 0.8024°. It can be observed that as muscle fatigue occurs more stimulation is required to produce the movement. This can be seen by the increase in the normalized stimulation in Fig. 5.4(b).

Table 5.1: Parameters used in the simulation of the cascaded, switched control system.

Parameter	J	m	l_c	d_1	d_2	d_3	d_4
Value	$0.275\,\mathrm{kgm^2}$	$6.09\,\mathrm{kg}$	$0.357\,\mathrm{m}$	17	0.6	0.005	5.048
Parameter	d_5	d_6	ϕ_0	c_1	c_2	c_3	
Value	98.57	-28.56	$0.5\,\mathrm{rad}$	$248.7\,\mathrm{N\,m}$	1.382	0.820	
Parameter	c_4	c_5	K_m	$\mu_{\min}$	T_f	T_r	
Value	0.587	1.105	$6\,\mathrm{N\,m/A}$	0.1	$2.9\,\mathrm{s}$	$28.5\,\mathrm{s}$	

Table 5.2: Control gains used in the simulation of the cascaded, switched control system.

Gain	α	k_1	k_2	k_3	κ_k	κ_m
Value	16.4	0.58	97.6	59.6	1	1

Note that the presented stability theorem does not place a restriction on gain k_3 of the VGSTA expressed in (5.19). When the variable gains, $k_1(e,t)$ and $k_2(e,t)$, are set to constant values and k_3 is set to zero the VGSTA equivalently becomes a super-twisting algorithm [131]. Therefore, if the uncertainty/disturbance terms, $\alpha_1(e,t)$ and $\alpha_2(e,t)$, can be bounded by constants then this stability proof is also a sufficient stability proof for super-twisting sliding mode control of the feedback linearized system. The advantage of using the additional gain term, $k_3 > 0$, is that it allows the VGSTA to compensate for perturbations that grow linearly outside of the sliding surface.

5.5 CONCLUSION

In this chapter a control scheme was presented that uses feedback linearization and second order sliding mode control for a hybrid FES/electric motor system. A Lyapunov stability analysis was used to determine sufficient gain conditions for the VGSTA that result in
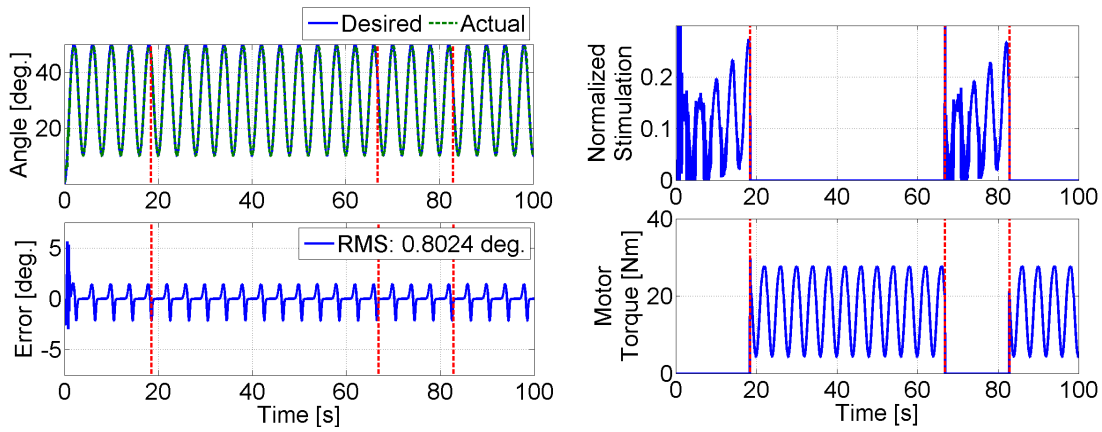
(a)

(b)
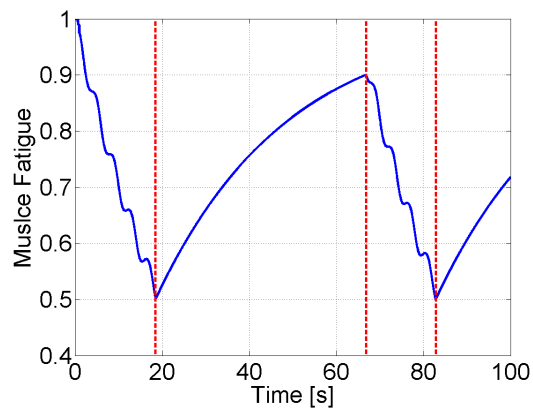
(c)

Figure 5.4: Results of the simulation of the cascaded, switched control system on a musculoskeletal model of knee extension. The vertical, red dashed lines indicate the times when the switching criteria is met and the controller switches from using FES to motor, or vice versa.

asymptotic tracking of the switched system. The developed control system was simulated on a musculoskeletal knee extension system to track a desired, sinusoidal shank angle. The simulations resulted in an RMS tracking error of $0.8024°$. Further research will validate the controller experimentally, and explore the robustness of the controller to variation in the estimated parameters of the system. To implement the switching control experimentally a model-based estimate of the fatigue state will be used.

6.0 NONLINEAR DYNAMIC CONTROL ALLOCATION OF A HYBRID NEUROPROSTHESIS

As was observed from the experimental results in Chapters 3 and 4, the only way that systems that strictly use electrical stimulation can compensate for the effects of muscle fatigue is by increasing the amplitude of the stimulation. However, increasing the amplitude of the stimulation only exacerbates the muscle fatigue, causing fatigue to occur even more rapidly and shortening the duration that neuroprostheses may be used. As previously mentioned in Chapter 1, some research has been done to develop actuated orthoses as an alternative to overcoming the challenge of FES-induced muscle fatigue. Actuated orthoses, or exoskeletons, such as the Vanderbilt exoskeleton [36], ReWalk [35], Mina [107], and EKSO [135, 136] are capable of walking durations that are significantly greater than what FES-based walking devices have been able to achieve. However, the duration that these devices may be used for strictly depends on the capacity of the power source. To achieve greater walking durations these devices would need to house larger batters, which would increase the size and weight of the devices. Also, these devices mostly use electric motors as the actuators, which can require a considerable amount of power to produce the torques necessary to produce the gait motion.

To overcome the challenge of rapid muscle fatigue caused by FES-based systems, and to potentially reduce the size, weight, and power consumption of powered exoskeleton devices, hybrid FES/exoskeleton gait restoration devices have been proposed [23, 55, 70, 112]. The challenge in controlling hybrid devices is that the FES and electric motors are redundant actuators. Therefore, the issue is how should control between the FES and electric motors be allocated. In [113], an adaptive control technique was tested to allocate control between a motor at the knee and stimulation of the quadriceps to produce a knee extension while

the subject was seated. From the calculations of the mechanical energy of the motor during knee extension motions with and without FES it was determined that the adaptive control technique yielded a 55.9% reduction in energy consumption. In [23] and [55] a hybrid neuroprostheses for gait restoration was controlled using a PID controller combined with an iterative learning controller was used to control FES, while the motors were controlled using joint angle feedback.

In Chapter 4 model predictive control (MPC) was used strictly for the control of FES. However, MPC can also be used to solve the control allocation problem by choosing how to allocate control to the redundant actuators based on the solution to a finite time optimal control problem [17,100]. When MPC is used in this way it is referred to as dynamic control allocation (DCA). Using DCA for the hybrid neuroprosthesis may allow us to use the minimal amount of electrical stimulation and motor torque to create the desired motion. Also, by including a model of muscle fatigue in the dynamics the DCA can allocate control from the FES to the electric motors as the muscles begin to fatigue; or conversely, the DCA can allocate control from the motors to the FES as the muscles recover.

In this chapter DCA of a hybrid neuroprosthesis using nonlinear model predictive control (NMPC) will be demonstrated through simulations of the leg extension model presented in Chapter 2. The model of the muscle fatigue dynamics that were introduced in Chapter 3 will also be used in the simulation model, as well as in the MPC. To solve the finite time optimal control allocation problem the gradient projection algorithm [50,67], which was used for NMPC of FES in Chapter 4, is also used here. This will allow the DCA that is performed in the simulations in this chapter to also be implemented in real time.
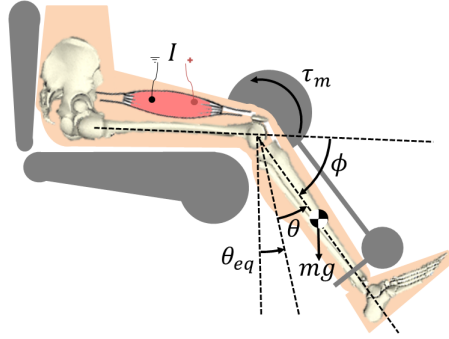
Figure 6.1: The hybrid leg extension neuroprosthesis uses a motor at the knee joint, τ_m, and electrical stimulation of the quadriceps muscles, I, to move the shank. The position of the shank relative to equilibrium is θ, and ϕ is the anatomical knee angle.

6.1 MODEL OF HYBRID NEUROPROSTHESIS SYSTEM

The dynamics of the hybrid leg extension neuroprosthesis system, illustrated in Fig. 6.1, can be modeled as

$$J\ddot{\theta} + G + \tau_p = \tau_m + \tau_{ke}, \tag{6.1}$$

where $\theta, \dot{\theta}, \ddot{\theta} \in \mathbb{R}$ are the angular position, velocity, and acceleration of the shank (lower leg and foot), respectively. The moment of inertia of the shank is $J \in \mathbb{R}^+$ and the gravitational term, $G \in \mathbb{R}$, is $G(\theta) = mgl_c \sin(\theta + \theta_{eq})$, where the variables $m, g, l_c \in \mathbb{R}^+$ are the mass of the shank, gravitational acceleration, and length from the knee joint to the center of mass of the shank, respectively. The torque $\tau_m \in \mathbb{R}$ is the torque of the motor, $\tau_p(\phi, \dot{\phi}) \in \mathbb{R}$ is the joint torque due to passive muscle dynamics, and $\tau_{ke}(\phi, \dot{\phi}, a_{ke}) \in \mathbb{R}$ is the knee extension torque due to stimulation of the quadriceps muscle. The passive joint torque can be expressed as a function of the anatomical knee joint angle, $\phi \in \mathbb{R}$, as [110]

$$\tau_p = d_1(\phi - \phi_0) + d_2\dot{\phi} + d_3 e^{d_4\phi} - d_5 e^{d_6\phi}, \tag{6.2}$$

105

where $d_i \in \mathbb{R} \forall i = \{1 - 6\}$ and $\phi_0 \in \mathbb{R}$ are subject specific parameters. The knee extension torque due to stimulation can be expressed as a function of the anatomical knee joint as [110]

$$\tau_{ke} = \left(c_2 \phi^2 + c_1 \phi + c_0 \right) \left(1 + c_3 \dot{\phi} \right) a_{ke} \mu, \tag{6.3}$$

where $c_j \in \mathbb{R} \forall j = \{1 - 3\}$ are subject specific parameters. The muscle activation, $a_{ke} \in [0, 1]$, in (6.3) can be modeled as [144]

$$\dot{a}_{ke} = \frac{u_{ke} - a_{ke}}{T_a}, \tag{6.4}$$

where $T_a \in \mathbb{R}^+$ is the muscle activation time constant. The normalized stimulation amplitude, $u_{ke} \in [0, 1]$ in (6.4), can be determined from the stimulation current amplitude, $I \in \mathbb{R}^+$, as

$$u_{ke} = \begin{cases} 0, & I < I_t \\ \frac{I_s - I}{I_s - I_t}, & I_t \leq I \leq I_s \\ 1, & I_s < I \end{cases} \tag{6.5}$$

where $I_t, I_s \in \mathbb{R}^+$ are the threshold and saturation limits of the muscle, respectively. The threshold current amplitude, I_t, is defined as the minimum stimulation amplitude required to produce the first significant muscle contraction. The saturation current amplitude, I_s, is defined as the minimum current amplitude that produces that maximum muscle contraction force.

The muscle fatigue, $\mu \in [\mu_{min}, 1]$ in (6.3), has dynamics that are dependent on the muscle activation and can be represented as [117]

$$\dot{\mu} = \frac{(\mu_{min} - \mu)a_{ke}}{T_f} + \frac{(1 - \mu)(1 - a_{ke})}{T_r}, \tag{6.6}$$

where $\mu_{min} \in (0, 1)$ is the minimum that the muscle can fatigue, $T_f \in \mathbb{R}^+$ is the fatigue time constant, and $T_r \in \mathbb{R}^+$ is the recovery time constant.

Using equations (6.1), (6.4), and (6.6) the dynamics of the hybrid neuroprosthesis system can be expressed in a state-space form as

$$\dot{x} = f(x, u) = \begin{bmatrix} x_2 \\ \frac{1}{J}(u_1 + \tau_{ke} - \tau_p - G) \\ \frac{u_2 - x_3}{T_a} \\ \frac{(\mu_{min} - x_4)x_3}{T_f} + \frac{(1 - x_4)(1 - x_3)}{T_r} \end{bmatrix}, \tag{6.7}$$

where $x = [x_1, x_2, x_3, x_4]^T = \left[\theta, \dot{\theta}, a_{ke}, \mu\right]^T$ are the states of the system and $u = [u_1, u_2]^T = [\tau_m, u_{ke}]^T$ are the inputs. To implement the gradient projection algorithm it is necessary that the state-space dynamics be continuously differentiable. From (6.7), it can be shown that $f(x, u)$ is in fact continuously differentiable.

6.2 GRADIENT PROJECTION DYNAMIC CONTROL ALLOCATION

The optimal control problem is stated as

$$\min_{u} \quad J(x, u) = V(\Delta x(T)) + \int_{t_0}^{T} l(\Delta x(\tau), \Delta u(\tau)) d\tau \tag{6.8}$$

$$\text{subject to:} \qquad \dot{x}(t) = f(x, u)$$

$$x(t_0) = x_0$$

$$u \in \mathcal{U}$$

where $J(x, u) \in \mathbb{R}^+$ is the cost function that will be minimized, $x_0 \in \mathbb{R}^4$ is the initial condition of the states, $\mathcal{U} = [u^-, u^+]$ are the bounds on u, t_0 is the initial time of the horizon, and T is the final time of the horizon. In the cost function $\Delta x = x_d - x$ where $x_d \in \mathbb{R}^4$ are the desired states, and $\Delta u = u_d - u$ where $u_d \in \mathcal{U}^2$ are the desired inputs. A quadratic cost function of the form

$$J(x, u) = \Delta x(T)^T P \Delta x(T) + \int_{t_0}^{T} \left(\Delta x(\tau)^T Q \Delta x(\tau) + \Delta u(\tau)^T R \Delta u(\tau) \right) d\tau \tag{6.9}$$

will be used as the cost function for the DCA. Therefore, it can be concluded from (6.8) and (6.9) that

$$
\begin{aligned}
V\left(\Delta x(T)\right) &= \Delta x(T)^T P \Delta x(T) \\
l\left(\Delta x(\tau), \Delta u(\tau)\right) &= \Delta x(\tau)^T Q \Delta x(\tau) + \Delta u(\tau)^T R \Delta u(\tau),
\end{aligned}
$$

where $P, Q \in \mathbb{R}^{4 \times 4}$ and $R \in \mathbb{R}^{2 \times 2}$ are positive definite and symmetric weight matrices that may be tuned to achieve the desired performance.

As was done in Chapter 4, a gradient projection-based method will be used for solving the optimal control allocation problem in (6.8). The gradient projection algorithm is summarized in Chapter 4, but for a detailed description of the algorithm see [49].

To ensure the stability of the gradient projection DCA a terminal cost, $V\left(x(T)\right)$, is used as a control Lyapunov function [62]. As was discussed in Chapter 4, a requirement for this terminal cost stabilization is that the set (x_{des}, u_{des}) are an equilibrium of $f(x, u)$. For the leg extension hybrid neuroprosthesis system presented in this chapter, given a desired joint angle the remaining elements of x_{des} and u_{des} can be solved from (6.7) as $f(x_{des}, u_{des}) = 0$. The control Lyapunov condition is approximately satisfied by solving the algebraic Riccati equation [49, 50]

$$
PA + A^T P - PBR^{-1} B^T P + Q = 0 \tag{6.10}
$$

for the gain matrix P, where the matrices $A \in \mathbb{R}^{4 \times 4}$ and $B \in \mathbb{R}^{4 \times 2}$ are the linearized state-space dynamics of the nonlinear system. The dynamics can be linearized using Jacobian

linearization about the desired states and control signals as

$$A = \left.\frac{\partial f(x,u)}{\partial x}\right|_{x=x_d,\ u=u_d}$$

$$= \begin{bmatrix} 0 & 1 & 0 & 0 \\ A_{21} & A_{22} & A_{23} & A_{24} \\ 0 & 0 & -\frac{1}{T_a} & 0 \\ 0 & 0 & A_{43} & A_{44} \end{bmatrix}$$

$$B = \left.\frac{\partial f(x,u)}{\partial u}\right|_{x=x_d,\ u=u_d}$$

$$= \begin{bmatrix} 0 & 0 \\ 1 & 0 \\ 0 & \frac{1}{T_a} \\ 0 & 0 \end{bmatrix}$$

where

$$\begin{aligned}
A_{21} = & -\beta\cos(x_d^{(1)} + \theta_{eq}) \\
& - \alpha\left[d_1 + d_3 d_4 e^{d_4(\frac{\pi}{2} - x_d^{(1)} - \theta_{eq})}\right. \\
& - d_5 d_6 e^{d_6(\frac{\pi}{2} - x_d^{(1)} - \theta_{eq})} \\
& + \left(2c_2\left(\frac{\pi}{2} - x_d^{(1)} - \theta_{eq}\right)\right. \\
& \left.\left. c_1\right)\left(1 - c_3 x_d^{(2)}\right) x_d^{(3)} x_d^{(4)}\right],
\end{aligned}$$

$$\begin{aligned}
A_{22} = & -\alpha\left[d_2 + (c_2(\frac{\pi}{2} - x_d^{(1)} - \theta_{eq})^2\right. \\
& \left. + c_1(\frac{\pi}{2} - x_d^{(1)} - \theta_{eq}) + c_0)c_3 x_d^{(3)} x_d^{(4)}\right],
\end{aligned}$$

$$\begin{aligned}
A_{23} = & \alpha\left[\left(c_2(\frac{\pi}{2} - x_d^{(1)} - \theta_{eq})^2\right.\right. \\
& + c_1\left(\frac{\pi}{2} - x_d^{(1)} - \theta_{eq}\right) \\
& \left.\left. + c_0)\left(1 - c_3 x_d^{(2)}\right) x_d^{(4)}\right],
\end{aligned}$$

109

$$A_{24} = \alpha \left[\left(c_2 (\frac{\pi}{2} - x_d^{(1)} - \theta_{eq})^2 \right. \right.$$
$$+ c_1 \left(\frac{\pi}{2} - x_d^{(1)} - \theta_{eq} \right)$$
$$\left. \left. + c_0 \right) \left(1 - c_3 x_d^{(2)} \right) x_d^{(3)} \right]$$

$$A_{43} = \frac{(\mu_{min} - x_d^{(4)})}{T_f} - \frac{(1 - x_d^{(4)})}{T_r}$$

$$A_{44} = -\frac{x_d^{(3)}}{T_f} - \frac{(1 - x_d^{(3)})}{T_r}$$

and $x_d^{(j)}$ for $j = \{1, 2, 3, 4\}$ is the jth element of x_d.

6.3   SIMULATIONS

The gradient projection algorithm based DCA was simulated on a hybrid neuroprosthesis leg extension model, whose dynamics are given in (6.7). The dynamics used by the gradient projection algorithm were equivalent to the dynamics used by the model. Therefore, this simulation reflects the exact model knowledge case.

The model used torque-length/velocity and viscoelastic muscle parameters that were estimated in [110] for a female participant with an SCI at the T10 level whose height and weight are $1.61\,\text{m}$ and $52\,\text{kg}$. The mass and inertial parameters were estimated using anthropometric data from [146] using the height and weight of the aforementioned SCI patient. The parameters of the muscle fatigue model that were used in the simulation were estimated by [117], and are the averaged results of five paraplegic participants. The parameters of the musculoskeletal model that were used in the simulations presented here are all given in Table 6.1.

The DCA was simulated for sixty seconds in Simulink (MathWorks, Inc.) with a sampling frequency of $100\,\text{Hz}$ using the same methods that were used in Chapter 4 to implement the NMPC of FES. This means that DCA may also be implemented in real-time. The horizon of the DCA was set to $0.5\,\text{s}$, an adaptive line search method was used to solve for the step size,

Table 6.1: Parameters used in the simulation of a hybrid neuroprosthesis using dynamic control allocation.

Parameter	α	β	θ_{eq}	ϕ_0	d_1	d_2
Value	$3.64\,/\mathrm{kgm}^2$	$64.1\,\mathrm{N/kgm}^2$	$0.561\,\mathrm{rad}$	$0.5\,\mathrm{rad}$	$17\,\mathrm{N\,m}$	$0.6\,\mathrm{N\,m\,s}$
Parameter	d_3	d_4	d_5	d_6	c_3	c_2
Value	$0.005\,\mathrm{N\,m}$	5.05	$98.6\,\mathrm{N\,m}$	-28.6	0.3	$-98.6\,\mathrm{N\,m}$
Parameter	c_1	c_0	T_a	$\mu_{\min}$	T_f	T_r
Value	$282\,\mathrm{N\,m}$	$43.2\,\mathrm{N\,m}$	$0.02\,\mathrm{s}$	0	$2.9\,\mathrm{s}$	$30\,\mathrm{s}$

Heun's method was used to integrate the dynamics, and trapezoidal integration was used to integrate the cost function. The Heun and trapezoidal numerical methods were chosen because they were found to be sufficiently accurate, and would allow for a faster solve time than if higher order methods were used.

The desired states and inputs used in the simulation are defined as

$$
x_{des} = \begin{cases} \begin{bmatrix} 0 \\ 0 \\ 0 \\ 1 \end{bmatrix}, & t < 2 \\ \begin{bmatrix} 40° \\ 0 \\ 0.083 \\ 0 \end{bmatrix}, & t \geq 2 \end{cases} \qquad u_{des} = \begin{cases} \begin{bmatrix} 0 \\ 0 \end{bmatrix}, & t < 2 \\ \begin{bmatrix} -10 \\ 0.083 \end{bmatrix}, & t \geq 2 \end{cases}, \tag{6.11}
$$

where the desired stimulation and motor torque were selected such that each actuator would contribute 50% of the torque required to make 40° an equilibrium position. The Q an R

weight matrices of the integral cost function were selected through tuning of their elements such that the desired performance was achieved. The weight matrices that were used in the simulation of the DCA were chosen to be

$$Q = \begin{bmatrix} 200 & 0 & 0 & 0 \\ 0 & 20 & 0 & 0 \\ 0 & 0 & 20 & 0 \\ 0 & 0 & 0 & 50 \end{bmatrix} \quad \text{and} \quad R = \begin{bmatrix} 1 & 0 \\ 0 & 20 \end{bmatrix}.$$

As was done for the NMPC of FES in Chapter 4, and mentioned previously in this chapter, a terminal cost was used in the simulation to ensure the stability of the gradient projection DCA. Using the parameters of the model, x_{des}, and u_{des} the matrices of the linearized dynamics were computed to be

$$A = \begin{bmatrix} 0 & 1 & 0 & 0 \\ -217 & -24.1 & -440 & -72.9 \\ 0 & 0 & -50 & 0 \\ 0 & 0 & -0.345 & -0.085 \end{bmatrix} \quad \text{and } B = \begin{bmatrix} 0 & 0 \\ 3.64 & 0 \\ 6.25 & 50 \\ 0 & 0 \end{bmatrix}. \tag{6.12}$$

From the weight matrices in (6.3) and the linearized A and B matrices the solution to the algebraic Riccati equation was computed to be

$$P = \begin{bmatrix} 65.5 & 0.381 & -0.513 & 14.9 \\ 0.381 & 0.162 & -0.318 & -0.189 \\ -0.513 & -0.318 & 1.20 & -0.203 \\ 14.9 & -0.189 & -0.203 & 424 \end{bmatrix}. \tag{6.13}$$

Because it can be shown that the matrices P, Q, and R are all positive definite it can be concluded that the quadratic cost function, of the form in (6.9), is strictly positive.

The simulation results of the DCA for regulation at a knee angle of 40° are shown in Fig. 6.2. The steady-state root mean square (RMS) of the error, which is defined as the RMS of the error from 5 s to 60 s, was computed to be 5.28°.
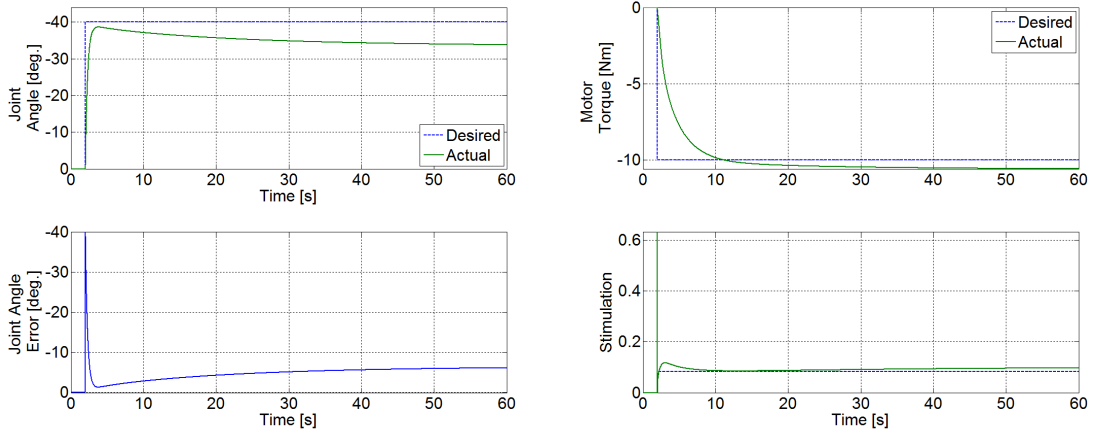
(a)

(b)
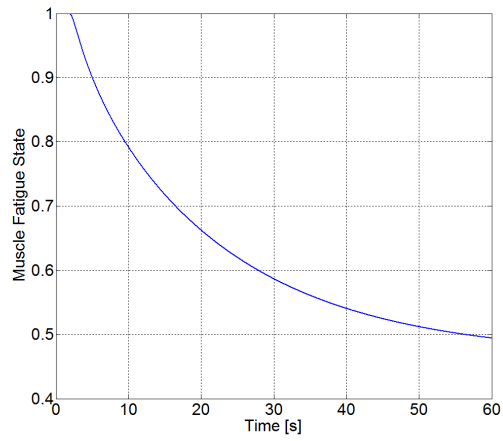
(c)

Figure 6.2: Results of the DCA simulation of a leg extension hybrid neuroprosthesis.

To illustrate the difference that the hybrid device can make in terms of inhibiting the muscle fatigue and its effects, NMPC of FES was simulated on the same musculoskeletal model using the same model and control parameters (note that $B = [0, 0, 50, 0]^T$ and $R = 20$ since FES is the only input). Unlike the simulation and experimental results presented in Chapter 4 the models used in this simulation of NMPC of FES the muscle fatigue dynamics have been included in the model. The results are shown in Fig. 6.3, which resulted in a steady-state RMS error of 28.7°.

6.4   CONCLUSION

This chapter illustrated how the gradient projection-based NMPC, which was first presented in Chapter 4, may be used for DCA in a hybrid neuroprosthesis. This was done through simulation of a hybrid neuroprosthesis leg extension model that used parameters estimated for an individual with SCI. NMPC of FES was also simulated using the SCI model parameters to illustrate the difference that the hybrid device can make in terms of inhibiting the muscle fatigue and maintaining regulation performance. From these results it can be observed that when the motor was not used the muscle fatigue state approximately reaches zero around 40 s, while the muscle fatigue state in the DCA simulation barely dropped below 0.5. Therefore, it may be concluded that the DCA induced approximately half as much muscle fatigue as when strictly FES is used. This allowed the DCA to maintain its performance significantly longer than the NMPC of FES, which resulted in a steady-state RMS error that was more than five times greater than the steady-state RMS error of the DCA. Further research will validate the controller experimentally through experimental trials on able-bodied persons and persons with SCI. As is the case with many of the control systems presented in this dissertation, the model parameter estimation procedures presented in Chapters 2 and 3 will need to be performed for each participant to implement the DCA in experiments.
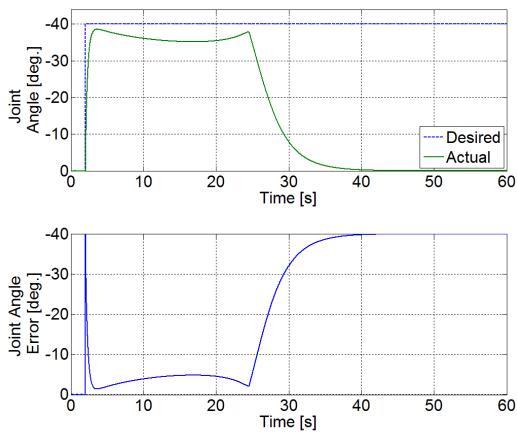
(a)
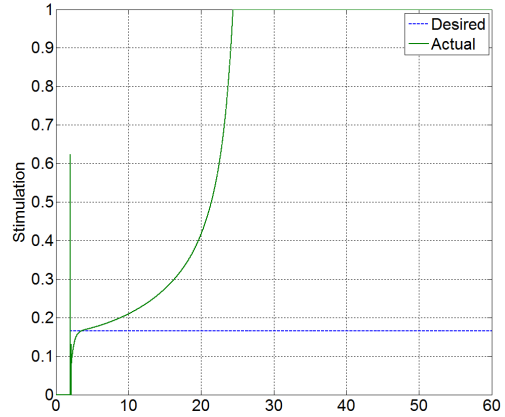
(b)
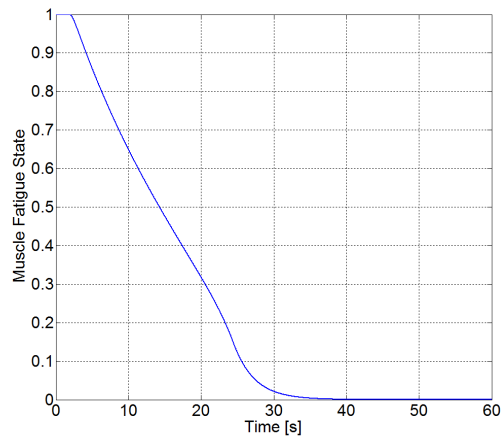
(c)

Figure 6.3: Results of the NMPC of a leg extension neuroprosthesis using the same model and control parameters as the DCA simulation.

7.0 DYNAMIC OPTIMIZATION OF A HYBRID NEUROPROSTHESIS FOR GAIT RESTORATION

The eventual goal of this research is to expand the control systems presented in this dissertation to a hybrid gait restoration device. The review of neuroprosthesis gait restoration devices in Chapter 1 showed that devices that strictly use functional electrical stimulation (FES) can only achieve limited walking durations. This is a result of the rapid muscle fatigue induced by trascutaneous stimulation. The muscles of paraplegic users can be trained using the FES to increase the duration that these devices may be used; however, on average persons with SCI that had been trained were still only able to achieve a walking distance of 100 m on average [76].

As an alternative to overcoming the challenge of rapid muscle fatigue fully actuated orthoses, or exoskeletons, have been developed. Exoskeleton devices such as the Vanderbilt exoskeleton [36], ReWalk [35], Mina [107], and Ekso (Ekso Bionics, Richmond, CA, USA) [135] have been shown to be capable of greater walking durations than FES-based devices. However, they are limited by the charge capacity of the batteries. Therefore, to achieve greater walking durations they would require larger, heavier batteries.

One method that shows promise for achieving greater walking durations is the combination of FES-based systems with exoskeletons. FES induced muscle contractions can produce large torques with little electrical power, and electric motors have consistent actuator dynamics that are not susceptible to fatigue. Therefore, by supplementing some of the torque required to produce the walking motion with electrical stimulation, smaller and lighter actuators may be used and the electrical power requirements of the device may be reduced. Thus producing a smaller, lighter, and more efficient device that may be used to restore

lower extremity functions to paraplegics. Little research has been done on combining FES with a lower extremity exoskeleton [23, 55, 113]. So far only the Vanderbilt exoskeleton has been combined with FES to explore the benefits of using a hybrid system [55, 56].

As was discussed in Chapters 5 and 6, the main problem that arises from using both FES and electric motors to restore the walking motion is that it creates a redundant actuation problem. In Chapter 5 this problem was solved using an estimate of the fatigue state to switch between FES and the electric motor as the muscles became too fatigued. In Chapter 6 DCA was used to allocate control between the FES and electric motors based on the solution to a finite-time optimal control problem. An adaptive control techniques was used in [113] to allocate control between stimulation of the quadriceps and an electric motor at the knee to produce a knee extension motion. In [23] and [55] an iterative learning controller was used to control stimulation of the quadriceps muscles while the motors of the exoskeleton were controlled using PID controllers with joint angle feedback during walking.

Of the aforementioned research on hybrid neuroprostheses that has been done to this point only Quintero et al. [113] assessed how much the energy efficiency may be improved by supplementing an exoskeleton with FES. This was done by computing the mechanical power of the motor during knee extension motions with and without FES. These results showed that a 55.9% energy reduction was achieved when FES was used with the electric motor. However, the mechanical energy is not equivalent to electrical energy, and the energy used by the FES was not measured or computed. Therefore, these results do not accurately approximate how supplementing an exoskeleton with FES may increase the overall electrical efficiency and potentially increase the duration that gait restoration devices may be used.

In this chapter forward dynamic optimizations of a four-link gait model are performed for three different actuation cases: FES only, electric motors only, and FES and electric motors combined (referred to as hybrid). These forward dynamic optimizations are similar to the DCA in Chapter 6 in the sense that they are both finite-time optimizations that compute how to allocate control to FES and electric motors to produce a desired functional movement. However, in these optimization the optimization is not solved at each time step of the control. Instead the optimization is performed for one complete step, then the resulting control signals are applied to the model. This work extends upon [71, 126] by using

a continuous dynamic model that includes modeling and actuation of the ankle and foot, as well as a ground reaction model. The results of the optimizations of the gait model for the three actuation cases will be compared and discussed. Specifically the energy consumption of the devices will be compared to show the potential of adding FES to exoskeleton systems to improve efficiency, and increase the duration that gait restoration devices may be used.

7.1   GAIT MODEL

One step of a gait cycle can be modeled as a fixed-free, four-link system as illustrated in Fig. 7.1 assuming that the motion occurs strictly in the sagittal plane, the position of the ankle of the stance leg is fixed, and the knee of the stance leg is locked by an orthosis. The locking of the knee joint of the stance leg simulates the use of an orthosis, such as a controlled brake orthosis [47, 48], which is used to reduce the stimulation required during standing or in between steps. This model also assumes that the user is capable of stabilizing their torso and propelling themselves forward using a walker. Therefore, the torso is not modeled as a rigid body; however, the mass of the head, arms, and trunk (HAT) are modeled as a point mass at the hip joints. Therefore, the model has five masses and four degrees of freedom.

The rigid body dynamics of the system described above, and illustrated in Fig. 7.1, can be defined as

$$M(q)\ddot{q} + C(q, \dot{q})\dot{q} + G(q) + \tau_p(q, \dot{q}) + \tau_g(q, \dot{q}) = \tau \tag{7.1}$$

where $q, \dot{q}, \ddot{q} \in \mathbb{R}^4$ are the angular position, velocity, and acceleration of the of the leg segments. The vector of positions is defined as $q = [q_1, q_2, q_3, q_4]^T$, where the elements of q, depicted in 7.1, are the absolute angles of the stance leg, upper leg, lower leg, and foot. The matrix $M(q) \in \mathbb{R}^{4 \times 4}$ is the mass/inertia matrix, $C(q, \dot{q}) \in \mathbb{R}^{4 \times 4}$ is the centripetal/Coriolis matrix, $G(q) \in \mathbb{R}^4$ is the gravity vector, and $\tau_p(q, \dot{q}) \in \mathbb{R}^4$ is the vector describing the viscoelastic dynamics of the muscles/ligaments.

The vector $\tau_g(q, \dot{q}) \in \mathbb{R}^4$ in (7.1) is the ground reaction torque, which can be modeled as a system of springs and dampers in the vertical direction and a friction model in the horizontal direction that acts on the points of contact on the foot when they reach the level
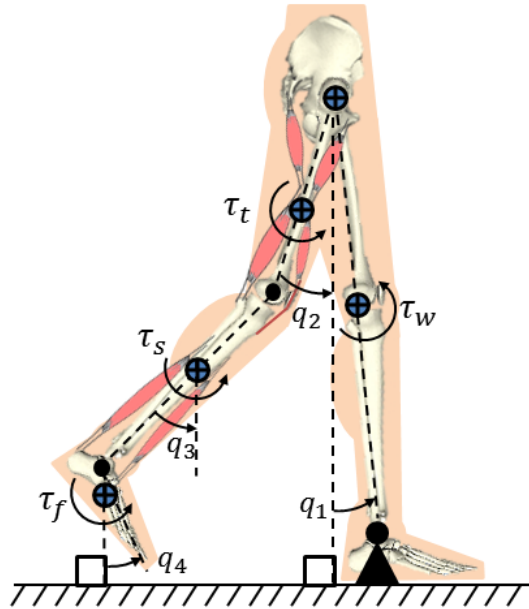
Figure 7.1: This figure illustrates the four-link gait model that was used to compute optimal motor joint torques and electrical stimulations. It is assumed that the position of the ankle of the stance leg is fixed, and the knee joint of the stance leg is locked using an orthosis. The model allows for electric motors at the hip, knee, and ankle joints as well as stimulation of hip flexors/extensors, knee flexors/extensors, and ankle plantar/dorsiflexion.
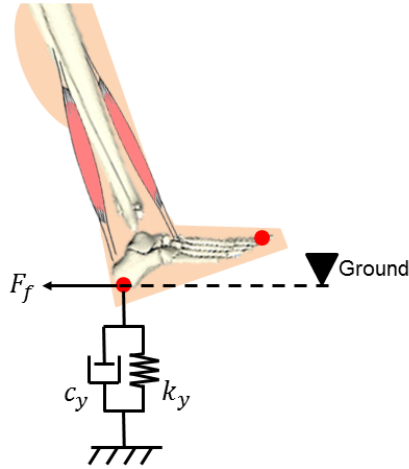
Figure 7.2: The interactions of the foot of the swing leg with the ground can be modeled as a system of spring mass dampers acting on the points of contact on the foot, which in this model are at the heel and toe, in the vertical direction and a friction model in the horizontal direction. The friction force, F_f, is modeled here using a Coulomb friction model.

of the ground [43]. The spring/damper system that models the ground reaction force has an equilibrium at the height of the ground in the vertical direction. In this model the points of contact on the foot are defined as the heel and toe of the foot of the swing leg, and the friction is modeled using a Coulomb friction model. The ground reaction model is illustrated in Fig. 7.2, which shows the heel of the swing leg in contact with the ground. Since the toe of the foot in Fig. 7.2 is above the ground, there is no ground reaction force acting on the foot at the toe. For a detailed description of the ground model see [43, 54, 108].

The passive viscoelastic torques at the joints that are caused by the muscles and ligaments, defined as τ_p in (7.1), can be modeled at each joint from [110] as

$$\tau_{pi} = d_{i1} \left(\phi_i - \phi_{i0} \right) + d_{i2} \dot{\phi}_i + d_{i3} \mathrm{e}^{d_{i4} \phi_i} - d_{i5} \mathrm{e}^{d_{i6} \phi_i},$$

where $\phi_i, \dot{\phi}_i \in \mathbb{R}$ for $i = \{h, k, a\}$ denotes the anatomical joint angle and angular velocity of the hip (h), knee (k), and ankle (a). The anatomical joint angles can be computed from the

120

absolute angles as

$$\phi_h = q_2$$
$$\phi_k = q_2 - q_3$$
$$\phi_a = q_4 - q_3 - \frac{\pi}{2}$$

The parameters d_{ik} for $i = \{h, k, a\}$ and $k = \{1 - 6\}$ are constants that depend on the subject. The parameters d_{i1} and ϕ_{i0} determine the linear stiffness of the joint, while the exponential functions are nonlinear stiffnesses that model the exponential increase in the stiffness of the joint in the regions of hyperextension and hyperflexion. The parameter d_{i2} models the damping of the musculotendon system at each joint. These parameters can be estimated for all three joints using the push/pull test and pendulum test that were presented in Chapter 2. From the passive torques at each of the joints, the vector that describes the viscoelastic dynamics of the muscles/ligaments is defined as

$$\tau_p = \begin{bmatrix} 0 \\ \tau_{ph} + \tau_{pk} \\ -\tau_{pk} + \tau_{pa} \\ -\tau_{pa} \end{bmatrix}.$$

In (7.1) the torque vector, $\tau \in \mathbb{R}^4$, is the vector of inputs to the system. The inputs to the system are electrical stimulation of the flexor/extensor muscles, motor torques at the joints, and a moment acting on the stance leg that models the use of a walker to assist in propelling the user forward. Assuming that all of these inputs are present the vector of input torques can be defined as $\tau = Bu$, where $B \in \mathbb{R}^{4 \times 10}$ and $u \in \mathbb{R}^{10}$ are defined as

$$
B = \begin{bmatrix}
1 & 0 & 0 & 0 & 0 & 0 \\
0 & K_m & K_m & 0 & \psi_{hf}\mu_{hf} & -\psi_{he}\mu_{he} \\
0 & 0 & K_m & K_m & 0 & 0 \\
0 & 0 & 0 & K_m & 0 & 0
\end{bmatrix}
$$

$$
\begin{bmatrix}
0 & 0 & 0 & 0 \\
\psi_{kf}\mu_{kf} & -\psi_{ke}\mu_{ke} & 0 & 0 \\
-\psi_{kf}\mu_{hf} & \psi_{ke}\mu_{ke} & \psi_{af}\mu_{af} & -\psi_{ae}\mu_{ae} \\
0 & 0 & -\psi_{af}\mu_{af} & \psi_{ae}\mu_{ae}
\end{bmatrix}
\tag{7.2}
$$

$$
u = \begin{bmatrix} \tau_w \\ u_m \\ u_s \end{bmatrix}.
$$

In (7.2) $K_m \in \mathbb{R}^+$ is the torque constant of the motors at the joints, and ψ_{ij} and μ_{ij} for $i = \{h, k, a\}$ and $j = \{f, e\}$ are functions that model the torque-length/velocity relationships and muscle fatigue of the flexor (f) and extensor (e) muscles at the hip, knee, and ankle joints. In (7.2), $\tau_w \in \mathcal{U}_w$ is the walker torque, $u_m \in \mathcal{U}_m^3$ is the vector of motor currents, and $u_s \in \mathcal{U}_s^6$ are the normalized muscle stimulations. The walker torque is bounded by the set $\mathcal{U}_w \subset \mathbb{R}$, which can be set to a reasonable bound based on the strength of a typical person. The motor currents are bounded by the set $\mathcal{U}_m \subset \mathbb{R}$, which depends on the motors being used in the exoskeleton or the power available.

The electrical stimulations used by the model, u_s, are normalized stimulations, which are bounded by the set $\mathcal{U}_s = [0, 1]$. The normalized stimulation can be thought of as the percentage of a corresponding muscle group that is recruited, where 0 means that no muscles are recruited (no force) and 1 means that 100% of the muscles are recruited (maximum force). This normalization is performed based on the stimulation current amplitude and can be computed as

$$
u_s = \begin{cases}
0, & I < I_t \\
\frac{I - I_t}{I_s - I_t}, & I_t \leq I \leq I_s \\
1, & I_s < I
\end{cases}
\tag{7.3}
$$

where $I \in \mathbb{R}^+$ is the stimulation current amplitude, $I_t \in \mathbb{R}^+$ is the threshold current amplitude, and $I_s \in \mathbb{R}^+$ is the saturation current amplitude. The threshold is the lowest current amplitude that produces the first significant muscle contraction, and the saturation is the lowest current amplitude that produces an increase in the muscle force generated. These values may be arbitrarily set in the optimizations, therefore this mapping is neglected during the optimizations to reduce calculations. The saturation and threshold parameters may be estimated using the methods presented in Chapter 2.

One of the goals of these simulations is to evaluate the potential of a hybrid gait restoration system to reduce the power required to create the walking motion compared to exoskeleton devices. To compute the electrical power used by stimulation assumptions will be made based on typical pulse trains and current amplitudes used in FES gait restoration devices, such as the Parastep system [76]. Since the stimulation commonly used in FES is not a continuous current, but instead a rectangular pulse train with a width of $w_p \in \mathbb{R}^+$ and a frequency of $f_s \in \mathbb{R}^+$, if the resistance of the skin, $R_s \in \mathbb{R}^+$, is known the electrical power used by each muscle stimulated can be computed as

$$P_{ij} = (f_s w_p I_{ij})^2 R_s, \tag{7.4}$$

where $I_{ij} \in \mathbb{R}^+$ is the stimulation amplitude of each muscle group computed from the inverse of (7.3).

In (7.2), $\psi_{ij}(\phi_i, \dot{\phi}_i)$ for $i = \{h, k, a\}$ and $j = \{f, e\}$ are functions of the anatomical joint angles and angular velocities that model the torque-length/velocity relationships of the hip, knee, and ankle flexors/extensors. From [30, 110] these functions are modeled as

$$\psi_{ij} = \left(c_{ij2}\phi_i^2 + c_{ij1}\phi_i + c_{ij0} \right) \eta_{ij}(\dot{\phi}_i)$$

where $\eta_{ij}(\dot{\phi}_i)$ is the torque-velocity relationship. The torque-velocity relationship can be modeled for flexion as

$$\eta_{if} = \begin{cases} c_{if4}, & \dot{\phi}_i < (1 - c_{if4})/c_{if3} \\ 1 - c_{if3}\dot{\phi}_i, & (1 - c_{if4})/c_{ij3} \le \dot{\phi}_i < 1/c_{if3} \\ 0, & 1/c_{ij3} \le \dot{\phi}_i \end{cases},$$

123

while for extension it is modeled as

$$\eta_{ie} = \begin{cases} 0, & \dot{\phi}_i < -1/c_{ie3} \\ 1 + c_{ie3}\dot{\phi}_i, & -1/c_{ie3} \leq \dot{\phi}_i < (c_{ie4} - 1)/c_{ie3} \\ c_{ie4}, & (c_{ie4} - 1)/c_{ie3} \leq \dot{\phi}_i \end{cases} \cdot$$

In the torque-length and torque-velocity relationships c_{ijk}, for $k = \{0 - 5\}$, are constant parameters. The two different torque-velocity relationships model the change in muscle force production during eccentric (muscle lengthening) and concentric (muscle shortening) muscle contractions.

The muscle fatigue of each muscle, μ_{ij} for $i = \{h, k, a\}$ and $j = \{f, e\}$ in (7.2), can be modeled as [117]

$$\dot{\mu}_{ij} = \frac{1}{T_{ij,f}}(\mu_{ij,\min} - \mu_{ij})u_{ij} + \frac{1}{T_{ij,r}}(1 - \mu_{ij})(1 - u_{ij}), \tag{7.5}$$

where $\mu_{ij} \in [\mu_{ij,\min}, 1]$ and $\mu_{ij,\min} \in (0, 1)$ is the minimum amount that the muscles can fatigue. Each muscle is considered to be fully rested when $\mu_{ij} = 1$ and fully fatigue when $\mu_{ij} = \mu_{ij,\min}$. The parameters $T_{ij,f}$ and $T_{ij,r}$ in (7.5) are time constants of the differential equation that model each muscles rate of fatigue and recovery, respectively. For persons with SCI, who suffer from muscle atrophy, the fatigue time constants tend to be significantly lower than able-bodied persons. In other words their muscle fatigue more rapidly than able-bodied persons, which greatly limits the duration that FES-based gait restoration devices may be used [44].

7.2 DYNAMIC OPTIMIZATION

Dynamic optimizations were used to compute the optimal control inputs to the previously described gait model to produce one step for three actuation cases: stimulation only, motors only, and hybrid (stimulation and motors). For all three actuation cases the optimal control problem can be expressed as

$$\min_{u} \quad J(u) = \int_{t_0}^{t_f} \left(u(\tau)^T R u(\tau) \right) d\tau \tag{7.6}$$

$$\text{subject to:} \qquad \dot{x}(t) = f(x, u)$$

$$x(t_0) = x_0$$

$$q(t_f) = q_f$$

$$\tau_w \in \mathcal{U}_w$$

$$u_s \in \mathcal{U}_s^6$$

$$u_m \in \mathcal{U}_m^3$$

where $J(u) \in \mathbb{R}$ is the cost function that we want to minimize. In the cost function t_0 is the time at which the step begins, t_f is the time at which the step is completed, and $R \in \mathbb{R}^{10 \times 10}$ is a positive definite weight matrix. For the stimulation only case all motor control signal are set equal to zero (i.e. $u_m = 0, \forall t \in [t_0, t_f]$), while for the motor only case all stimulation control signal are set equal to zero (i.e. $u_s = 0, \forall t \in [t_0, t_f]$).

In the constraints of the optimal control problem $\dot{x}(t) = f(x, u)$ are the dynamics of the system from (7.1) and (7.5) in a state space formulation, where the states and their initial conditions are defined as

$$
x = \begin{bmatrix} q_1 \\ q_2 \\ q_3 \\ q_4 \\ \dot{q}_1 \\ \dot{q}_2 \\ \dot{q}_3 \\ \dot{q}_4 \\ \mu_{hf} \\ \mu_{he} \\ \mu_{kf} \\ \mu_{ke} \\ \mu_{af} \\ \mu_{ae} \end{bmatrix} \quad \text{and} \quad x_0 = x(t_0) = \begin{bmatrix} \alpha \\ -\alpha \\ -\alpha \\ \frac{\pi}{2} \\ 0 \\ 0 \\ 0 \\ 0 \\ \mu_{hf,0} \\ \mu_{he,0} \\ \mu_{kf,0} \\ \mu_{ke,0} \\ \mu_{af,0} \\ \mu_{ae,0} \end{bmatrix} ,
\tag{7.7}
$$

where the angle α is determined from the step length, L_s, and the length of the leg (thigh and shank), L_l, from the equation $\alpha = \sin^{-1}\left(\frac{L_s}{2L_l}\right)$. The values for L_s and L_l can be determined from anthropometric data based on the height of the individual, H, as $L_s = 0.447H$ and $L_l = 0.491H$ [105, 146]. From these relations α can be expressed as a constant value as $\alpha = \sin^{-1}(0.455) = 0.472\,\mathrm{rad}$. The initial condition in (7.7) models the person starting flat footed with feet apart by a distance L_s starting from rest. The initial conditions of the muscle fatigue states, $\mu_{ij,0}$ for $i = \{h, k, a\}$ and $j = \{f, e\}$, are all set equal to one on the first simulated step. In other words on the first step it is assumed that all muscle groups are fully rested. On subsequently simulated steps the muscle fatigue states are initialized with the values at the end of the previous step. It is unnecessary to constrain the angular velocities and muscle fatigue at the end of the step, therefore only the terminal angular positions are

constrained to ensure that one step is completed. The terminal position constraint in (7.6) was defined in the optimizations as

$$
q_f = \begin{bmatrix} -\alpha \\ \alpha \\ \alpha \\ \frac{\pi}{2} \end{bmatrix},
\tag{7.8}
$$

which models the person completing their step flat footed with feet apart by a distance L_s.

The control signals are bounded in the constraints given in (7.6) to mimic the physical limitations on the electrical stimulations, electric motors, and assistance from the walker. In the optimizations the normalized stimulations are bounded by the set $\mathcal{U}_s = [0, 1]$. The motor torques are bounded by the set $\mathcal{U}_m$, which depends on the motors that are being used at the joints of the exoskeleton. The walker torque is bounded by the set $\mathcal{U}_w$, which depends on the strength of the individual using the device.

7.3 RESULTS OF DYNAMIC OPTIMIZATIONS

The aforementioned gait model was modeled in Simulink and optimized using Matlab's fmincon function (MathWorks, Inc.) for the stimulation only, motor only, and hybrid (stimulation and motor) actuation cases. The optimizations were performed for 100 steps with each step was completed in 0.75 s (i.e. for each optimized step $t_f - t_0 =0.75\,\text{s}$). The parameters of the active and passive muscle torques that were used in the model are parameters estimated from an SCI patient as presented in [110] for the hip and knee joint and [5] for the ankle joint. The muscle fatigue parameters ($\mu_{ij,\text{min}}$, $T_{ij,f}$, and $T_{ij,r}$ in (7.5)) were set equal to the values that were estimated for a paraplegic patient in [117]. The mass and inertial parameters were determined using anthropometric data from [147] for a person with a mass of 91 kg and a height of 1.8 m. The weight of any components (e.g. stimulator unit and electric motors) were neglected so that the results of all three actuation cases may be comparable independent of device weight.

For the simulated actuation case where only electrical stimulation is used it is assumed that $u_m = 0 \forall t \in [t_0, t_f]$, and for the actuation case where only electric motors are used it is assumed that $u_s = 0 \forall t \in [t_0, t_f]$. The set that bounds the electrical stimulations are defined by the model to be $\mathcal{U}_s = [0, 1]$. The bounds on the walker torque ($\mathcal{U}_w$) and motor currents ($\mathcal{U}_m$) were selected in agreement with realistic values. It was assumed that an LPA-17-100-SP electric motor (Harmonic Drive, LLC) was used at all of the joints of the swing leg, which has a maximum current of $9\,\text{A}$ and a torque constant of $6\,\text{N\,m/A}$. Therefore, the bound on the current and the torque constants of all of the motors were set to $\mathcal{U}_m = [-9, 9]\text{A}$ and $K_m = 6\,\text{N\,m/A}$. The Harmonic Drive motor was selected to define the bounds on the motor current and the torque constant because it is capable of generating the torques and velocities required to generate the gait motion, and because it has been used in the design of a hybrid orthosis for gait restoration [70]. For the walker torque the bound was defined as $\mathcal{U}_w = [-200, 200]\text{N\,m}$.

The gait kinematics from the results of the optimizations of the first and last steps are shown for all three actuation cases in Fig. 7.3. It is understandable that for the motors only case, where no muscle fatigue occurs, that there is no change in the kinematics. For the stimulation only and hybrid cases, where the muscle groups fatigue as they are stimulated, there is also no observable change in the gait kinematics. This indicates that although muscle fatigue occurred the optimizations were able to appropriately allocate control, despite the effects of muscle fatigue, such that the gait kinematics were preserved and the step was achieved.

All of the control signals for one leg during the swing phase for the first and last steps of all three simulated actuation cases are shown in Figs. 7.4-7.7. Fig. 7.4 show the walker moments, which is approximately equal for all actuation cases and for the first and last step. The motor torque and flexion/extension normalized stimulations at the hip, knee, and ankle joints are shown in Figs. 7.5-7.7. These plots illustrate how the hybrid actuation case can reduce the stimulation and motor torque required to produce the gait motion. They also illustrate how the muscle fatigue model causes an increase in the amount of stimulation required to produce the gait motion.

First Step (a) / Last Step (b) — Hip Angle [deg.]
First Step (c) / Last Step (d) — Knee Angle [deg.]
First Step (e) / Last Step (f) — Ankle Angle [deg.]
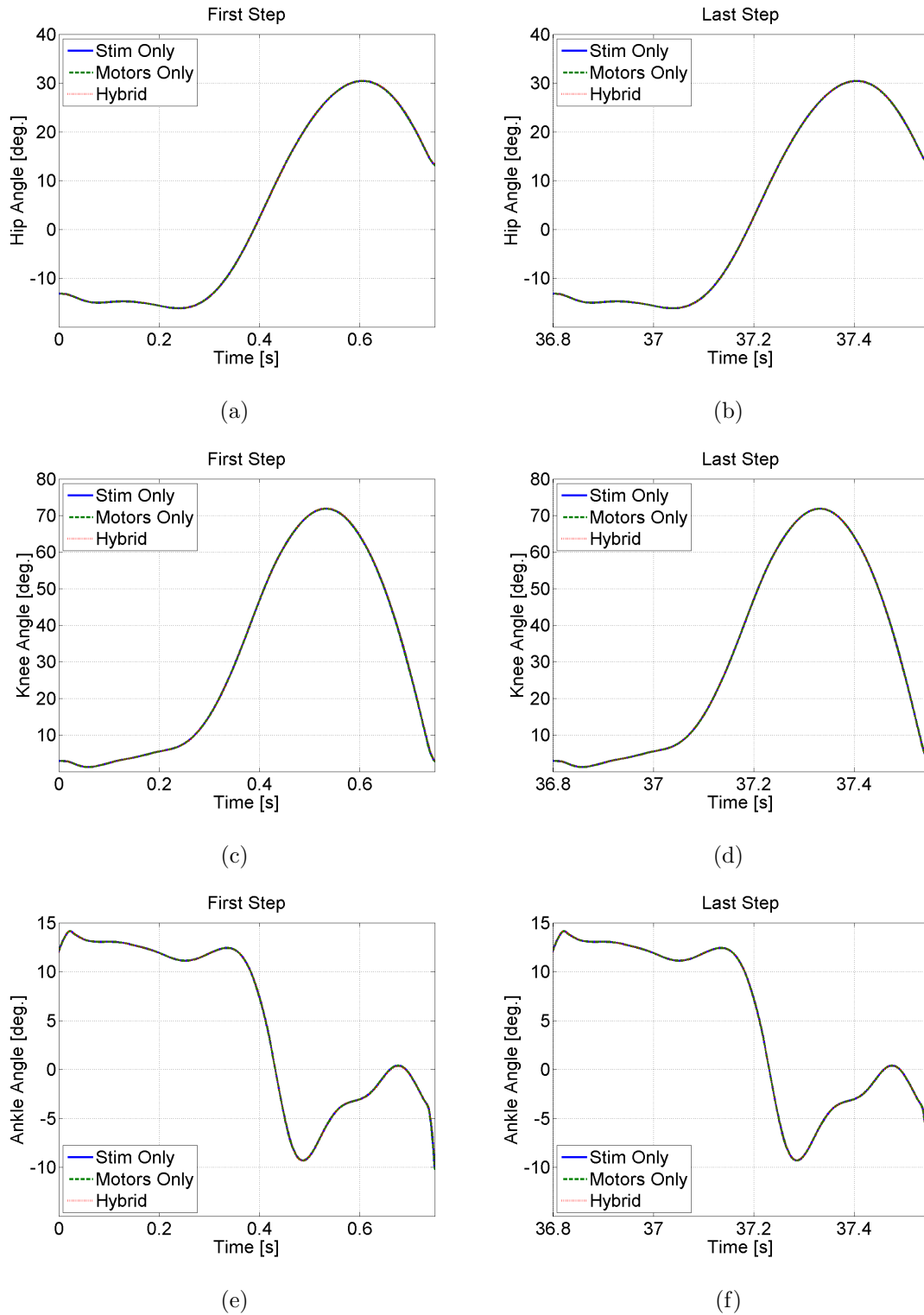
Figure 7.3: Plots of the gait kinematics (hip, knee, and ankle joint angles of the swing leg) for all three actuation cases on the first and last steps simulated.
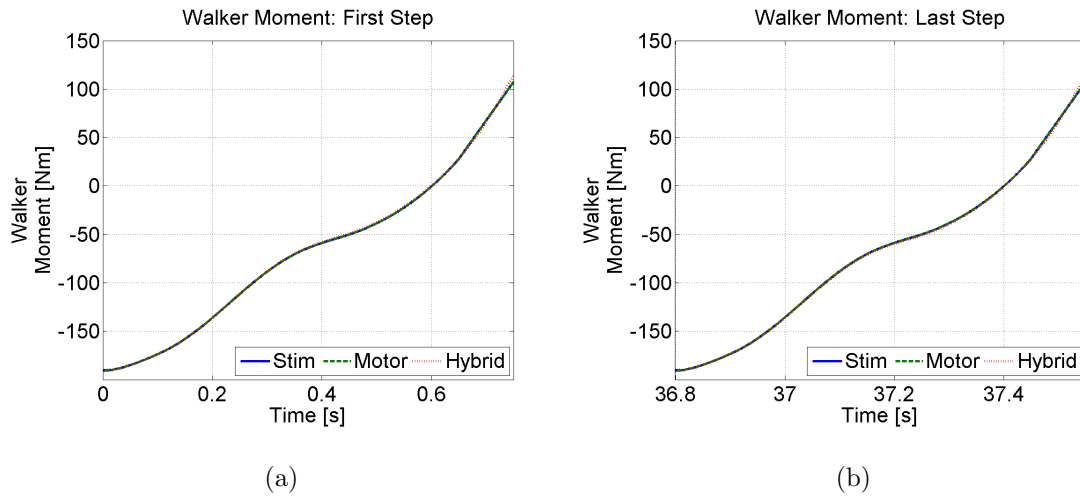
Figure 7.4: Plots of the walker moments for the first (a) and last (b) steps of all three simulated actuation cases.
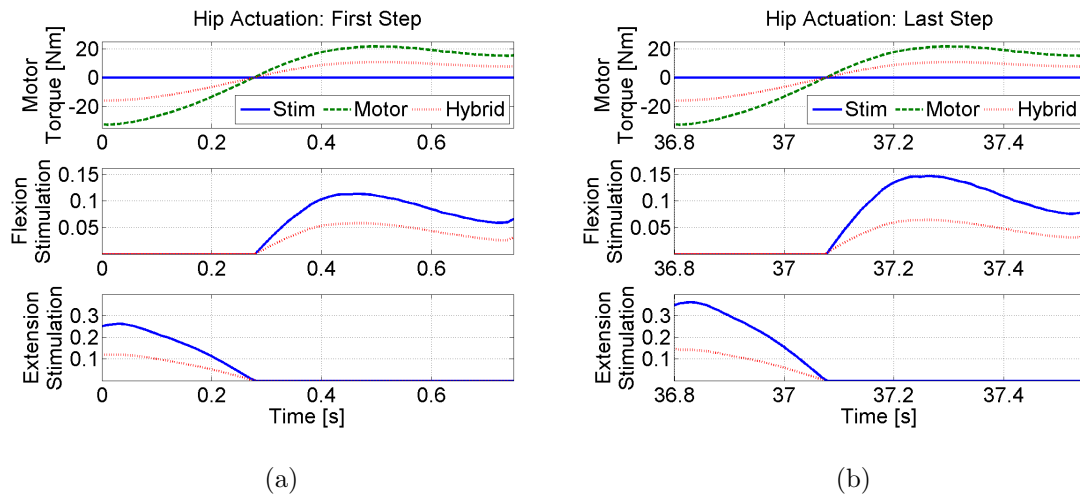
Figure 7.5: Plots of the hip motor torque and hip flexion/extension normalized stimulation for the swing phase of the first (a) and last (b) steps of all three simulated actuation cases.
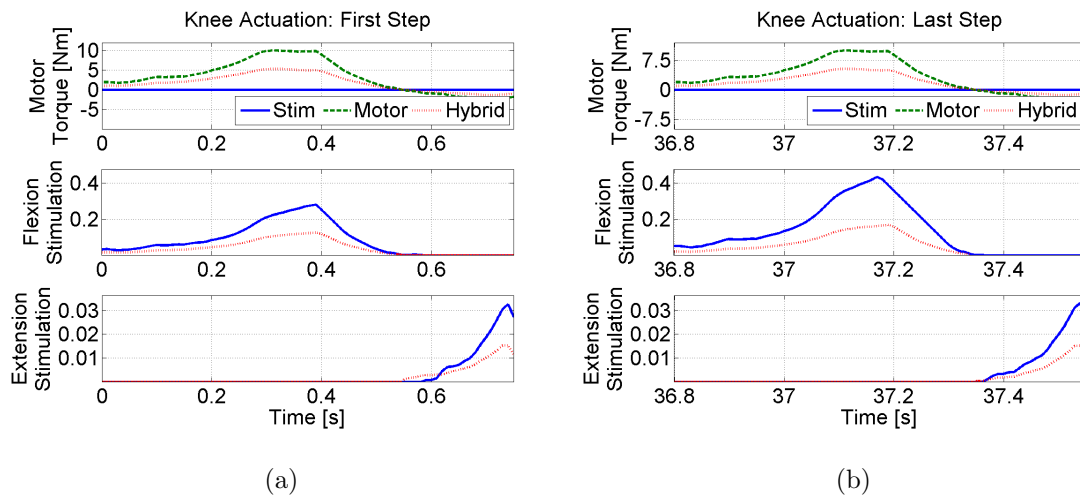
Figure 7.6: Plots of the knee motor torque and knee flexion/extension normalized stimulation for the swing phase of the first (a) and last (b) steps of all three simulated actuation cases.
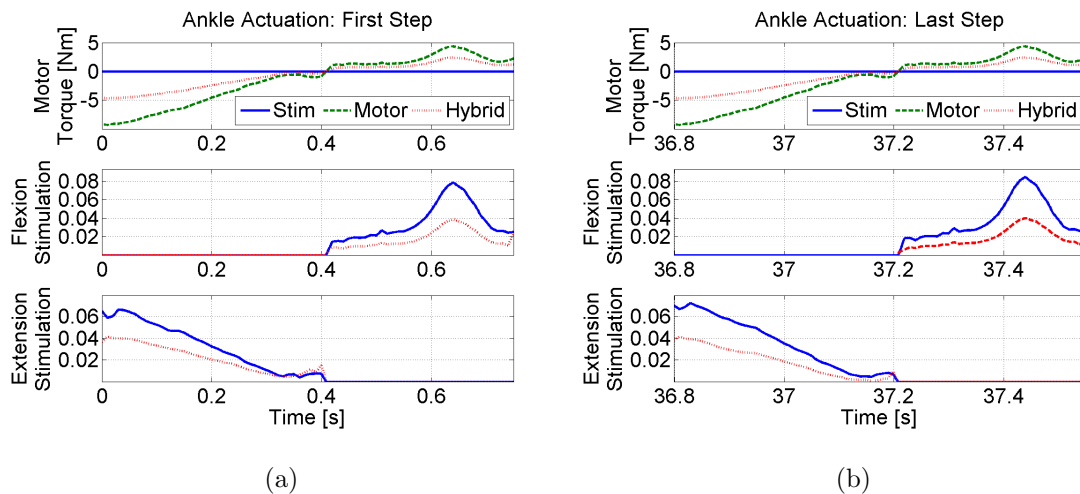
Figure 7.7: Plots of the ankle motor torque and ankle flexion/extension normalized stimulation for the swing phase of the first (a) and last (b) steps of all three simulated actuation cases.
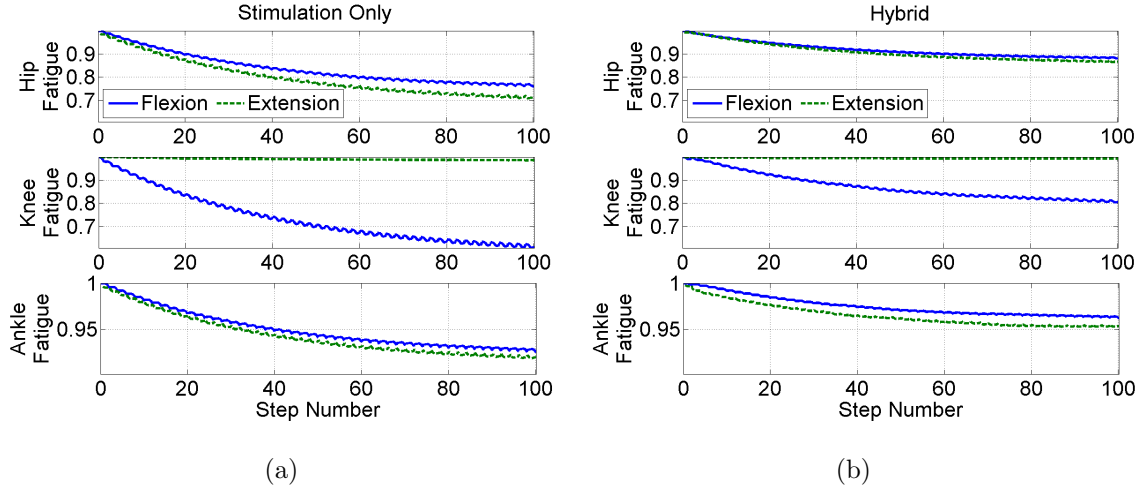
Figure 7.8: Plot of the fatigue states of all stimulated muscle groups for the stimulation only (a) and hybrid (b) actuation cases.

The muscle fatigue states for all stimulated muscles of one leg and all simulated steps of the stimulation only and hybrid actuation cases are shown in Fig. 7.8. During the stance phase, since the stance leg is not stimulated, some recovery occurs. However, due to the relatively large muscle recovery time constant very little recovery occurs during this time. Note that the motor only actuation case is not shown here because stimulation is not used in that cases, and therefore muscle fatigue does not occur.

The control signals in Figs. 7.5-7.7 were used to compute the total instantaneous power for all three actuation cases. The electrical power consumed by the motors was calculated using the mechanical power of each motor and the efficiency of the aforementioned Harmonic Drive motors, which is approximately 80%. The electrical power consumed by the stimulation was calculated using (7.4) based on parameters of commonly used pulsed trains and an approximation of the resistivity of the skin when FES is applied. The parameters of the stimulation train that were used to compute power were based on the parameters used by the Parastep system: $F_s =24$ Hz stimulation frequency, $W =150\,\mu$s pulse width, and a maximum current amplitude of $300\,$mA [76]. Assuming that the threshold current is $100\,$mA and the saturation current is $300\,$mA, the normalized currents solved by the optimizations can be
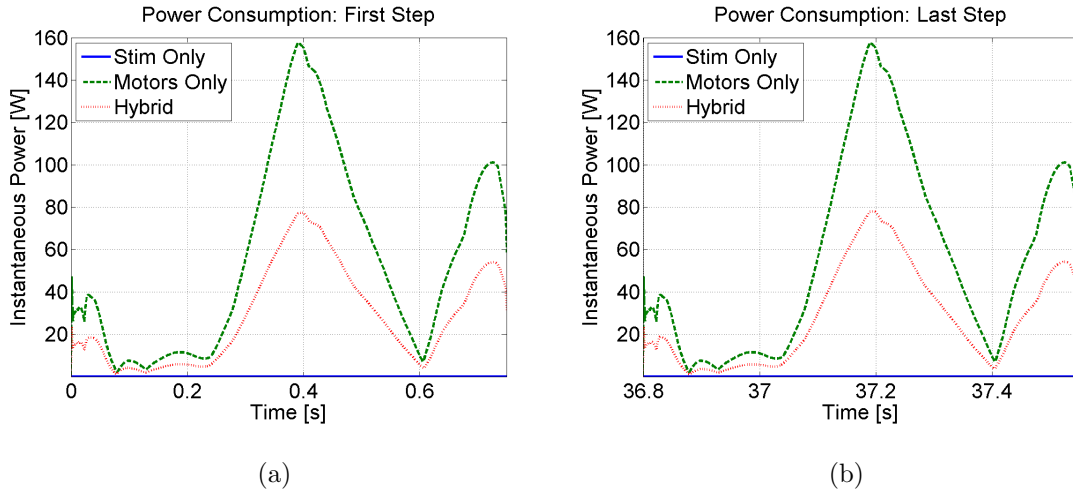
Figure 7.9: Total instantaneous power consumed by the FES and motors for the three actuation cases for the first (a) and last (b) simulated steps.

mapped to a current amplitude using the inverse of (7.3). The resistivity of the human skin can vary based on many different parameters, such as the frequency of the stimulation [85] and the size of the size of the electrodes [143]. From the data in [115], which was compiled from a number of sources, the electrical impedance of the skin for a frequency range of 30-60 Hz was determined to be in the range 60-80 kΩcm². Assuming that electrodes with a surface area of approximately 80 cm² (surface area of commonly used 2.5"×5" electrode pads) are used the resistivity can be over-approximated to be 1 kΩ.

Using the aforementioned methods and parameters the instantaneous electrical power consumed by the stimulation and motors were computed for the first and last simulated steps, and the results are shown in Fig. 7.9. As can be seen from these results the power consumption of FES is almost negligible when compared to the power consumption of the motors. Also, because the FES is more efficient than the electric motors (i.e., FES produces more torque with less electrical power) the power consumption of the hybrid actuation case is approximately half the power consumption of the motor only actuation case.

133

Table 7.1: The energy consumption of the first and last step for the three simulated actuation cases that included a model of muscle fatigue were computed.

	Energy Consumption [J]	
Actuation Method	First Step	Last Step
Stimulation Only	6.85×10^{-4}	7.35×10^{-4}
Motor Only	41.7	41.7
Hybrid	21.3	21.4

The instantaneous power consumption that was calculated and plotted in Fig. 7.9 was integrated to compute the energy consumption for all three actuation cases of the first and last steps that were simulated. The calculated energy consumptions are shown in Table 7.1. From these results it can be concluded that the use of a hybrid system would result in a reduction in power consumption of approximately 50% throughout 100 steps.

7.4 DISCUSSION

First, it should be noted that although the energy consumption of the stimulation only case was almost negligible compared to the energy used by the motor only case, exoskeleton gait restoration devices have been shown to be able to achieve significantly greater walking durations. This is a result of the rapid muscle fatigue that is caused by the application of FES. Although the addition of the muscle fatigue model had little effect on the results of the simulation over 100 steps it has been observed that in application the muscle fatigue can greatly limit the duration that FES-based gait restoration devices can be used [76]. The minimal effects that the muscle fatigue model had on the simulations were likely a result of the short step durations and the musculoskeletal parameters used in the model. The musculoskeletal parameters, which were obtained from [5, 110, 117], may have been estimated from paraplegic participants whose muscles had previously been trained using

FES. Participants' muscles that have been trained using FES have been shown to see a substantial increase in muscle force production and fatigue resistance [80]. If this were the case it would mean that the results of these simulations are idealistic, and not necessarily generalizable to the paraplegic population.

The results of the simulations of the hybrid case illustrate its advantages over systems that use strictly FES or strictly electric motors. The hybrid case resulted in approximately half as much stimulation being used, which resulted in approximately half as much muscle fatigue being induced. This indicates that a hybrid system could potentially double the walking duration of FES only systems. The hybrid case also used half as much energy as the motor only case, which could also result in increased walking durations. In [112] an electric motor was used with and without FES to produce a knee extension motion. The energy was then calculated for both cases based on the mechanical energy of the motor. The results indicated that a 55.9% energy reduction was achieved when FES was used with the electric motor. Although their calculations were based strictly on mechanical power and they did not take into account the power consumption of the electrical stimulation, this value approximately agrees with the simulation results presented here that calculated a 50% energy reduction when FES is used to supplement electric motors.

7.5   CONCLUSION

The results of the simulations presented here illustrated that a hybrid gait restoration device has the potential to be more efficient than exoskeleton devices, allowing it to achieve greater walking durations than a system that is strictly driven by FES or electric motors. The increased walking durations would result from two factors. First, the decrease in FES used by the hybrid systems compared to the FES only system would result in less muscle fatigue, allowing the stimulation to be used for a longer duration. Second, the hybrid case used half as much energy as the motor only case, which indicates that a hybrid system would be capable or running for twice as long as an exoskeleton system.

These results may also be used for open-loop control of a hybrid orthosis. However, it would be more favorable to use a closed-loop optimal control technique, such as model predictive control that was used on the leg extension system in Chapters 4 and 6 or in [72, 104]. The closed-loop optimal control would make the system more robust to modeling uncertainties and disturbances. The use of the model predictive control for the hybrid gait system would also solve the actuator redundancy problem, as was shown in Chapter 6; however, the gait system is of a higher order than the leg extension system. This means that the computation time of the optimal control problem will be greater, and it will become more challenging to implement the DCA control technique for the gait restoration system in real-time.

Another control method that has been proposed to robustify the results of the optimizations that were computed here is a muscle synergy-inspired adaptive control scheme [4]. This control method uses the computed control signals to extract synergies, which can then be used to reduce the order of the control system. This lower dimensional control system is simpler to adapt because the number of required signals are reduced due to the lower number of synergies used.

8.0   FINITE-STATE MACHINE CONTROL OF A SEMI-ACTIVE NEUROPROSTHESIS FOR RESTORING LOWER LIMB FUNCTION IN PARAPLEGICS

As demonstrated in the previous chapters, a hybrid gait restoration device that uses functional electrical stimulation (FES) and electric motors has the potential to be more energy efficient than exoskeleton devices and be capable of greater walking durations than FES-based or exoskeleton devices. Therefore, work has begun to develop a hybrid gait restoration device that may be used to experimentally validate the previously discussed control systems, as well as any other forthcoming control systems. This chapter summarizes the development of a semi-active orthosis (SEAHO) that is controlled using a finite state machine (FSM) whose states are dependent on the phase of the hip angle during the gait cycle. SEAHO uses trancutaneous FES of the quadriceps, hamstrings, and gastrocnemii to actuate knee flexion/extension and plantar flexion, while hip flexion/extension is actuated using electric motors. Wrap spring clutches have been added to the knee joints so that stimulation is not required to keep the knee joints extended during standing. This chapter will discuss the individual components of the SEAHO, the FSM control system that is being used, and present results from initial testing of the device on an able-bodied participant.

8.1   SEAHO AND ITS CONTROL SYSTEM

SEAHO, which is shown in Fig. 8.1, can be broken down into three primary components: electric motors, FES, and wrap spring clutches. The electric motors (Harmonic Drive LLC, MA, USA), located at the hip joints, can generate a maximum torque of $40\,\mathrm{N\,m}$ and are the
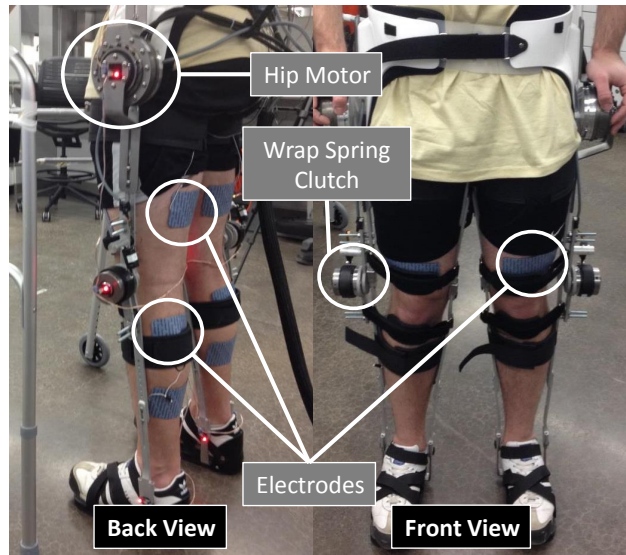
Figure 8.1: Semi-active orthosis (SEAHO) for individuals with paraplegia. Motors at the hip joints generate hip flexion/extension through position feedback control. The electrodes placed at the gastrocnemius, hamstrings, and quadriceps generate plantar flexion, knee flexion, and knee extension, respectively. When the wrap spring clutches are locked they prevent motion in the direction of flexion, but the user may always move freely in the direction of extension.

motors that were considered in the gait optimizations in Chapter 7. Electric motors are used at the hip joints, and not FES, because it can be difficult to stimulate the hip flexors. This is because these muscle groups are not easily accessible using surface electrodes. It possible to generate reflexive hip flexion using surface electrodes via peroneal nerve stimulation; however, this technique is often unreliable and suffers from habituation that causes a rapid reduction in the magnitude of the response [51]. Also, the use of peroneal nerve stimulation can be considerably uncomfortable for able-bodied persons who have complete sensation in their lower extremities. Therefore, for the preliminary tests of this system, which are performed on an able-bodied subject, peroneal nerve stimulation was not used. The hip motors were controlled using the robust integral of the sign of the error (RISE) controller [129], where the error signal was defined as a desired hip angle minus the hip angle measured from the incremental encoders of the motors. The desired hip angle trajectories used for the position feedback control were recorded from an able-bodied person while taking a step in the brace. The hip desired hip angles were measured while wearing the brace, instead of using hip angles from a normal gait, because of the movement constraints created by the brace (e.g., the brace prevents hip abduction/adduction).

The hybrid orthosis uses FES of the gastrocnemii, quadriceps, and hamstrings. Electrical stimulation of the gastrocnemius induces plantar flexion of the foot, which is used to help achieve push-off of the swing leg. Stimulation of the quadriceps and hamstrings elicits knee extension and knee flexion, respectively. Since sensors were not used to measure the knee and ankle angles feedback control of the stimulation was not used. Instead a bang-bang control method was used. Bang-bang control has only two states, on and off. The stimulation amplitude used for each muscle was the amplitude that achieved a maximum muscle contraction while still being comfortable for the user. The maximum contraction stimulation amplitude was determined experimentally for the participant before they put on the brace.

The FES was turned on and off to each muscle group depending on where the user was in their gait cycle. Since the hip angles were the only signals measured that indicate the phase of the persons gait cycle they were used to control the FES. The gait phase-based triggering of the stimulation with respect to the hip angles were determined from gait analysis data
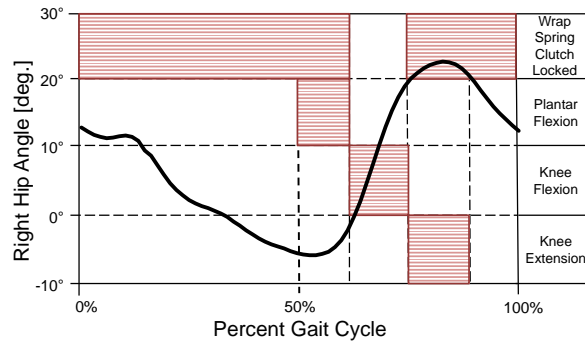
Figure 8.2: The logic for the finite state machine control of SEAHO is strictly dependent on hip angle. The approximate timing of the control of the system as a function of hip angle for one full gait cycle is illustrated here. The shaded in regions indicate when a component of the system is active.

in [87, 146]. The timing for the FES of the three muscle groups with respect to the hip angle during one complete gait cycle are shown in Fig. 8.2. The regions illustrated in Fig. 8.2 were adjusted during the testing to achieve the best results without over-stimulating the muscles.

The final components of SEAHO are the wrap spring clutches at the knee joints. The purpose of the wrap spring clutch (WSC) is to prevent flexion of the knee joints when locked, while still allowing extension. When the WSC is unlocked, which is controlled using a linear actuator, it allows free motion in the directions of knee extension and knee flexion. This feature reduces the amount of stimulation required since it is not required to keep the knees extended so that the person remains standing between steps. The WSC is also used to lock the knee joint of the stance leg so that only the swing leg needs to be stimulated when taking a step. The function of the WSC was mimicked in the gait model presented in Chapter 7, which assumes that the knee joint of the stance leg is fixed. The WSC is only unlocked when knee flexors were stimulated, as is illustrated in Fig. 8.2.

For the initial testing of the device only three states were used in the FSM to achieve walking. Since the user starts from standing with both feet together the first state was a half step, which transitioned the user from standing with both feet together to the initial gait position. The other two states of the FSM were a state for a left step and a state for a right step. The final two states are repeated cyclically to achieve walking. Transition from one state to the next was initiated by the user pressing a button on the walker when they felt prepared to move to the next state. Future work will add more states to the FSM control such that other motions, such as sit-to-stand and stand-to-sit transfers, may be achieved in the brace.

8.2 RESULTS

The developed hybrid gait restoration system was tested on one able-bodied participant. Once the individual was standing with feet together while wearing the brace they were asked to completely relax their lower extremities and allow the hip motors and electrical stimulation to produce all of the motion. The results of the initial testing of the hybrid device on an able-bodied participant can be seen in Figs. 8.4 and 8.5. In the first half of the gait cycle the right leg is the stance leg and the left leg is the swing leg. Therefore, the wrap spring clutch was locked and no stimulation was applied to the right leg.

In Region 1, which occurs from approximately 50%-65% of the gait cycle, the right gastrocnemius was stimulated to achieve heel-off. Then, as the right hip began to flex, the stimulation of the gastrocnemius was stopped, the WSC was unlocked, and the stimulation of the right hamstrings was initiated. The stimulation of the hamstrings caused flexion of the knee joint, which helped the foot to clear the ground as the right hip is flexed by the motor. This is illustrated as Region 2 in Fig. 8.3, which occurred from approximately 65%-75% of the gait cycle. When the hamstrings were no longer being stimulated, the wrap spring clutch was locked again. Note that when the WSC is locked it only prevents motion in the direction of flexion. Therefore, although the clutch was locked the knee may still extend.

141
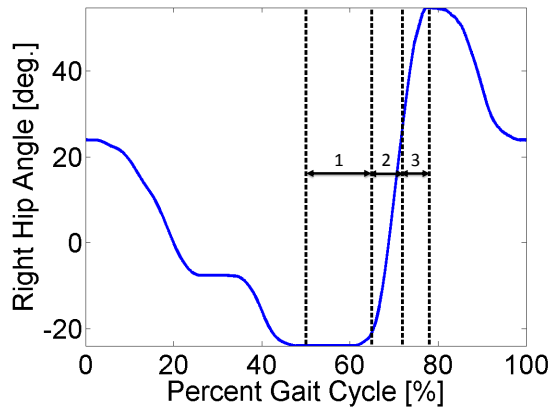
Figure 8.3: The right hip angle, measured from the hip motor, and the stimulation regions for the right leg are shown for a full gait cycle. In Region 1 the gastrocnemius is stimulated, in Region 2 the wrap spring clutch is unlocked and the hamstring is stimulated, and in Region 3 the right quadriceps is stimulated.

Once the right hip angle exceeded approximately 30° the stimulation of the hamstrings stops and the stimulation of the quadriceps was initiated, causing the right knee to extend. This is illustrated as Region 3 of Fig. 8.3, which occurred from approximately 75%-80% of the gait cycle. Less stimulation to the quadriceps was required because once the knee was fully extended the WSC prevented the knee from flexing. If a measurement of the knee angle was accessible feedback control of the hamstring and quadriceps muscles may be used to further reduce the amount of stimulation used to elicit knee flexion/extension.

The RISE controller, which was used for the position tracking control of the hip motors, was able to track the desired hip angles with an RMS error of 0.346° and a peak error magnitude of approximately 1.5°. As can be seen in Fig. 8.5, the peak RMS position tracking error for one complete gait cycle occurred at approximately 65% of the gait cycle. This corresponds to the moment when right hip flexion began, and the largest hip motor torque was required.

142
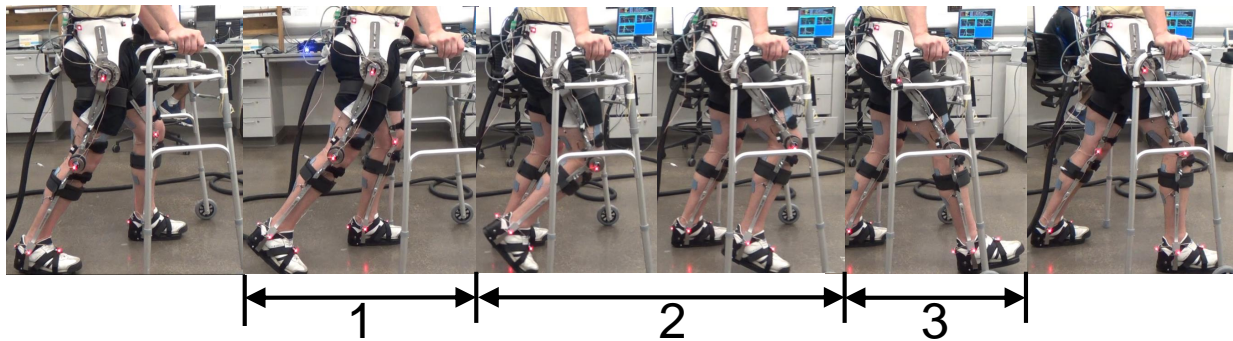
Figure 8.4: This sequence of photos shows the testing of SEAHO for a full gait cycle. The top sequence of photos shows the left step, and the bottom sequence of photos shows the subsequent right step. The regions in this figure, numbered 1-3, correspond to the regions in Fig. 8.3.
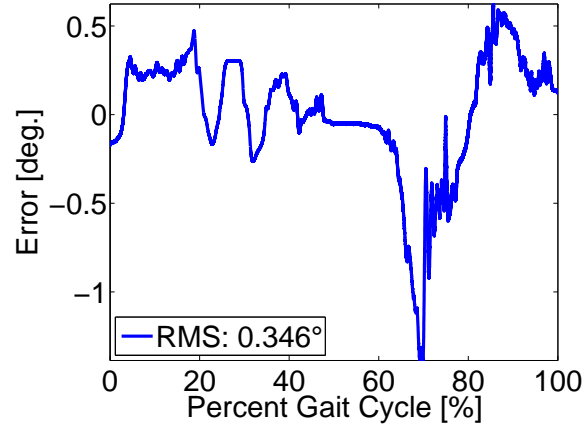
Figure 8.5: The RISE controller was used for the position tracking control of the hip motors. The motors tracked the desired hip angle with an RMS error of 0.346° over one full gait cycle.

8.3 CONCLUSION

As a result of the ability of an able-bodied participant to perform multiple steps in SEAHO it can be concluded that the device is ready for testing on paraplegic subjects. The brace is also being modified to allow the control systems presented in this dissertation and other, forthcoming control systems to be validated experimentally. Encoders have been added to the knee joints so that closed-loop feedback control of the FES of the quadriceps and hamstrings may be used. Future designs of the device will also include motors at the knee joints to further reduce the requirement of electrical stimulation for the hamstrings and quadriceps. Force sensitive resistors are being added to the feet of the devices to be used as another form of gait detection and for center of pressure gait control methods. For persons with SCI, stimulation of the peroneal nerve may be used. This will assist the hip motors in producing hip flexion, and may also assist in producing knee flexion. Note that the addition of motors at the knee joint and peroneal nerve stimulation create an actuator redundancy. Therefore, control methods, such as the ones presented in Chapters 5 and 6, will need to be modified so that they may be applied to a full gait system.

Finally, although the device does not currently use the same actuators as the model in Chapter 7, the model may be modified to match the current state of the brace. Then a forward dynamic optimization of the modified model may be used to compute the optimal control signals to achieve gait. The computed control signals may then be used as an open-loop optimal control for the developed gait restoration system, as previously discussed in Chapter 7. The computation and implementation of this open-loop optimal control would require identification of the musculoskeletal parameters, which can be performed using methods similar to those presented in Chapter 2.

9.0 SUMMARY

Over 5,000 people are diagnosed with paraplegia each year in the United States, and their loss of motor and/or sensory function of their lower extremities greatly affects their every day lives [137]. Research has explored the use of functional electrical stimulation (FES) [8, 51, 58, 78, 80, 97] and actuated orthoses [35, 36, 107, 135, 136], also known as exoskeletons, to restore functional movement to these people. However, transcutaneous FES causes the muscles to fatigue more rapidly than volitional muscle contractions, and the duration that exoskeleton devices may be used are limited by the capacity of their batteries. Some research has explored the development of hybrid (FES and electric motor) systems to potentially decrease the size and weight of the devices, and to increase the duration that they may be used [23, 55, 72, 112]. However, these hybrid systems present a number of new research challenges. The preeminent challenge being the actuator redundancy created through the use of actuators that act on the same degree of freedom.

The primary goal of this research was the study and development of control methods to compensate for and/or inhibit the effects of muscle fatigue in FES and hybrid neuroprosthetic devices. The results presented here illustrated that FES-based systems can compensate for the effects of muscle fatigue by considering the fatigue dynamics in the control development. However, because these systems compensated for muscle fatigue by increasing the amount of stimulation or by sacrificing performance they were unable to inhibit the onset of muscle fatigue. Simulation results illustrated that a hybrid gait restoration system is capable of achieving greater walking durations than systems that use strictly FES or strictly electric motors by decreasing FES induced muscle fatigue and power consumption compared to exoskeleton devices. These promising results facilitated the necessity for continued study of hybrid gait restoration systems.

In the case of systems that strictly use FES, error-based feedback control of FES can compensate for the effects of muscle fatigue by increasing the amount of stimulation used [2, 3, 125, 129]. However, none of the previously developed FES controllers took into consideration how muscle fatigue would effect the musculoskeletal dynamics. In Chapter 3 a nonlinear controller that incorporates muscle activation and fatigue dynamics was developed. The purpose of this controller was to use information of the muscle fatigue dynamics to compensate for its effects, allowing the controller to maintain performance over longer durations. The developed controller required knowledge of unmeasurable states, specifically the muscle activation and fatigue states. Therefore, model-based estimation techniques were used based on the modeling and system identification in Chapter 2. This controller showed a statistically significant improvement over a proportional-derivative (PD) controller in terms of performance, but caused approximately the same amount of muscle fatigue as the PD controller. Therefore, it was concluded that the new controller compensated for how the muscle fatigue can affect performance in closed-loop feedback control of FES, but it did not inhibit the onset of muscle fatigue.

Another control method with potential to reduce the muscle fatigue in systems that strictly use FES that was investigated in this research is model predictive control (MPC). In FES systems, as more stimulation is applied the effects of muscle fatigue are perpetuated. Therefore, it was theorized that MPC may be used to solve for and apply the minimum amount of stimulation necessary to produce a desired movement. In Chapter 4 nonlinear MPC (NMPC) was implemented on three able-bodied subjects using a gradient projection method to solve the finite-time optimal control problem. The modeling and parameter estimation procedures in Chapter 2 were used to allow for the implementation of this model-based control method. Although this was not the first proposal of MPC or NMPC for FES-based systems [11, 34, 104] it is the first real-time implementation of such a controller. To determine if the NMPC achieved the goal of reducing the muscle fatigue compared to a typical feedback controller, muscle fatigue was measured after a trial using NMPC and a trial using a proportional-integral-derivative (PID) controller. The results indicated that the NMPC caused the muscles to fatigue less than the PID controller. However, this came at the price of sacrificing performance. The NMPC induced approximately 25% less muscle

fatigue than the PID controller (based on normalized force-time integrals); however, the regulation performance of the PID controller was approximately two times better than the NMPC (based on steady-state root mean square errors). The tradeoff between performance and muscle fatigue that was observed in these results can be adjusted through tuning of the parameters of the cost function, but as long as strictly FES is used this tradeoff will remain.

One method for inhibiting the muscle fatigue in neuroprostheses is to add an electric motor to supplement some of the control, which may reduce the amount of stimulation required. However, the addition of an electric motor creates an actuator redundancy. One solution to the actuator redundancy problem is to switch discretely between FES and an electric motor. In Chapter 5 a controller was developed that is capable of stable switching between FES and an electric motor based on an estimate of the muscle fatigue. The controller switches from FES to an electric motor when the muscle fatigue becomes severe, and then switches back to FES once the muscle has sufficiently recovered. The developed control system was demonstrated through simulations on a musculoskeletal hybrid neuroprosthesis model, using model parameters estimated for a person with an SCI. Future work will validate this controller experimentally through trials on able-bodied individuals and persons with SCI. The developed controller requires estimated model parameters to be implemented. Therefore, the methods in Chapter 2 will be used to estimate the necessary parameters of the research participants.

As an alternative to switching between the FES and an electric motor, in Chapter 6 it was shown how the NMPC in Chapter 4 may be used for dynamic control allocation (DCA) to allocate control to FES and electric motors simultaneously. The DCA was simulated on a hybrid neuroprosthesis leg extension model, which used musculoskeletal parameters estimated from persons with SCI. The results of the DCA of a hybrid neuroprosthesis in Chapter 6 showed how NMPC can be used to optimally allocate control to the FES and electric motor. The results of the DCA were compared with simulation results of NMPC of FES using the same SCI parameter models that were used in the DCA simulations. The comparison of these two simulations showed how supplementing FES with an electric motor can inhibit the onset of muscle fatigue and improve the performance when such a device is used for long durations. Future work will validate the DCA of a hybrid neuroprosthesis

experimentally through trials on able-bodied persons and persons with SCI. Like the NMPC of FES in Chapter 4 and the switching controller in Chapter 5, the DCA requires that the musculoskeletal parameters be estimated. Therefore, to implement this controller in experimental trials the methods in Chapter 2 will be used.

The major concerns with the use of MPC is that it is very dependent on the accuracy of the system identification, and the use of a terminal cost function is weak form of stability that is dependent on the linearized model. One technique that may be used to robustify the MPC is the use of tube-based MPC [99]. Tube-based MPC uses the error between the measured states and the states predicted by the MPC as feedback to compensate for mismatches between the actual system and the model. This robustifying technique can easily be added to the NMPC of FES in Chapter 4 and to the DCA in Chapter 6 to make them more robust to uncertainties that occur in the system identification procedures. One method that may be used to improve the stability of the MPC is Lyapunov-based MPC [103]. This control method uses the Lyapunov function of a stable controller as an inequality constraint that bounds the same Lyapunov function evaluated for the MPC. When this constraint is satisfied it ensures that the MPC has the same stability as the controller whose Lyapunov function is used to bound it. This would allow the MPC to inherit the stability of other controllers that have been developed for FES systems and have been shown to be robust to phenomenon present in FES systems that are not included in the model used by the MPC (e.g. spasticity and electromechanical delay).

The control systems developed in this dissertation require either partial or complete models of the systems to be implemented. Therefore, phenomenological musculoskeletal models, specifically Hill-type muscle models [146], and a systematic parameter identification procedure were used. A major limitation of this method is that the parameter identification procedure, presented in Chapter 2, requires numerous steps to identify all of the parameters of the system. Not only is it time consuming to conduct all of the necessary procedures but they are also subject to propagation of estimation error (i.e., errors incurred in any one procedure are carried over to all following procedures). Also, because the system being controlled is biological it is subject to day-to-day changes that may require the system identification procedures to be performed regularly. Using non-phenomenological models,

such as Hammerstein models [42,86] or neural network models [22], could significantly reduce the amount of time required to identify the model and may be used to implement the MPC and DCA in place of the phenomenological model. Also, these models may be adapted online, which would make the model-based controllers presented here more robust to day-to-day changes in the system that result from it being biological.

To illustrate the advantages of using a hybrid gait restoration system over systems that strictly use FES or electric motors, forward dynamic optimizations of a four-link gait model were performed in Chapter 7 for the three actuation cases: FES only, motors only, and hybrid (FES and motors). From the results of the optimizations it was concluded that a hybrid system may be capable of greater walking durations than systems that use either FES or electric motors. The optimizations showed that an FES only system induced approximately twice as much muscle fatigue as a hybrid system, and the motor only system used twice as much electrical energy as a hybrid system. These results are indications that a hybrid system is capable of achieving greater walking durations than systems that strictly use FES or electric motors, and facilitate the necessity for the continued study and development of hybrid gait restoration systems. Future work will directly measure the power consumption of a hybrid gait restoration device, such as the one presented in Chapter 8, to experimentally validate the results of these simulations.

The methods used in Chapter 7 can also be used to compute user specific optimal controls for use in a hybrid neuroprostheses. The musculoskeletal parameters of a user may be estimated using methods similar to the ones presented in Chapter 2, then the forward dynamic optimizations can be used to determine that user's optimal stimulations and motor torques. The computed control signals may then be used in open-loop control to achieve walking with the device. The major drawback to this open-loop optimal control method is that it would not be robust to disturbances or uncertainties in the model. Another, more robust, utility for the computed control signals is that they may be used in feedforward/feedback control schemes, such as the newly developed synergy based controller [4]. This new control method uses principal component analysis (PCA) of the computed control signals to reduce the order of the control problem and solve the control allocation problem based on how the

optimization allocates the control. The synergies computed by the PCA are then used in an adaptive feedforward control scheme, with feedback to the electric motors, to make the system robust to disturbances and modeling uncertainties.

The results of this dissertation facilitate the need for continued research in the presented topics. Some future work items have been presented and discussed in the preceding chapters and in this summary. These items can be summarized as follows:

- Non-phenomenological musculoskeletal models for model-based control methods
    - Neural networks or Hammerstein models can be used
    - Require less procedures for identification
    - Can be adapted in real time to compensate for time-varying system characteristics
- Ultrasound for real-time measurement of muscle fatigue
- Improvements to MPC and MPC-based DCA
    - Tube-based methods to robustify the MPC and DCA
    - Lyapunov-based MPC can be used to strengthen the stability of MPC and DCA
    - Non-phenomenological models can be used for adaptive MPC/DCA
- Gait model and dynamics optimizations
    - Can be used to compute user-specific optimal control signals
    - Optimal control signals can be used in newly developed synergy-based feedforward/feedback control scheme
- Hybrid neuroprosthesis modifications
    - Addition of new states to FSM control such as sit-to-stand and stand-to-sit
    - Motors at the knee joints
    - Force sensitive resistors to foot plate for gait detection and center of pressure control

BIBLIOGRAPHY

[1] J. Abbas and H. Chizeck. Feedback control of coronal plane hip angle in paraplegic subjects using Functional Neuromuscular Stimulation. *IEEE Trans. Biomed. Eng.*, 38(7):687–698, 1991.

[2] A. Ajoudani and A. Erfanian. A neuro-sliding-mode control with adaptive modeling of uncertainty for control of movement in paralyzed limbs using functional electrical stimulation. *IEEE Trans. Biomed. Eng.*, 56(7):1771–1780, 2009.

[3] N. Alibeji, N. Kirsch, S. Farrokhi, and N. Sharma. Further results on predictor-based control of neuromuscular electrical stimulation. *IEEE Trans. Neural Syst. Rehabil. Eng.*, 2015.

[4] N. Alibeji, N. Kirsch, and N. Sharma. A muscle synergy-inspired adaptive control scheme for a hybrid walking neuroprosthesis. *Front. Bioeng. Biotechnol.*, 2015.

[5] F. Anderson and M. Pandy. Dynamic optimization of human walking. *J. Biomech. Eng.*, 123(5):381–390, 2001.

[6] B. Andrews and T. Bajd. Hybrid orthoses for paraplegics. In *Int. Symp. Extern. Control Hum. Extrem.*, 1984.

[7] E. Asmussen. Muscle fatigue. *Med. Sci. Sport. Exerc.*, 11(4):313–321, 1979.

[8] T. Bajd, A. Kralj, R. Turk, H. Benko, and J. Šega. The use of a four-channel electrical stimulator as an ambulatory aid for paraplegic patients. *Phys. Ther.*, 63(7):1116–1120, 1983.

[9] L. Baker. http://www.axelgaard.com/education.

[10] M. Bellman, T. Cheng, R. Downey, and W. Dixon. Stationary cycling induced by switched functional electrical stimulation control. In *Am. Control Conf.*, pages 4802–4809, 2014.

[11] M. Benoussaad, K. Mombaur, and C. Azevedo-Coste. Nonlinear model predictive control of joint ankle by electrical stimulation for drop foot correction. In *Int. Conf. Intell. Robot. Syst.*, pages 983–989, 2013.

[12] C. Bickel, C. Gregory, and J. Dean. Motor unit recruitment during neuromuscular electrical stimulation: a critical appraisal. *Eur. J. Appl. Physiol.*, 111(10):2399–2407, 2011.

[13] S. Binder-Macleod, J. Dean, and J. Ding. Electrical stimulation factors in potentiation of human quadriceps femoris. *Muscle and Nerve*, 25(2):271–279, 2002.

[14] M. Blanke and J. Schröder. *Diagnosis and fault-tolerant control.* Springer Berlin, 2006.

[15] G. Brindley, C. Polkey, and D. Rushton. Sacral anterior root stimulators for bladder control in paraplegia. *Spinal Cord*, 20(6):365–381, 1982.

[16] W. Buford, F. Ivey, J. Malone, R. Patterson, G. Peare, D. Nguyen, and A. Stewart. Muscle balance at the knee-moment arms for the normal knee and the ACL-minus knee. *IEEE Trans. Rehabil. Eng.*, 5(4):367–379, 1997.

[17] E. Camacho and C. Alba. *Model predictive control.* Springer, 2013.

[18] P. Cavanagh and P. Komi. Electromechanical delay in human skeletal muscle under concentric and eccentric contractions. *Eur. J. Appl. Physiol. Occup. Physiol.*, 42(3):159–163, 1979.

[19] G. Chang, J. Lub, G. Liao, J. Lai, C. Cheng, B. Kuo, and T. Kuo. A neuro-control system for the knee joint position control with quadriceps stimulation. *IEEE Trans. Rehabil. Eng.*, 5(1):2–11, 1997.

[20] H. Chen and F. Allgöwer. A quasi-infinite horizon nonlinear model predictive control scheme with guaranteed stability. *Automatica*, 34(10), 1998.

[21] Y. Chen, W. Chen, C. Hsiao, T. Kuo, and J. Lai. Development of the FES system with neural network + PID controller for the stroke. In *Proc. IEEE Int. Symp. Circuits Syst.*, pages 5119–5121, 2005.

[22] T. Cheng, Q. Wang, R. Kamalapurkar, H. Dinh, M. Bellman, and W. Dixon. Identification-based closed-loop NMES limb tracking with amplitude-modulated control input. *IEEE Trans. Cybern.*, 2015.

[23] A. Del-Ama, A. Gil-Agudo, J. Pons, and J. Moreno. Hybrid FES-robot cooperative control of ambulatory gait rehabilitation exoskeleton. *J. Neuroeng. Rehabil.*, 11(1):1–15, 2014.

[24] J. Ding, A. Wexler, and S. Binder-Macleod. A mathematical model that predicts the force-frequency relationship of human skeletal muscle. *Muscle and Nerve*, 26(4):477–485, 2002.

[25] J. Ding, A. Wexler, and S. Binder-Macleod. A predictive fatigue model. I. Predicting the effect of stimulation frequency and pattern on fatigue. *IEEE Trans. Rehabil. Eng.*, 10(1):48–58, 2002.

[26] J. Ding, A. Wexler, and S. Binder-Macleod. A predictive fatigue model. II. Predicting the effect of resting times on fatigue. *IEEE Trans. Neural Syst. Rehabil. Eng.*, 10(1):59–67, 2002.

[27] B. Doll, N. Kirsch, and N. Sharma. Optimization of a stimulation train based on a predictive model of muscle force and fatigue. In *IFAC Symp. Biol. Med. Syst.*, 2015.

[28] A. Dollar and H. Herr. Lower extremity exoskeletons and active orthoses: challenges and state-of-the-art. *IEEE Trans. Robot*, 24:144–158, 2008.

[29] W. Dong and K. Kuhnert. Robust adaptive control of nonholonomic mobile robot with parameter and nonparameter uncertainties. *IEEE Trans. Robot*, 21(2):261–266, 2005.

[30] S. Dosen and D. Popovic. Moving-window dynamic optimization: design of stimulation profiles for walking. *IEEE Trans. Biomed. Eng.*, 56(5):1298–1309, 2009.

[31] R. Downey, M. Bellman, H. Kawai, C. Gregory, and W. Dixon. Comparing the induced muscle fatigue between asynchronous and synchronous electrical stimulation in able-bodied and spinal cord injured populations. *IEEE Trans. Neur. Sys. Rehab. Eng.*, 23(6):964–972, 2014.

[32] R. Downey, M. Bellman, N. Sharma, Q. Wang, C. Gregory, and W. Dixon. A novel modulation strategy to increase stimulation duration in neuromuscular electrical stimulation. *Muscle Nerve*, 44(3):382–7, 2011.

[33] R. Downey, T. Cheng, M. Bellman, and W. Dixon. Closed-loop asynchronous electrical stimulation prolongs functional movements in the lower body. *IEEE Trans. Neural Syst. Rehabil. Eng.*, 23(6):1117–1127, 2015.

[34] R. Esfanjani and F. Towhidkhah. Application of nonlinear model predictive controller for FES-assisted standing up in paraplegia. In *Eng. Med. Biol. 27th Annu. Conf.*, volume 6, pages 6210–6213, 2005.

[35] A. Esquenazi, M. Talaty, A. Packel, and M. Saulino. The ReWalk powered exoskeleton to restore ambulatory function to individuals with thoracic-level motor-complete spinal cord injury. *Am. J. Phys. Med. Rehabil.*, 91(11):911–921, 2012.

[36] R. Farris, H. Quintero, and M. Goldfarb. Preliminary evaluation of a powered lower limb orthosis to aid walking in paraplegic individuals. *IEEE Trans. Neural Syst. Rehabil. Eng.*, 19(6):652–659, 2011.

[37] R. Farris, H. Quintero, S. Murray, K. Ha, C. Hartigan, and M. Goldfarb. A preliminary assessment of legged mobility provided by a lower limb exoskeleton for persons with paraplegia. *IEEE Trans. Neural Syst. Rehabil. Eng.*, 22(3):482–490, 2014.

[38] M. Ferrarin, F. Palazzo, R. Riener, and J. Quintern. Model-based control of FES-induced single joint movements. *IEEE Trans. Neural Syst. Rehabil. Eng.*, 9(3):245–257, 2001.

154

[39] M. Ferrarin and A. Pedotti. The relationship between electrical stimulus and joint torque: a dynamic model. *IEEE Trans. Rehabil. Eng.*, 8(3):342–352, 2000.

[40] R. Fierro and F. Lewis. Control of a nonholonomic mobile robot using neural networks. *IEEE Trans. Neural Netw.*, 9(4):589–600, 1998.

[41] C. Freeman. Upper limb electrical stimulation using input-output linearization and iterative learning control. *Control Syst. Technol.*, 23(4):1546–1554, 2014.

[42] C. Freeman, A. Hughes, J. Burridge, P. Chappell, P. Lewin, and E. Rogers. A model of the upper extremity using fes for stroke rehabilitation. *J. Biomech. Eng.*, 131(3):031011, 2009.

[43] H. Geyer and H. Herr. A muscle-reflex model that encodes principles of legged mechanics produces human walking dynamics and muscle activities. *IEEE Trans. Neural Syst. Rehabil. Eng.*, 18(3):263–273, 2010.

[44] L. Giangregorio and N. McCartney. Bone loss and muscle atrophy in spinal cord injury: epidemiology, fracture prediction, and rehabilitation strategies. *J. Spinal Cord Med.*, 29(5):489–500, 2006.

[45] Y. Giat, J. Mizrahi, and M. Levy. A musculotendon model of the fatigue profiles of paralyzed quadriceps muscle under FES. *IEEE Trans. Biomed. Eng.*, 40(7):664–674, 1993.

[46] J. Giuffrida and P. Crago. Functional restoration of elbow extension after spinal-cord injury using a neural network-based synergistic FES controller. *IEEE Trans. Neural Syst. Rehabil. Eng.*, 13(2):147–152, 2005.

[47] M. Goldfarb and W. Durfee. Design of a controlled-brake orthosis for FES-aided gait. *IEEE Trans. Rehabil. Eng.*, 4(1):13–24, 1996.

[48] M. Goldfarb, K. Korkowski, B. Harrold, and W. Durfee. Preliminary evaluation of a controlled-brake orthosis for FES-aided gait. *IEEE Trans. Neural Syst. Rehabil. Eng.*, 11(3):241–248, 2003.

[49] K. Graichen and B. Käpernick. *A real-time gradient method for nonlinear model predictive control.* INTECH Open Access Publisher, 2012.

[50] K. Graichen and A. Kugi. Stability and incremental improvement of suboptimal MPC without terminal constraints. *IEEE Trans. Automat. Contr.*, 55(11):2576–2580, 2010.

[51] M. Granat, A. Ferguson, B. Andrews, and M. Delargy. The role of functional electrical stimulation in the rehabilitation of patients with incomplete spinal cord injury - observed benefits during gait studies. *Spinal Cord*, 31(4):207–215, 1993.

[52] D. Graupe and K. Kohn. Functional neuromuscular stimulator for short-distance ambulation by certain thoracic-level spinal-cord-injured paraplegics. *Surg. Neurol.*, 50(3):202–207, 1998.

[53] W. Gstoettner, O. Adunka, J. Hamzavi, and W. Baumgartner. Rehabilitation of hearing-impaired patients with cochlear implants: a review. *Wien. Klin. Wochenschr.*, 112(11):464–472, 2000.

[54] M. Günther and H. Ruder. Synthesis of two-dimensional human walking: A test of the λ-model. *Biol. Cybern.*, 89(2):89–106, 2003.

[55] K. Ha, S. Murray, and M. Goldfarb. An approach for the cooperative control of fes with a powered exoskeleton during level walking for persons with paraplegia. *IEEE Trans. Neural Syst. Rehabil. Eng.*, 2015.

[56] K. Ha, H. Quintero, R. Farris, and M. Goldfarb. Enhancing stance phase propulsion during level walking by combining FES with a powered exoskeleton for persons with paraplegia. In *IEEE EMBC*, pages 344–347, 2012.

[57] R. Happee. Inverse dynamic optimization includin muscular dynamics, a new simulation method applied to goal directed movements. *J. Biomech.*, 27(7):953–960, 1994.

[58] E. Hardin, R. Kobetic, L. Murray, M. Corado-Ahmed, G. Pinault, J. Sakai, S. Bailey, C. Ho, and R. Triolo. Walking after incomplete spinal cord injury using an implanted FES system: a case report. *J. Rehabil. Res. Dev.*, 44(3):333–346, 2007.

[59] H. Hatze. A myocybernetic control model of skeletal muscle. *Biol. Cybern.*, 25(2):103–119, 1977.

[60] K. Hunt, B. Stone, N. Negard, T. Schauer, M. Fraser, A. Cathcart, C. Ferrario, S. Ward, and S. Grant. Control strategies for integration of electric motor assist and functional electrical stimulation in paraplegic cycling: utility for exercise testing and mobile cycling. *IEEE Trans. Neural Syst. Rehabil. Eng.*, 12(1):89–101, 2004.

[61] E. Isakov, R. Douglas, and P. Berns. Ambulation using the reciprocating gait orthosis and functional electrical stimulation. *Spinal Cord*, 30(4):239–245, 1992.

[62] A. Jadbabaie and J. Hauser. Stabilizing receding horizon control of nonlinear systems: a control Lyapunov function approach. In *Am. Control Conf.*, volume 3, pages 1535–1539, 1999.

[63] S. Jezernik, R. Wassink, and T. Keller. Sliding mode closed-loop control of FES: controlling the shank movement. *IEEE Trans. Biomed. Eng.*, 51(2):263–272, 2004.

[64] T. Johansen and T. Fossen. Control allocation–a survey. *Automatica*, 49(5):1087–1103, 2013.

[65] T. Johnston, R. Betz, B. Smith, B. Benda, M. Mulcahey, R. Davis, T. Houdayer, M. Pontari, A. Barriskill, and G. Creasey. Implantable FES system for upright mobility and bladder and bowel function for individuals with spinal cord injury. *Spinal Cord*, 43(12):713–723, 2005.

[66] A. Kantrowitz. Electronic physiologic aids. *Rep. Maimonides Hosp. Brooklyn*, 1963.

[67] B. Käpernick and K. Graichen. The gradient based nonlinear model predictive control software GRAMPC. In *IEEE Eur. Control Conf.*, pages 1170–1175, 2014.

[68] B. Käpernick and K. Graichen. GRAMPC - A gradient based MPC software for real-time applications, 2015.

[69] H. Khalil. *Nonlinear Systems*. Prentice Hall, 3rd edition, 2002.

[70] N. Kirsch, N. Alibeji, L. Fisher, C. Gregory, and N. Sharma. A semi-active hybrid neuroprosthesis for restoring lower limb function in paraplegics. In *IEEE EMBC*, 2014.

[71] N. Kirsch, N. Alibeji, and N. Sharma. Optimized control of different actuation strategies for FES and orthosis aided gait. In *ASME Dyn. Syst. Control Conf.*, Palo Alto, CA, 2013.

[72] N. Kirsch, N. Alibeji, and N. Sharma. Model predictive control-based dynamic control allocation in a hybrid neuroprosthesis. In *ASME Dyn. Syst. Control Conf.*, San Antonio, TX, 2014.

[73] N. Kirsch, N. Alibeji, and N. Sharma. Nonlinear model predictive control of functional electrical stimulation. In *ASME DSCC*, 2015.

[74] N. Kirsch, N. Alibeji, and N. Sharma. Nonlinear model predictive control of functional electrical stimulation. *Control Eng. Pract.*, Accepted.

[75] C. Klauer, T. Schauer, W. Reichenfelser, J. Karner, S. Zwicker, M. Gandolla, E. Ambrosini, S. Ferrante, M. Hack, A. Jedlitschka, A. Duschau-Wicke, M. Gföhler, and A. Pedrocchi. Feedback control of arm movements using neuro-muscular electrical stimulation (NMES) combined with a lockable, passive exoskeleton for gravity compensation. *Front. Neurosci.*, 8(262), 2014.

[76] K. Klose, P. Jacobs, J. Broton, R. Guest, B. Needham-Shropshire, N. Lebwohl, M. Nash, and B. Green. Evaluation of a training program for persons with SCI paraplegia using the Parastep 1 ambulation system: part 1. Ambulation performance and anthropometric measures. *Arch. Phys. Med. Rehabil.*, 78(8):789–793, 1997.

[77] R. Kobetic, C. To, J. Schnellenberger, M. Audu, T. Bulea, R. Gaudio, G. Pinault, S. Tashman, and R. Triolo. Development of hybrid orthosis for standing, walking, and stair climbing after spinal cord injury. *J. Rehabil. Res. Dev.*, 46(3):447–462, 2009.

[78] R. Kobetic, R. Triolo, and E. Marsolais. Muscle selection and walking performance of multichannel FES systems for ambulation in paraplegia. *IEEE Trans. Rehabil. Eng.*, 5(1):23–9, 1997.

[79] H. Kordylewski and D. Graupe. Control of neuromuscular stimulation for ambulation by complete paraplegics via artificial neural networks. *Neurol. Res.*, 23(5):472–481, 2001.

[80] A. Kralj and T. Bajd. *Functional electrical stimulation: standing and walking after spinal cord injury.* CRC Press, 1989.

[81] J. Krevolin, M. Pandy, and J. Pearce. Moment arm of the patellar tendon in the human knee. *J. Biomech.*, 37(5):785–788, 2004.

[82] M. Krstic, P. Kokotovic, and I. Kanellakopoulos. *Nonlinear and adaptive control design.* John Wiley & Sons, Inc., 1995.

[83] N. Lan, P. Crago, and H. Chizeck. Control of end-point forces of a multijoint limb by functional neuromuscular stimulation. *IEEE Trans. Biomed. Eng.*, 38(10):953–965, 1991.

[84] N. Lan, P. Crago, and H. Chizeck. Feedback control methods for task regulation by electrical stimulation of muscles. *IEEE Trans. Biomed. Eng.*, 38(12):1213–1223, 1991.

[85] J. Lawler, M. Davis, and E. Griffith. Electrical characteristics of the skin. *J. Invest. Dermatol.*, 34(5):301–308, 1960.

[86] F. Le, I. Markovsky, C. Freeman, and E. Rogers. Recursive identification of Hammerstein systems with application to electrically stimulated muscle. *Control Eng. Pract.*, 20(4):386–396, 2012.

[87] D. Levine, J. Richards, and M. Whittle. *Whittle's gait analysis.* Elsevier Health Sciences, fifth edition, 2012.

[88] M. Levy, J. Mizrahi, and Z. Susak. Recruitment, force and fatigue characteristics of quadriceps muscles of paraplegics, isometrically activated by surface FES. *J. Biomed. Eng.*, 12(2):150–156, 1990.

[89] F. Lewis. *Optimal Control.* John Wiley & Sons, 1986.

[90] F. Lewis. Neural network control of robot manipulators. *IEEE Intell. Syst.*, 11(3):64–75, 1996.

[91] F. Lewis, J. Campos, and R. Selmic. *Neuro-fuzzy control of industrial systems with actuator nonlinearities.* Society for Industrial and Applied Mathematics, 2002.

[92] D. Liberzon. *Switching in systems and control.* Systems & Control: Foundations & Applications. Birkhauser, 2003.

[93] D. Luenberger and Y. Ye. *Linear and nonlinear programming.* Springer Science & Business Media, 2008.

[94] C. Lynch and M. Popovic. A comparison of closed-loop control algorithms for regulating electrically stimulated knee movements in individuals with spinal cord injury. *Neural Syst. Rehabil.*, 20(4):539–548, 2012.

[95] G. Lyons, T. Sinkjaer, J. Burridge, and D. Wilcox. A review of portable FES-based neural orthoses for the correction of drop foot. *IEEE Trans. Neur. Sys. Rehab. Eng.,*, 10(4):260–279, 2002.

[96] R. Maladen, R. Perumal, A. Wexler, and S. Binder-Macleod. Effects of activation pattern on nonisometric human skeletal muscle performance. *J. Appl. Physiol.*, 102(5):1985–1991, 2007.

[97] E. Marsolais and R. Kobetic. Functional electrical stimulation for walking in paraplegia. *J. Bone Jt. Surg.*, 69(5):728–733, 1987.

[98] K. Masani and M. Popovic. Functional electrical stimulation in rehabilitation and neurorehabilitation. In *Springer Handb. Med. Technol.*, pages 877–896. Springer, 2011.

[99] D. Mayne, E. Kerrigan, E. van Wyk, and P. Falugi. Tube-based robust nonlinear model predictive control. *Int. J. Robust Nonlinear Control*, 21(11):1341–1353, 2011.

[100] D. Mayne, J. Rawlings, C. Rao, and P. Scokaert. Constrained model predictive control: stability and optimality. *Automatica*, 36(6):789–814, 2000.

[101] M. McClelland, B. Andrews, J. Patrick, and W. Masri. Augmentation of the Oswestry Parawalker orthosis by means of surface electrical stimulation: gait analysis of three patients. *Spinal Cord*, 25(1):32–38, 1987.

[102] L. Mendell and E. Henneman. Terminals of single Ia fibers: location, density, and distribution withing a pool of 300 homonymous motorneurons. *J. Neurophysiol.*, 34(1):171–187, 1971.

[103] P. Mhaskar, N. El-Farra, and P. Christofides. Stabilization of nonlinear systems with state and control constraints using Lyapunov-based predictive control. *Syst. Control Lett.*, 55(8):650–659, 2006.

[104] S. Mohammed, P. Poignet, P. Fraisse, and D. Guiraud. Toward lower limbs movement restoration with input-output feedback linearization and model predictive control through functional electrical stimulation. *Control Eng. Pract.*, 20(2):182–195, 2012.

[105] M. Murray, A. Drought, and R. Kory. Walking patterns of normal men. *J. Bone Joint Surg. Am.*, 46(2):335–60, 1964.

[106] S. Nandurkar, E. Marsolais, and R. Kobetic. Percutaneous implantation of iliopsoas for functional neuromuscular stimulation. *Clin. Orthop. Relat. Res.*, 389:210–217, 2001.

[107] P. Neuhaus, J. Noorden, T. Craig, T. Torres, J. Kirschbaum, and J. Pratt. Design and evaluation of Mina: a robotic orthosis for paraplegics. In *IEEE Int. Conf. Rehabil. Robot.*, pages 1–8, 2011.

[108] T. Oda, H. Kanehisa, and K. Chino. In vivo length-force relationships on muscle fiber and muscle tendon complex in the tibialis anterior muscle. *International Journal of Sport and Health Science*, 3:245–252, 2005.

[109] P. Peckham and J. Knutson. Functional electrical stimulation for neuromuscular applications. *Annu. Rev. Biomed. Eng.*, 7:327–360, 2005.

[110] D. Popović, R. Stein, M. Namik Oguztoreli, M. Lebiedowska, S. Jonic, and S. Joni. Optimal control of walking with functional electrical stimulation: a computer simulation study. *IEEE Trans. Rehabil. Eng.*, 7(1):69–79, 1999.

[111] M. Popović, D. Popović, and T. Keller. Neuroprostheses for grasping. *Neurol. Res.*, 24(5):443–452, 2002.

[112] H. Quintero, R. Farris, W. Durfee, and M. Goldfarb. Feasibility of a hybrid-FES system for gait restoration in paraplegics. In *IEEE EMBS*, pages 483–486, 2010.

[113] H. Quintero, R. Farris, K. Ha, and M. Goldfarb. Preliminary assessment of the efficacy of supplementing knee extension capability in a lower limb exoskeleton with FES. In *IEEE EMBC*, pages 3360–3363, 2012.

[114] K. Ragnarsson. Functional electrical stimulation after spinal cord injury: current use, therapeutic effects and future directions. *Spinal Cord*, 46(4):255–274, 2007.

[115] J. Reilly. *Applied bioelectricity: from electrical stimulation to electropathology.* Springer Science & Business Media, 2012.

[116] R. Riener and T. Fuhr. Patient-driven control of FES-supported standing up: a simulation study. *IEEE Trans. Rehabil. Eng.*, 6(2):113–124, 1998.

[117] R. Riener, J. Quintern, and G. Schmidt. Biomechanical model of the human knee evaluated by neuromuscular stimulation. *J. Biomech.*, 29(9):1157–1167, 1996.

[118] I. Ross. *A primer on Pontryagin's Principle in optimal control.* Collegiate Publishers, 2009.

[119] D. Russ, K. Vandenborne, and S. Binder-Macleod. Factors in fatigue during intermittent electrical stimulation of human skeletal muscle. *J. Appl. Physiol.*, 93(2):469–478, 2002.

[120] O. Rutherford and D. Jones. Measurement of fibre pennation using ultrasound in the human quadriceps in vivo. *Eur. J. Appl. Physiol.*, 65:433–437, 1992.

[121] T. Schauer, N. Negard, F. Previdi, K. Hunt, M. Fraser, E. Ferchland, and J. Raisch. Online identification and nonlinear control of the electrically stimulated quadriceps muscle. *Control Eng. Pr.*, 13:1207–1219, 2005.

[122] E. Schearer, Y. Liao, E. Perreault, M. Tresch, W. Memberg, R. Kirsch, and K. Lynch. Multi-muscle FES force control of the human arm for arbitrary goals. *IEEE Trans. Neural Syst. Rehabil. Eng.*, 22:654–663, 2014.

[123] A. Scheiner, R. Stein, D. Ferencz, and H. Chizeck. Improved models for the lower leg in paraplegics. *Proc. 15th Annu. Int. Conf. IEEE Eng. Med. Biol. Soc.*, pages 1151–1152, 1993.

[124] F. Sepulveda. Artificial neural network techniques in human mobility rehabilitation. In *Computational Methods in Biophysics, Biomaterials, Biotechnology and Medical Systems*, pages 327–362. Springer, 2003.

[125] N. Sharma, S. Bhasin, Q. Wang, and W. Dixon. Predictor-based control for an uncertain Euler-Lagrange system with input delay. In *Am. Control Conf.*, pages 1422–1427, 2010.

[126] N. Sharma and A. Dani. Nonlinear estimation of gait kinematics during functional electrical stimulation and orthosis-based walking. In *Am. Control Conf.*, pages 4778–4783, 2014.

[127] N. Sharma, C. Gregory, and W. Dixon. Predictor-based compensation for electromechanical delay during neuromuscular electrical stimulation. *IEEE Trans. Neural Syst. Rehabil. Eng.*, 19(6):601–611, 2011.

[128] N. Sharma, P. Patre, C. Gregory, and W. Dixon. Nonlinear control of NMES: incorporating fatigue and calcium dynamics. In *ASME Dyn. Syst. Control Conf.*, pages 705–712, 2009.

[129] N. Sharma, K. Stegath, C. Gregory, and W. Dixon. Nonlinear neuromuscular electrical stimulation tracking control of a human limb. *IEEE Trans. Neural Syst. Rehabil. Eng.*, 17(6):576–584, 2009.

[130] N. Sharma and R. Stein. Gait planning and double support phase model for functional electrical stimulation-based walking. In *IEEE Eng. Med. Biol. Soc.*, pages 1904–1907, 2012.

[131] Y. Shtessel, C. Edwards, L. Fridman, and A. Levant. *Sliding mode control and observation.* Springer New York, 2014.

[132] M. Solomonow, R. Baratta, S. Hirokawa, N. Rightor, W. Walker, P. Beaudette, H. Shoji, and R. D'Ambrosia. The RGO generation II: muscle stimulation powered orthosis as a practical walking system for thoracic paraplegics. *Orthopedics*, 12(10):1309–1315, 1989.

[133] M. Solomonow, H. Shoji, R. D'Ambrosia, and R. Douglas. Electromechanical walking system for paraplegics. In *IEEE Annu. Conf. Eng. Med. Biol. Soc.*, pages 4–7, 1985.

[134] R. Stein, E. Zehr, M. Lebiedowska, D. Popovic, A. Scheiner, and H. Chizeck. Estimating mechanical parameters of leg segments in individuals with and without physical disabilities. *IEEE Trans. Rehabil. Eng.*, 4(3):201–211, 1996.

[135] K. Strausser and H. Kazerooni. The development and testing of a human machine interface for a mobile medical exoskeleton. In *IEEE/RSJ Int. Conf. Intell. Robot. Syst.*, pages 4911–4916, 2011.

[136] E. Strickland. Good-bye, wheelchair. *IEEE Spectr.*, 49(1):30–32, 2012.

[137] The National Spinal Cord Injury Statistical Center. Spinal cord injury (SCI) facts and figures at a glance. *J. Spinal Cord Med.*, 2015.

[138] D. Thelen, F. Anderson, and S. Delp. Generating dynamic simulations of movement using computed muscle control. *J. Biomech.*, 36(3):321–328, 2003.

[139] C. To, R. Kobetic, J. Schnellenberger, M. Audu, and R. Triolo. Design of a variable constraint hip mechanism for a hybrid neuroprosthesis to restore gait after spinal cord injury. *IEEE/ASME Trans. Mechatronics*, 13(2):197–205, 2008.

[140] R. Tomović, D. Popović, R. Stein, R. Tomović, and D. Popović. *Nonanalytical methods for motor control.* World Scientific, 1995.

[141] R. Tomović, .M Vukobratovic, and L. Vodovnik. Hybrid actuators for orthotic systems - hybrid assistive system. In *Int. Symp. Extern. Control Hum. Extrem.*, page 73, 1973.

[142] K. Tong and M. Granat. Gait-control system for functional electrical stimulation using neural networks. *Med. Biol. Eng. Comput.*, 37:35–41, 1999.

[143] R. Treagear. *Physical functions of the skin.* Academic Press, 1966.

[144] P. Veltink, H. Chizeck, P. Crago, and A. El-Bialy. Nonlinear joint angle control for artificially stimulated muscle. *IEEE Trans. Biomed. Eng.*, 39(4):368–380, 1992.

[145] Q. Wang, N. Sharma, M. Johnson, C. Gregory, and W. Dixon. Adaptive inverse optimal neuromuscular electrical stimulation. *IEEE Trans. Cybern.*, 43(6):1710–1718, 2013.

[146] D. Winter. *Biomechanics and motor control of human movement.* John Wiley & Sons, 2009.

[147] D. Winter, A. Patla, J. Frank, and S. Walt. Biomechanical walking pattern changes in the fit and healthy elderly. *Phys. Ther.*, 70(6):340–347, 1990.

[148] J. Winters. Hill-based muscle models: a systems engineering perspective. In *Mult. Muscle Syst.*, pages 69–93. Springer New York, 1990.

[149] F. Zajac. Muscle and tendon: properties, models, scaling, and application to biomechanics and motor control. *Crit. Rev. Biomed. Eng.*, 17(4):359–411, 1989.

[150] D. Zhang and K. Zhu. Simulation study of FES-assisted standing up with neural network control. In *IEEE Eng. Med. Biol. Soc.*, volume 2, pages 4877–4880, 2004.

[151] S. Zhou, D. Lawson, W. Morrison, and I. Fairweather. Electromechanical delay in isometric muscle contractions evoked by voluntary, reflex and electrical stimulation. *Eur. J. Appl. Physiol. Occup. Physiol.*, 70(2):138–145, 1995.